

Magnetic-Based NDE of Prestressed and Post-Tensioned Concrete Members—The MFL System

PUBLICATION NO. FHWA-RD-00-026

MAY 2000



U.S. Department of Transportation
Federal Highway Administration

Research, Development, and Technology
Turner-Fairbank Highway Research Center
6300 Georgetown Pike
McLean, VA 22101-2296

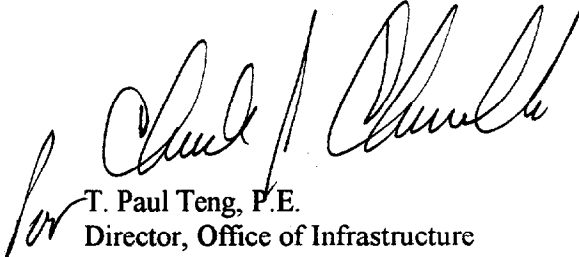
FOREWORD

This report presents information on the development of a nondestructive evaluation (NDE) system for assessing the condition of prestressing or post-tensioning steel in concrete structures. The technique is based on the magnetic flux leakage (MFL) concept. The basic methodology is based on introducing a direct-current (magnetic field in close proximity of the prestressing or post-tensioning steel and monitoring the variations of the field due to loss of cross-sectional area of steel from corrosion or fracture.

Although most of the effort made during this study was associated with the development of the MFL system, limited laboratory and field investigations were conducted to assess the capabilities and limitations of the system. During both the laboratory and field investigations, it was demonstrated that the installation and operation of the MFL system were successful. System installation on a test beam is accomplished easily and in a time period not longer than a few minutes. During the laboratory study, steel prestressing strands with partial localized cross-sectional area losses from 7% to 71% percent were used as test specimens. Also, prestressing strands with real corrosion were used for the same purpose. It was found that the smallest flaw in a strand that could be detected had a 7% percent reduction in the cross-sectional area. This capability was demonstrated for the strands that were placed at a distance of up to 128 mm (5 in) from the magnet and sensor assembly of the system. A field demonstration was conducted that showed that the installation and operation of the MFL system were successful.

It is recommended that additional laboratory and field investigations beyond this study be conducted with the use of the new MFL system in order to fully evaluate its capabilities and limitations. This would also facilitate the establishment of a more comprehensive database that can enhance the data interpretation capability and the overall reliability of the system.

This report will be of interest to maintenance; materials and bridge engineers; practicing structural engineers; construction engineers; prestressing steel producers; and owners of reinforced, prestressed, and post-tensioned structures.



T. Paul Teng, P.E.
Director, Office of Infrastructure
Research and Development

NOTICE

This document is disseminated under the sponsorship of the Department of Transportation in the interest of information exchange. The United States Government assumes no liability for its contents or use thereof. This report does not constitute a standard, specification, or regulation.

The United States Government does not endorse products or manufacturers. Trade or manufacturers' names appear herein only because they are considered essential to the object of the document.

Technical Report Documentation Page

1. Report No. FHWA-RD-00-026	2. Government Accession No.	3. Recipient's Catalog No.	
4. Title and Subtitle MAGNETIC-BASED NDE OF PRESTRESSED AND POST-TENSIONED CONCRETE MEMBERS – THE MFL SYSTEM		5. Report Date May 2000	6. Performing Organization Code
7. Author(s) A. Ghorbanpoor, R. Borchelt, M. Edwards, and E. Abdel Salam,		8. Performing Organization Report No.	
9. Performing Organization Name and Address Department of Civil Engineering and Mechanics University of Wisconsin-Milwaukee 3200 N. Cramer Street Milwaukee, WI 53211		10. Work Unit No. (TRAVIS)	11. Contract or Grant No. DTFH61-95-C-00161
12. Sponsoring Agency Name and Address Office of Infrastructure Research and Development Federal Highway Administration 6300 Georgetown Pike McLean, VA 22101-2296		13. Type of Report and Period Covered Final Report 1995-1999	
15. Supplementary Notes Contracting Officer's Technical Representative (COTR): Y.P. Virmani, HRDI-09		14. Sponsoring Agency Code	
<p>16. Abstract</p> <p>This report describes all aspects of a study to develop a nondestructive evaluation (NDE) system based on the concept of magnetic flux leakage (MFL) to detect corrosion and fracture of prestressing steel in pretensioned and post-tensioned concrete bridge members. The basic methodology is based on introducing a direct-current magnetic field in close proximity of the prestressing or post-tensioning steel and monitoring the variations of the field due to loss of cross-sectional area of steel from corrosion or fracture.</p> <p>The mechanical and electrical components of the MFL system include a lightweight structural frame that supports the source of the required magnetic field and an array of sensors for measuring the magnetic field variation. The frame also supports a series of mechanical and electrical components that facilitate the operation of the system. Two strong permanent magnets provide the required magnetic field. A set of 10 Hall-effect sensors in the system measure the variations in the magnetic field due to the presence of flaws in prestressing or post-tensioning steel. Software is developed to acquire and analyze the MFL data as well as to control all hardware, including the mechanical and electrical components of the system. The system is designed and fabricated to offer ease of use during the field operation. The operation of the system includes attaching the structural frame of the system to a test beam and conducting the test by controlling the frame and its components by a notebook computer from a remote site via wireless communication.</p> <p>Although most of the effort made during this study was associated with the development of the MFL system, limited laboratory and field investigations were conducted to assess the capabilities and limitations of the system. During both the laboratory and field investigations, it was demonstrated that the installation and operation of the MFL system were successful. System installation on a test beam may be accomplished easily and in a time period not longer than a few minutes. During the laboratory study, steel prestressing strands with partial localized cross-sectional area losses from 7% to 71% were used as test specimens. Also, prestressing strands with real corrosion were used for the same purpose. It was found that the smallest flaw in a strand that could be detected had a 7% reduction in the cross-sectional area. This capability was demonstrated for the strands that were placed at a distance of up to 128 mm (5 in) from the magnet and sensor assembly of the system. A field demonstration was conducted that showed that the installation and operation of the MFL system were successful.</p> <p>It is recommended that additional laboratory and field investigations beyond this study be conducted with the use of the new MFL system in order to fully evaluate its capabilities and limitations. This would also facilitate the establishment of a more comprehensive database that can enhance the data interpretation capability and the overall reliability of the system.</p>			
17. Key Words Nondestructive evaluation (NDE), magnetic flux leakage (MFL), bridges, concrete, prestressing steel, corrosion, Hall effect, wireless communication.		18. Distribution Statement No original distribution by the sponsoring agency. This document is available to the public through the National Technical Information Service, Springfield, VA 22161.	
19. Security Classif. (of this report) Unclassified	20. Security Classif. (of this page) Unclassified	21. No. of Pages 107	22. Price

SI* (MODERN METRIC) CONVERSION FACTORS

APPROXIMATE CONVERSIONS TO SI UNITS					APPROXIMATE CONVERSIONS FROM SI UNITS				
Symbol	When You Know	Multiply By	To Find	Symbol	Symbol	When You Know	Multiply By	To Find	Symbol
LENGTH					LENGTH				
in	inches	25.4	millimeters	mm	mm	millimeters	0.039	inches	in
ft	feet	0.305	meters	m	m	meters	3.28	feet	ft
yd	yards	0.914	meters	m	m	meters	1.09	yards	yd
mi	miles	1.61	kilometers	km	km	kilometers	0.621	miles	mi
AREA					AREA				
in ²	square inches	645.2	square millimeters	mm ²	mm ²	square millimeters	0.0016	square inches	in ²
ft ²	square feet	0.093	square meters	m ²	m ²	square meters	10.764	square feet	ft ²
yd ²	square yards	0.836	square meters	m ²	m ²	square meters	1.195	square yards	yd ²
ac	acres	0.405	hectares	ha	ha	hectares	2.47	acres	ac
mi ²	square miles	2.59	square kilometers	km ²	km ²	square kilometers	0.386	square miles	mi ²
VOLUME					VOLUME				
fl oz	fluid ounces	29.57	milliliters	mL	mL	milliliters	0.034	fluid ounces	fl oz
gal	gallons	3.785	liters	L	L	liters	0.264	gallons	gal
ft ³	cubic feet	0.028	cubic meters	m ³	m ³	cubic meters	35.71	cubic feet	ft ³
yd ³	cubic yards	0.765	cubic meters	m ³	m ³	cubic meters	1.307	cubic yards	yd ³
MASS					MASS				
oz	ounces	28.35	grams	g	g	grams	0.035	ounces	oz
lb	pounds	0.454	kilograms	kg	kg	kilograms	2.202	pounds	lb
T	short tons (2000 lb)	0.907	megagrams (or "metric ton")	Mg (or "t")	Mg (or "t")	megagrams (or "metric ton")	1.103	short tons (2000 lb)	T
TEMPERATURE (exact)					TEMPERATURE (exact)				
°F	Fahrenheit temperature	5(F-32)/9 or (F-32)/1.8	Celsius temperature	°C	°C	Celsius temperature	1.8C + 32	Fahrenheit temperature	°F
ILLUMINATION					ILLUMINATION				
fc	foot-candles	10.76	lux	lx	lx	lux	0.0929	foot-candles	fc
fl	foot-Lamberts	3.426	candela/m ²	cd/m ²	cd/m ²	candela/m ²	0.2919	foot-Lamberts	fl
FORCE and PRESSURE or STRESS					FORCE and PRESSURE or STRESS				
lbf	poundforce	4.45	newtons	N	N	newtons	0.225	poundforce	lbf
lbf/in ²	poundforce per square inch	6.89	kilopascals	kPa	kPa	kilopascals	0.145	poundforce per square inch	lbf/in ²

* SI is the symbol for the International System of Units. Appropriate rounding should be made to comply with Section 4 of ASTM E380.

(Revised September 1993)

TABLE OF CONTENTS

	Page
CHAPTER 1. INTRODUCTION	1
BRIDGE CONDITION EVALUATION.....	1
HISTORY OF MAGNETIC-BASED NDE.....	2
SCOPE OF THE STUDY.....	3
CHAPTER 2. THEORY OF MAGNETISM	5
BACKGROUND.....	5
MAGNETIC FLUX LEAKAGE CONCEPT	6
CHAPTER 3. SYSTEM INSTRUMENTATION	9
INTRODUCTION.....	9
THE MECHANICAL SYSTEM.....	10
The Sensing-Head Unit	10
The Beam-Rider Unit.....	12
THE ELECTRICAL SYSTEM.....	14
The DAC Unit.....	14
The Sensing-Head	14
The Motor Control Circuit for the Beam-Rider Unit	15
The Radio Modem Transceivers	16
Electrical Circuit Diagrams and Schematics.....	17
Identification of Primary Components/Parts	17
CHAPTER 4. SOFTWARE	19
INTRODUCTION	19
DATA ACQUISITION.....	19
System Control Software.....	19
Data-Acquisition Software	20
DATA ANALYSIS (post-processing).....	21

TABLE OF CONTENTS (Continued)

	Page
CHAPTER 5. SYSTEM OPERATION	33
INTRODUCTION.....	33
SYSTEM INSTALLATION AND OPERATION.....	34
Steps for Adjusting the Width of the Beam-Rider Unit.....	34
Installing the Beam-Rider Unit on a Concrete Test Beam.....	35
Safety Considerations.....	36
Operation of the Beam-Rider Unit.....	37
CHAPTER 6. SYSTEM EVALUATION	41
INTRODUCTION.....	41
LABORATORY INVESTIGATION.....	41
Laboratory Evaluation Results.....	44
FIELD INVESTIGATION.....	54
ANALYSIS METHODS AND SUMMARY OF FINDINGS.....	60
Data Interpretation.....	60
Post-Processing Methods for the Recorded Data.....	60
Correlation Parameters Based on Test Results.....	62
CHAPTER 7. CONCLUSIONS	65
APPENDIX A. TECHNICAL DATA FOR PERMANENT MAGNETS	67
APPENDIX B. TECHNICAL DATA FOR HALL-EFFECT SENSORS	73
APPENDIX C. TECHNICAL DATA FOR ELECTRICAL AND CONTROL SYSTEMS	77
APPENDIX D. PRIMARY COMPONENTS/PARTS DESCRIPTION	81
APPENDIX E. DATA ACQUISITION, DATA ANALYSIS, AND SYSTEM CONTROL SOFTWARE SUBROUTINES	83
REFERENCES	99

LIST OF FIGURES

Figure No.		Page
1.	Overall view of the magnetic-based NDE system (the beam-rider unit).....	9
2.	Block diagram for the MFL system design concept.....	10
3.	Overall view of the sensing head	11
4.	Components of the beam-rider unit.....	13
5.	Printed circuit boards for the Hall sensors.....	16
6.	System control part of the user's interface software for the MFL system.....	20
7.	Data-acquisition software for the MFL system.....	20
8.	MFL data post-processing options window.....	22
9.	User interface window for MFL data analysis Option One.....	23
10.	User interface window for MFL data analysis Option Two.....	24
11.	User interface window for MFL data analysis Option Three.....	25
12.	User interface window for MFL data analysis Option Four.....	27
13.	User interface window for MFL data analysis Option Five.....	28
14.	User interface window for MFL data analysis Option Six.....	29
15.	User interface window for MFL data analysis Option Seven.....	30
16.	User interface window for MFL data analysis Option Eight.....	31
17.	User interface window for MFL data analysis Option Nine.....	32
18.	The wooden beam used for laboratory testing of the beam-rider unit.....	42
19.	Strands with mechanically introduced flaws and real corrosion.....	43
20.	Graphs of a sensor amplitude output and correlation analysis for Cable #1 (distance to magnet/sensor = 51 mm (2 in), no adjacent steel).....	45
21.	Graphs of a sensor amplitude output and correlation analysis for Cable #2 (distance to magnet/sensor = 51 mm (2 in), no adjacent steel).....	46
22.	Graphs of a sensor amplitude output and correlation analysis for Cable #3 (distance to magnet/sensor = 51 mm (2 in), no adjacent steel).....	47
23.	Graphs of a sensor amplitude output and correlation analysis for Cable #1 (distance to magnet/sensor = 89 mm (3.5 in), no adjacent steel).....	48
24.	Graphs of a sensor amplitude output and correlation analysis for Cable #2 (distance to magnet/sensor = 89 mm (3.5 in), no adjacent steel).....	49
25.	Graphs of a sensor amplitude output and correlation analysis for Cable #3 (distance to magnet/sensor = 89 mm (3.5 in), no adjacent steel).....	49
26.	Graphs of a sensor amplitude output and correlation analysis for Cable #1 (distance to magnet/sensor = 128 mm (5 in), no adjacent steel).....	50
27.	Graphs of a sensor amplitude output and correlation analysis for Cable #2 (distance to magnet/sensor = 128 mm (5 in), no adjacent steel).....	51
28.	Graphs of a sensor amplitude output and correlation analysis for Cable #3 (distance to magnet/sensor = 128 mm (5 in), no adjacent steel).....	51
29.	Graphs of a sensor amplitude output and correlation analysis for Cable #1 (distance to magnet/sensor = 51 mm (2 in), 14 adjacent steel cables).....	52
30.	Graphs of a sensor amplitude output and correlation analysis for Cable #2 (distance to magnet/sensor = 51 mm (2 in), 14 adjacent steel cables).....	53
31.	Graphs of a sensor amplitude output and correlation analysis for Cable #4 (distance to magnet/sensor = 51 mm (2 in), no adjacent steel).....	54

LIST OF FIGURES (Continued)

Figure No.		Page
32.	Overall layout of the structural framing of the bridge span tested by the MFL system.....	55
33.	Close-up view of the beam-rider unit on a concrete girder	55
34.	View of the beam-rider unit with the details of the safety clamps and cables	56
35.	Graphs of a sensor amplitude output and correlation analysis for field test data.....	57
36.	Amplitude data for tracks 1 and 2 of a girder during field testing	58
37.	Three-dimensional graph for tracks 1 and 2 of a girder during field testing (only 3.0 m (10 ft) of data is shown for clarity).....	59
38.	Required parameters for the correlation analysis.....	61
C-1.	Block diagram describing data acquisition and conditioning.....	79
C-2.	Circuit diagram for overall electrical control for the MFL system.....	80

LIST OF TABLES

Table No.		Page
1.	Functional description for the controllers and indicators in the system control software	21
2.	Signal amplitudes for a single prestressing tendon at different cover depths	62
3.	Optimum B and N values for post-processing of MFL data.....	63
C-1.	Hall-effect sensor and power connection data (Cable #1).....	77
C-2.	Pin identification and function description for digital/analog Cable #2.....	77
C-3.	Pin identification and function description for motor control Cable #3	78
D-1.	Primary components/parts data for the MFL system.....	81

CHAPTER 1. INTRODUCTION

In April 1995, the Federal Highway Administration (FHWA) issued a request for proposal for a research study on "Magnetic-Based System for NDE of Prestressing Steel in Pretensioned and Post-Tensioned Concrete Bridges." The objectives of the study were to design, fabricate, and demonstrate a nondestructive evaluation (NDE) system based on the principle of magnetic flux variation that can detect corrosion and fracture of reinforcing or prestressing steel in concrete bridge members. It was required to develop a system that was based on a modular concept to allow application to various bridge members with different geometrical configurations. It was also required to offer field operation efficiency for the system in terms of its overall operation and, specifically, its installation and removal on and from various bridge components.

Upon approval of a research study proposal, the University of Wisconsin-Milwaukee was authorized by the FHWA to initiate work on the project on October 1, 1995. A conceptual design was developed by the research staff that was submitted to the FHWA in April 1996 in the form of an interim report. Upon approval of the interim report in June 1996, the research staff initiated the required tasks of detailed design and fabrication of the NDE system. The efforts devoted to the study have led to the development of a modular-based NDE system based on the principle of magnetic flux variation that can be used to evaluate the condition of reinforcing or prestressing steel in concrete bridge members. This report presents all aspects of the development of the system and other relevant details.

BRIDGE CONDITION EVALUATION

The majority of bridge structures in the United States and throughout the world are more than 30 to 40 years old. With the aging of these structures, bridge engineers and owners have experienced significant problems associated with their overall condition and performance. Various components of these structures have deteriorated to a varying extent during their service lives and have significantly affected the safe and reliable performance of these structures. To deal with the problem, a significant amount of funds and resources have been used for repair, rehabilitation, and replacement of these structures. In most cases, the deterioration of the components could not be recognized or identified by the maintenance personnel in time or before extensive damage had taken place. When deterioration is first identified at a relatively late stage, the cost of correcting the problem could be very high. This cost may be in terms of needed funds and other resources and often includes disruption of traffic and flow of commerce. The problem has been mainly due to the use of ineffective inspection methods that have adversely affected the evaluation of these structures.

A large number of bridge structures are constructed using concrete as the primary construction material. To make concrete effective in resisting tension, reinforcing, prestressing, or post-tensioning steel is normally placed in the tension region of concrete structural members. Deficiencies in concrete structures are associated with either the quality of concrete or the deterioration of concrete and steel reinforcement. The most common problems related to the quality of concrete include low density and the presence of voids, honeycombing, delamination, and cracking. In addition, concrete could deteriorate during the normal service life from the effect of environment and exposure to harmful chemicals. These problems can directly or indirectly lead to additional deficiencies that adversely affect the performance of concrete structural members. The problem associated with the deterioration of steel within concrete has been primarily due to the corrosion phenomenon caused by chloride ions from deicer application or marine environments. Concrete structures depend primarily on steel to resist tensile stresses that are induced from the effect of service loads. Corrosion causes a reduction in the cross-sectional area of steel in addition to concrete cracking and delamination. Reduction in the steel cross-sectional area, as well as formation of

stress raisers at the location of corrosion pits, will directly increase the stress level in the steel that could reach a critical level.

Bridge maintenance engineers and owners are continuously faced with the task of evaluating the existing condition of the prestressed concrete (PS/C) structures. Generally, visual inspection is the most commonly used method. While a thorough visual inspection can offer valuable information concerning the condition of a bridge structure, it may only reveal the aftereffects of various deteriorating mechanisms that can take place in concrete structures. For example, surface cracks or corrosion stains on concrete structures can indicate that some deteriorating mechanisms have been active within the concrete for some time. Often, the extent of the problem cannot be determined through visual inspection. In recent years, the use of various NDE techniques has become more desirable for the PS/C structures. Some NDE methods can offer reliable results that can be used to assess the condition of a structure. Normally, different NDE methods should be employed to evaluate concrete or prestressing steel within the concrete. Several NDE methods are applicable to PS/C structures. The choice of the methods depends on what information is required to be obtained. Methods that are suitable for evaluation of concrete materials are discussed in numerous available publications, but are not the focus of this study. In contrast, only a limited number of NDE methods have been identified as being applicable for assessing the condition of prestressing steel in concrete. The most appropriate of the methods are those based on the radiographic and magnetic flux leakage (MFL) concepts. Nondestructive evaluation methods based on the radiographic concept offer the capability of producing images of various types of steel within concrete. While these methods can help to accurately determine the location of steel or voids within most concrete members, they have some inherent limitations and disadvantages that limit their use for field application. These include issues related to the adequacy of the resolution of the images produced for identifying the extent of corrosion in steel, the reliability of the results, the time required for the test, safety concerns and requirements, and the relative cost. Using the concept of MFL has been effective in developing the capability of assessing the condition of prestressing steel within concrete structures. Therefore, the focus of this study has been placed on developing state-of-the-art instrumentation to enhance this capability.

HISTORY OF MAGNETIC-BASED NDE

The first instrumentation based on the MFL concept was developed in the late 1970's to allow inspection of prestressed concrete bridge girders.⁽¹⁻²⁾ The system was based on using a direct-current electromagnet to introduce a magnetic field inside the concrete near its surface. The instrumentation was subjected to an evaluation in 1984⁽³⁾ and an additional evaluation and upgrade in the late 1980's.⁽⁴⁾ During these studies, extensive laboratory and field evaluation of various bridge members were conducted using the developed MFL system. The laboratory investigation included evaluation of manmade flaws as well as real corrosion in reinforcing bars and prestressing steels. The field studies were comprised of several tests of concrete bridge structures of reinforced, prestressed, and post-tensioned construction types. Based on these studies, it was shown that the concept had excellent potential for application to concrete bridge structures. It was shown that reinforcing or prestressing steel flaws equivalent to 5- to 10-percent loss of cross-section could be detected using the MFL system.⁽⁴⁾ Various data analysis techniques were developed to aid the interpretation of the relevant test results.

Although the concept was proven to be very promising, there were several limitations and disadvantages associated with the mechanical operation of the developed MFL system. The weight of the equipment was excessive and it required extensive effort for set-up and testing for the evaluation of a single concrete member. Limitations also included difficulties in terms of operation and speed of testing, data acquisition, and data processing. The shortcomings mostly stemmed from the fact that the computing machines, data acquisition hardware, and control devices of the mid- to late 1970's were relatively limited in their capabilities compared with those available today.

Based on the promise of the concept and the relatively successful use of the initially developed instrumentation, the FHWA provided support to initiate this study in 1995. The primary goal of the study was to develop a state-of-the-art MFL system that can overcome the limitations of the previous instrumentation. The main focus was placed on the design and fabrication of a reliable system that would be efficient for field application in terms of installation on and removal from various bridge components, as well as on improving its reliability. To meet that requirement, a modular design concept was adapted and implemented that can allow a variety of structural components with varying geometrical configurations to be tested by the new system. During this study, an NDE system was designed and fabricated for testing rectangular or I-shaped concrete girders. The system includes a structural frame that supports all associated components and instrumentation. The frame is designed to be attached to a concrete girder for the purpose of scanning it. The frame is maintained on the girder through the frictional forces developed by a series of contact wheels that are compressed against the sides of the girder by spring forces. The system employs a wireless communications concept that allows the control of the test equipment and the acquisition of the test data by a remote computer. Through the remote computer control, the equipment is capable of scanning the length of the girder and recording test data. The data is obtained based on the variations in an induced magnetic field in the concrete due to the presence of different discontinuities, such as corrosion or fractures of the steel. The recorded data is then analyzed in the computer to assess the condition of the steel.

Most of the effort in the current study was devoted to the development and fabrication of the new system. Performance evaluation of the system was accomplished at various stages of the equipment development. However, this effort was limited to only a few laboratory tests that evaluated the condition of reinforcing and prestressing steels with manmade flaws and real corrosion. In addition, two demonstration field tests were performed after the system was completely fabricated. Based on experience from the laboratory and field tests, system optimization was performed during the study. The potential of the MFL concept for detecting corrosion and fracture in reinforcing or prestressing steel within concrete bridge members has already been demonstrated through past studies.⁽¹⁻⁴⁾ However, more comprehensive laboratory and field evaluations of the new system, with possible additional development and/or optimization, are recommended to follow this study.

SCOPE OF THE STUDY

The primary objective of this study was to develop and fabricate a state-of-the-art NDE system based on the concept of MFL that could offer efficient and reliable field assessment of the condition of prestressing steel within concrete. To achieve field-worthiness and efficiency, it was decided that a modular design concept should be used to allow the use of the system with different bridge or structural members. It was also decided that the installation and removal of the system on and from bridge components should be possible without requiring excessive time and effort. To further increase the field efficiency of the system, it was decided that wireless communication capability should be added to allow remote control of the equipment, data acquisition, and data transfer from the equipment to a host computer.

CHAPTER 2. THEORY OF MAGNETISM

BACKGROUND

Magnetism in permanent magnets is caused by the presence of molecular current loops within the magnetic material. Those current loops are due to two phenomena, the motion of electrons within the atoms and the spin direction of the electrons. The electron spin is a quantum mechanical property of the electron. The basic magnetic interaction within the magnet is that moving charges exert magnetic forces on other moving charges. It is important to realize that the force is in addition to any electrical force exerted due to opposite charges attracting one another.

External magnetic fields exhibit a force on all ferromagnetic materials, such as iron. Magnetic fields are characterized by regions of differing strength and are represented by field lines. These lines always form a closed loop that emanates from the north pole and follows a curved path to the south pole. The field line travels through the magnet to complete the loop. If there are two magnets in the system, the field lines travel from north on the first magnet to south on the second magnet. They travel through the second magnet to its north pole, whereupon they then travel to the first magnet's south pole and through it to the originating north pole to form a closed loop.

In the presence of a magnetic field, a moving charge has a magnetic force exerted upon it. The relationship that governs the force on moving charges through a magnetic field is called Faraday's Law. It states:

$$\underline{F} = q \cdot \underline{V} \cdot \underline{B} \quad (1)$$

where:

- \underline{F} = Magnetic force
- q = Charge
- \underline{V} = Velocity
- \underline{B} = Applied magnetic field

The above relationship implies that as a charge q moves with a velocity \underline{V} in a magnetic field \underline{B} , it experiences a magnetic force \underline{F} . It should be noted that this relationship follows the right-hand rule in that by directing the right-hand fingers from \underline{V} to \underline{B} , the force \underline{F} will be in the direction of the right-hand thumb. The International System of Units for the magnetic field is Tesla, T, where:

$$1 \text{ T} = (1 \text{ newton/coulomb}) / (1 \text{ meter/second}).$$

As a charge of 1 coulomb moves with a velocity of 1 m/s perpendicular to a magnetic field of 1 tesla, a force of 1 Newton. It should be noted that a tesla is a large unit of magnetic field (most magnets have a field strengths of less than 1 tesla). The U.S. System of Units is based on the International System of Units. The U.S. unit of magnetic field is the gauss, G (1 T is equal to 10,000 G). A field strength of 1 gauss is a relatively small quantity.

When referring to the application of permanent magnets, it is necessary to understand the basic properties associated with them. They can be described with eight basic axioms. They are:

1. Flux lines, like electrical currents, will always follow the path of least resistance. In magnetic terms, this means that flux lines will follow the path of greatest permeance or lowest reluctance.
2. Flux lines repel each other if their direction of flow is the same.
3. As a corollary to axiom (2), flux lines can never cross each other.
4. As a corollary to axiom (1), flux lines will always follow the shortest path through any medium. Therefore, they can only travel in straight lines or on curved paths. Meeting the conditions of this axiom, flux lines will normally move on curved paths; although over short distances, these paths may be considered straight for practical purposes.
5. Flux lines always leave and enter the surface of ferromagnetic materials at right angles.
6. All ferromagnetic materials have a limited ability to carry flux. When they reach this limit, they are saturated and behave as transparent materials (like air or aluminum). Below the level of saturation, a ferromagnetic material will substantially contain the flux lines passing through it. As saturation is approached, because of axioms (1) and (2), the flux lines may travel as readily through the air as through the material.
7. Flux lines will always travel from the nearest north pole to the nearest south pole in a path that forms a closed loop. They need not travel to their own opposite pole; although they ultimately do if the poles of another magnet are closer and/or there is a lower path of reluctance (greater permeance) between them.
8. Magnetic poles are not unit poles. In a magnetic circuit, any two points equidistant from the neutral axis function as poles so that flux will flow between them (ensuring that they meet the above conditions).

MAGNETIC FLUX LEAKAGE CONCEPT

To use the concept of MFL as an NDE tool, it is necessary to have the ability to measure changes in the path of magnetic field force lines, or flux, near a ferromagnetic material, such as steel, that has discontinuities or defects. Ferromagnetic materials have properties that are conducive to this process. These materials can be defined by their ability to undergo some changes in the presence of a magnetic field. First, in the presence of a magnetic field, they align their electric dipoles with the external field. They do this in relationship to the strength of the magnetic field such that for a stronger field, more dipoles are aligned than for a weaker one. Second, the magnetic flux intensity is increased within the material as a result of the dipole alignment. Third, there is a saturation level at which all dipoles are aligned and no further alignment is possible. Finally, below the saturation level, the following relationship is valid:

$$\underline{B} = \mu \cdot \underline{H} \quad (2)$$

where:

\underline{B} = Magnetic flux (weber/m²)

μ = Magnetic permeability of the material (weber/Ampere meter)

\underline{H} = Magnetic field strength (Ampere/meter)

When an external magnetic field is applied to reinforced or prestressed concrete members, the flux within the reinforcing or prestressing steel remains unchanged until it must leave the steel to travel back to the south pole of the magnet. If the flux encounters a flaw such as a corroded area, broken strand, or complete fracture, some or all of the flux leaks out of the steel. This magnetic flux leakage is detected by one or more sensors and is analyzed to determine the extent or severity of the discontinuity.

The applied magnetic field strength has a dominant influence on the concentration of the flux within ferromagnetic materials and subsequently on the extent of the flux leakage. Adequate flux leakage must take place at the location of a flaw or discontinuity in the steel so it can be measured by appropriate sensors that have their inherent limitations in terms of sensitivity, signal-to-noise ratio, etc. The field strength, therefore, must be large enough to overcome problems due to system noise, distance between the magnetic field source and the ferromagnetic material, and the masking effect of large quantities of steel found in many prestressed and reinforced concrete members. Relatively large irregularities in the steel, such as manufacturing defects or handling damage, can cause MFL that might be misinterpreted as defects. In addition, the presence of other ferromagnetic materials in the concrete, such as wrapping wires, chairs, or dropped nails, can result in the disturbance of the magnetic field. Various signal analysis techniques need to be used to enhance the interpretation capability of the recorded data.

It should be noted that due to the presence of some particles, such as magnetite or iron oxide in concrete, there could be a small effect on the distribution of the applied field. This effect is small, however, and can normally be neglected during a test. More important is the effect of the distance between the sensor and the steel on the magnitude of the flux leakage due to the presence of discontinuities in the steel. The induced magnetic field strength should be adequately large to preferably cause the saturation of the steel. This will allow maximum flux leakage to occur when there are small defects in the steel. As a result, small flaws in the steel could be detected using the MFL concept.

The device most often used to detect and measure the extent of MFL is the Hall-effect sensor. Hall elements are crystals of specially grown semi-conductor materials that, when excited by the passage of current, react to the presence of an external magnetic field by developing a voltage difference across the two parallel faces of the crystal (known as the Hall effect). The sensors can be made in any size to fulfill any intended testing application. Sensors can be made small to allow small flaws in the steel to be detected.

CHAPTER 3. SYSTEM INSTRUMENTATION

INTRODUCTION

The NDE system developed under this study is comprised of a magnetic field source, a series of magnetic field detection sensors, structural support framing, mechanical control devices, electrical control devices and circuits, wireless communication devices, software, and a notebook computer. Figure 1 shows an overall view of the system that can be used to evaluate I-shaped and rectangular concrete members.

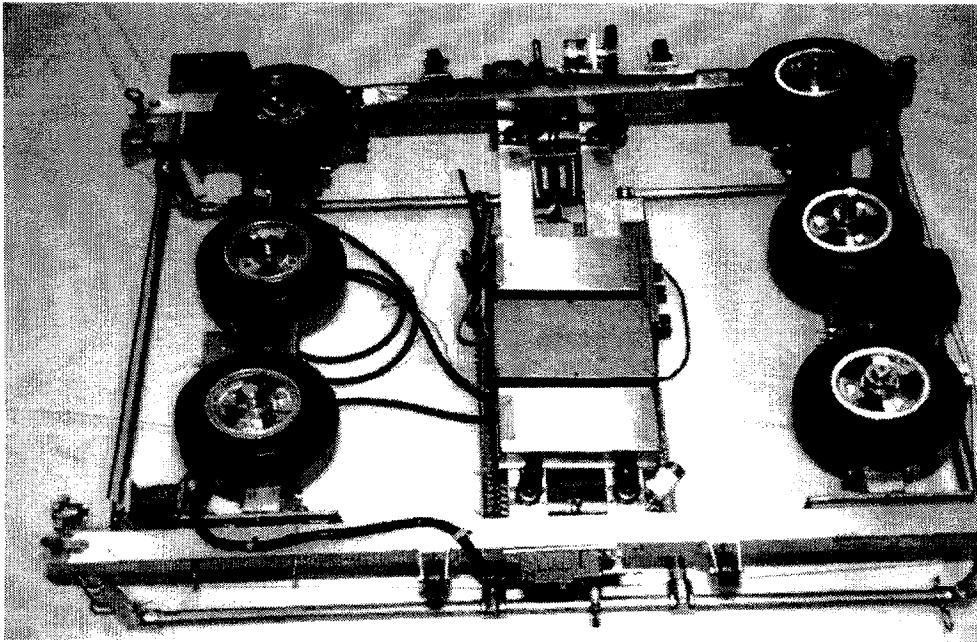


Figure 1. Overall view of the magnetic-based NDE system (the beam-rider unit).

A system block diagram is shown in figure 2 that describes the design concept used for the development of the MFL system.

A modular concept was used in the design of the system. This facilitated the use of the system for evaluation of various concrete bridge members with different geometric configurations. The primary component of the developed system is a modular unit called the sensing head that is comprised of two permanent magnets and a series of Hall-effect sensors with appropriate signal-conditioning circuits. These components are mounted on an aluminum frame that can be used independently as a hand-held unit or as a subcomponent of other units for testing different bridge members. For example, the sensing-head unit can be installed in a system called the beam-rider unit to allow the testing of I-shaped or rectangular concrete girders. In addition, it could be installed in two other units, namely the pier-climber or the pushcart units, to allow the testing of round concrete piers or flat concrete slabs or pavements. A significant portion of the efforts of this study was devoted to the development of the sensing head and the beam-rider units. While design details for the pier-climber and the pushcart units were completed, the component fabrication could not be accomplished in this study due to a lack of time and funds. Therefore, the materials presented here address the details of the sensing-head and beam-rider units, along with all relevant subcomponents, control units, applicable software, and operational details. The following is a

discussion on the details and functionality of the mechanical and electrical design concepts and components used for the MFL system.

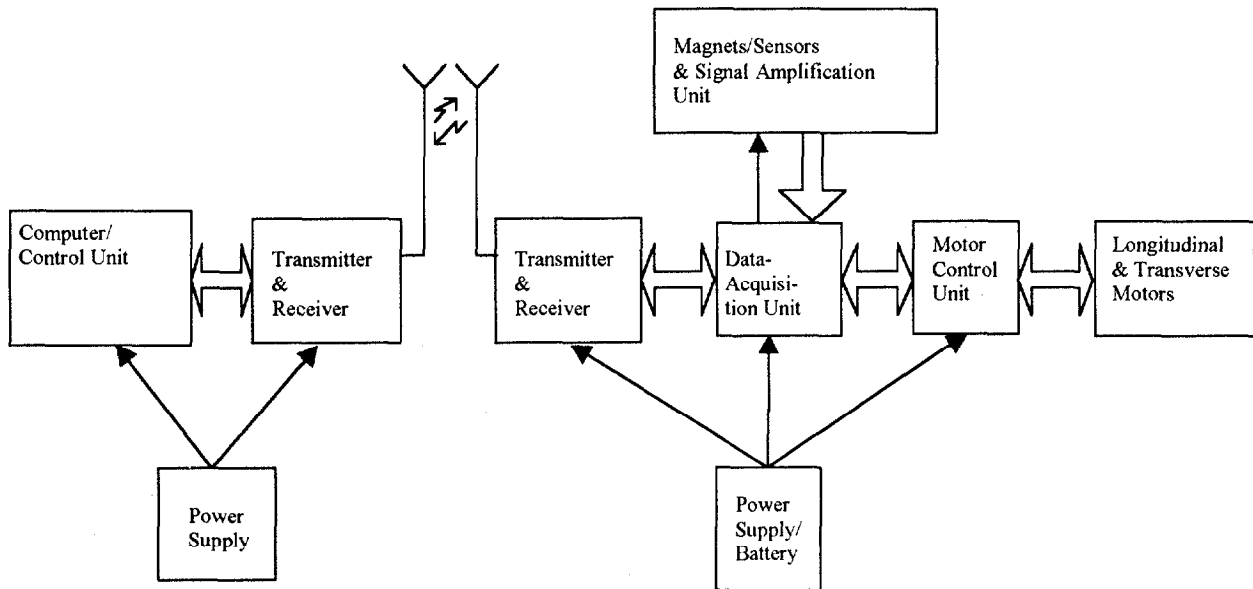


Figure 2. Block diagram for the MFL system design concept.

THE MECHANICAL SYSTEM

As described above, the new NDE system is primarily comprised of the sensing-head and the beam-rider units. For evaluating the concrete beams of I-shaped or rectangular sections, the sensing head is mounted onto the beam-rider unit, which along with a remote host computer form a complete magnetic-based NDE system.

The Sensing-Head Unit

Three stainless steel and aluminum enclosures are used to house two permanent magnets and a series of Hall-effect sensors with their associated signal-conditioning circuits. These enclosures are mounted on an aluminum structural frame that is independent of other system components. In addition, the frame is configured to allow for installation of an electrical encoder to identify the longitudinal position of the frame when it is used during an independent operation (when the sensing head is not installed in the beam-rider unit). A photograph of the sensing-head unit is presented in figure 3 where the enclosures for the magnets and the sensors are shown mounted on an aluminum structural frame. At the left-hand side, two contact wheels are used to provide constant distance between the top of the enclosures and the bottom of the concrete beam under test. Also shown, is an eye-bar at the left end of the frame that is used for

installing the frame onto the beam-rider unit. The detail at the right end is similar to what is shown for the left end of the sensing-head frame.

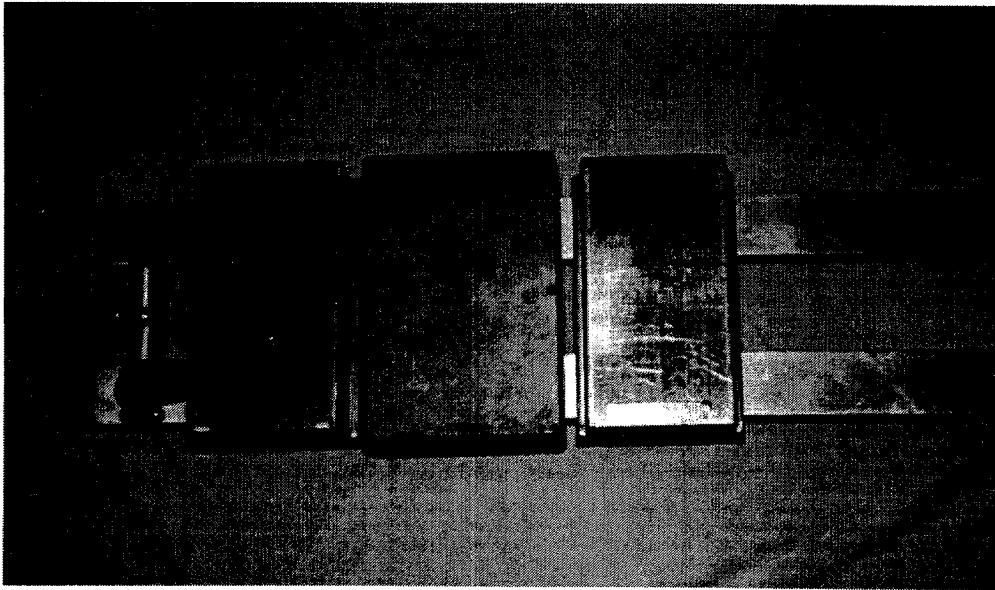


Figure 3. Overall view of the sensing head.

The permanent magnets selected for the MFL system are two large Neodymium Iron Boron magnets that have a strength of approximately 2,200 gauss at the center of each piece. Each one of the two magnets is actually a packed assembly of eight individual magnets of approximately 50 mm x 50 mm x 38 mm (2 in x 2 in x 1.5 in) that is housed in a sealed stainless steel enclosure. The overall dimension of each magnet with the enclosure is approximately 210 mm x 108 mm x 46 mm (8.25 in x 4.25 in x 1.8 in). The weight of each magnet is approximately 6.2 kg (13.6 lb). Each magnet was mapped for its flux intensity at the time of delivery (February 1997) and again 2 years later. No significant degradation of the magnet flux intensity was noticed over this period. Technical data regarding the properties and dimensions of the magnets is presented in Appendix A of this report.

Detection of the MFL is made possible through the use of Hall-effect sensors. An array of 10 Hall sensors, in 2 stacks of 7 and 3 sensors each, is housed in a sealed aluminum enclosure and is installed on the same structural frame that supports the permanent magnets. The sensors are positioned precisely at the mid-point between the two magnets where the effect of the flux lines on the sensors is at a minimum. Adjustment of the position of the sensor enclosure should not be attempted in the field since it has a significant effect on the output of the sensors.

Because of the high strength associated with the magnets used in the MFL system, they have been secured on a relatively rigid structural frame to minimize deformation of the frame due to the magnet forces. Great care should be taken in handling these magnets during transport and operation of the system due to large forces that are imposed by them.

The sensing-head unit may be used independently in a manual mode of operation where it is moved along the length of the member under test. The frame is configured to allow installation of a longitudinal encoder that is required for the manual mode of operation. Normally, the sensing-head unit is installed

onto the beam-rider unit. The installation is made through a specially designed support mechanism that, with its spring loading, allows vertical motion adjustment of the sensing head. The applied constant spring force ensures that the sensing-head unit is kept at a constant distance from the beam under test. Maintaining this constant distance is important since a varying distance between the magnet/sensor assembly and a ferromagnetic material (such as steel in the concrete) can result in signals with varying amplitudes and durations, which can make data interpretation difficult.

The modular concept used for the new NDE system allows the sensing-head unit to be installed on other structural frames to facilitate testing of various bridge members with different geometric configurations. Two examples are for the evaluation of round concrete piers and flat slabs or pavements. For the NDE of round concrete piers, the sensing-head unit may be mounted onto a vertical frame that is attached to the pier so it is possible to scan the pier along its height. Upon completion of one scan, the frame will be moved to a new location along the circumference of the pier to allow for a new scan to be performed. To have complete coverage for the evaluation of the pier, the sensing head and its carrier frame are moved only to the extent that there will be a slight overlap of the previous scan. This will be repeated until complete coverage around the perimeter of the pier is achieved. For the evaluation of flat slabs or pavements, the sensing-head unit may be installed onto a simple cart on wheels that can be pushed forward by the operator. Again, several scans, with a slight overlap for each, must be performed in order to achieve coverage of an area that needs to be evaluated.

The Beam-Rider Unit

The beam-rider unit includes an aluminum structural support frame, a series of wheels that exert lateral pressure against the sides of the concrete beam under test, a series of electrical switches and control devices, a series of contact wheels acting against the bottom surface of the beam under test, a spring-loaded encoder device to identify longitudinal position, a data-acquisition unit, a wireless communications device, a suspension mechanism to support the sensing-head unit, and a dc power source. The various components of the beam-rider unit are shown in figure 4.

The beam-rider unit is designed to allow relatively easy and quick installation on and removal from concrete beams. The total weight of the beam-rider unit, including the power supply and data acquisition units, is 68 kg (150 lb). The installation and removal of the beam-rider unit can be accomplished by a two-person crew and without the need for any lift or special equipment. The installation may be made easier if the dc power supply and data-acquisition units are installed after the beam-rider unit is secured on the concrete beam. The beam-rider unit is maintained on a concrete test beam through a frictional force that is developed between the unit's spring-loaded wheels and the side surfaces of the concrete beam. One of the two inside wheels is linked with a dc motor that provides power to drive the beam-rider unit along a test beam. The beam-rider unit's travel speed on a concrete test beam is 50 mm/s (2 in/s). The second inside wheel acts as a stabilizer wheel. A set of two outside wheels on each side of the beam-rider unit operates in a tilted position during the motion of the unit. A tilt angle of approximately 4 degrees was calculated and implemented for the wheels to pull the beam-rider unit up against the bottom surface of the concrete beam. A tilt angle smaller than an optimum value could result in an inadequate frictional force to maintain the unit on the beam, and a greater tilt angle could cause an operational inefficiency. Using dc electric motors and a specially designed mechanism, the tilting wheels are automatically repositioned with a tilt angle equal to the mirror image value upon a change in the direction of travel of the unit.

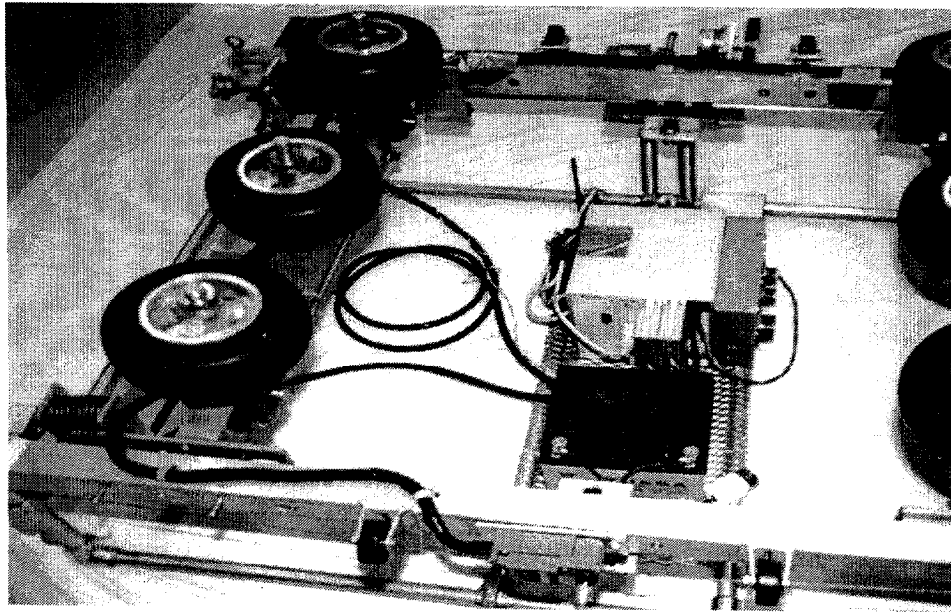


Figure 4. Components of the beam-rider unit.

An encoder device is installed on the beam-rider unit's support frame that identifies the longitudinal position of the unit along a concrete beam during a testing operation. The rolling of a wheel of the encoder device that is spring-loaded against the concrete surface produces an electrical pulse every 2.5 mm (0.1 in) of travel of the beam-rider unit along the concrete beam. These electrical pulses indicate the position of the beam-rider unit along the concrete beam. The encoder output is communicated to the host computer and is integrated with the MFL data from each sensor to relate them to the longitudinal position along the length of the concrete beam under test. In addition, the encoder's output is used here as an external trigger source for the system's MFL data acquisition. In other words, if the encoder wheel is not in contact with the surface of a concrete beam under test, then there will be no data collection by the MFL system.

There is no limit on the length of a concrete beam that can be tested by the new MFL system. The only effect from the length of a beam is on the size of the data files that are associated with that beam. Concrete beams with various widths may be tested by the newly developed MFL system. The structural frame of the beam-rider unit is designed to allow installation on concrete beams with wide variations in width. This may be achieved by selecting specific existing connectors, with the appropriate spacing, on the cross-frame members for the attachment of the longitudinal frame members. The longitudinal frame members are those that support the drive and tilting wheels. The current system allows installation of the beam-rider unit on concrete beams with widths from 356 mm (14 in) to 610 mm (24 in). The cross-frame members of the beam-rider unit can be easily replaced with longer pieces to allow installation on wider beams.

Only 203 mm (8 in) of the width of a concrete beam may be scanned as the beam-rider unit travels along the length of the beam. This is due to the limiting width of the permanent magnets and the sensing array that are integrated with the sensing-head unit. For beams with widths wider than 203 mm (8 in), multiple scans need to be made to cover the entire width of the beam. The choice of the current magnet width was made to optimize the weight of the system for efficient field usage. A control mechanism is incorporated

into the beam-rider unit that allows positioning of the sensing-head unit at any desired location across the width of a concrete beam via remote computer control. The MFL data analysis software uses the sensing-head position information data from the output of a potentiometer to appropriately display the MFL data from different test scans.

THE ELECTRICAL SYSTEM

The electrical system for the MFL device is centered on the data-acquisition and control (DAC) unit. A 12-V deep-cycle marine battery with a 38-Amp-h rating provides power for the system. This would allow for approximately 4 h of operation of the MFL system during field testing under normal conditions. Both an internal fuse and an internal polarity protection device are provided to protect the power connection. Special connectors are used between the battery and the DAC unit that allow connection with only proper polarity. The DAC unit itself serves two major functions. It gathers data from the Hall-effect sensor array in the sensing head and it monitors and controls the various devices that comprise the remainder of the beam-rider system. Three cables (Cables #1 through #3) are used to connect the control devices, switches, and the sensing head to the DAC unit. The data gathered by the system, and the various monitoring and control functions of the system, are communicated to the host computer via a 900-MHz broad-spectrum digital radio modem. One transceiver is located with the DAC unit and is connected to the serial port adapter on the National Instruments SCXI chassis. The other is connected to the serial port of the host computer. This radio modem connection is “transparent” to the host computer and DAC unit. It operates the same way that a cable would, except for a few details that will be discussed below.

The DAC Unit

The primary task of the DAC unit is to condition and gather the data from the sensing head and broadcast it down to the host computer. One of the cards in the National Instruments SCXI Chassis (the SCXI-2400 card) is a communications adapter that allows a serial interface to be used. The normal configuration utilizes a parallel interface that is found on the SCXI-1200 card (the label of this card is normally obscured by its SCXI-1302 front-mounted terminal block). The SCXI-1200 card is the multi-function data-acquisition card that communicates with the host computer and acts as the controller for the SCXI-1100 multiplexer/amplifier card (the label of this card is normally obscured by its SCXI-1300 front-mounted terminal block). The SCXI-1100 is the card that gathers the Hall-effect sensor data and, because of a unique need of the longitudinal motor control circuit, also gathers the status of the two “end-of-travel” switches that regulate longitudinal travel. In addition to controlling the SCXI-1100 card, the SCXI-1200 monitors the two transverse axis switches, the longitudinal encoder, and the transverse potentiometer. These input devices control the movement of the sensing head across the width of the beam (for the transverse potentiometer) and indicate position along the length of the beam (for the longitudinal encoder). The SCXI-1200 card also handles the control of the two motor circuits (both transverse and longitudinal axes) by manipulating a set of four motor control relays. This set of relays will be described below.

The Sensing-Head

The electrical system of the sensing-head is connected to the DAC unit through Cable #3 and is connected to the DAC control box (Box #1) via a large green 14-pin military-specification connector. The two large central pins of that cable provide the ± 12 -V power levels for the operation of the amplifier circuits on the sensor array. The remaining pins carry the ground bus and the individual amplified voltage values from the Hall-effect sensors. The ± 12 -V power comes from a power supply chip mounted to the circuit board

inside of the control box. This chip converts the +12-V supply from the battery to the ± 12 -V needed by the amplifier circuits.

On the sensing head, in the center enclosure, there are two printed circuit boards populated by various operational amplifier chips (op-amps), resistors, capacitors, and the Hall-effect sensors. The top board contains the main sensor array, which is comprised of seven Hall-effect sensors located approximately 25 mm (1 in) apart and positioned in the center of the dead-zone of the magnetic field generated by the two large permanent magnets. The bottom board is located directly beneath the top board and contains three additional sensors that make up the secondary array that is used to help determine the depth and location of any detected flaws. Each sensor circuit is comprised of an individually matched constant-current source and an amplifier that conditions the output from the Hall-effect sensor prior to "sending it down the cable" to the DAC unit. The overall offset of the board and the individual sensor circuit amplifications can be calibrated through the adjustment of the potentiometers that make up the various amplifier circuits. (Note: This procedure should not be attempted by field operators.)

The Hall-effect sensors were manufactured by the W.F. Bell Co. for this study under a special arrangement. Technical data, including sensor component details and signal conditioning circuit diagram for one Hall-effect sensor along with the circuit boards' layout schematics, is presented in Appendix B of this report. Figure 5 shows a photograph of the circuit boards for the Hall-effect sensors as they are installed on the structural frame that is also supporting the permanent magnets for the MFL system. The protective cover of the Hall-effect sensors is removed in the figure to show the boards and associated components.

The Motor Control Circuit for the Beam-Rider Unit

In addition to handling the Hall-effect sensor data, the DAC unit serves as the controller for the remote operation of the motors. On a box located on the side of the beam-rider unit, there is a three-position switch that can be set to manual mode, automatic mode, or a neutral position. When in manual mode, the operation of the longitudinal motors is controlled by a momentary rocker switch that allows the operator to control the direction of travel by pressing and holding the rocker switch in a certain direction. This feature is used primarily for initially mounting and positioning the beam-rider unit on a concrete beam. The automatic mode disables the manual switch and puts the host computer in charge of the longitudinal motor. The transverse motor is always under host computer control only. The neutral position, as might be expected, leaves the motors inoperable.

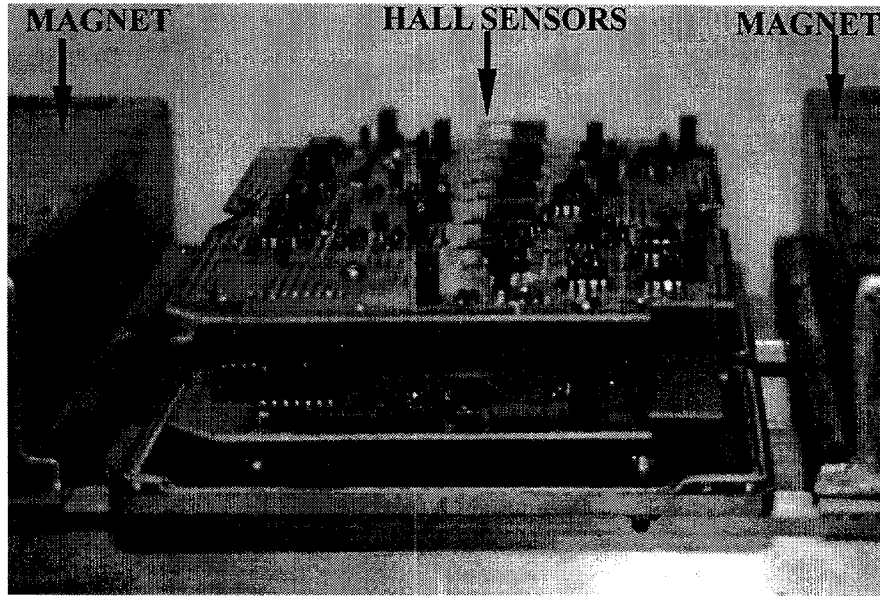


Figure 5. Printed circuit boards for the Hall sensors.

Because of the unique nature of the wheel and motor combination, the motor control circuit for the system is quite complex. The circuit has redundant safety features that make it shutoff the motors whenever the end-of-travel switches are activated, even if communications with the host computer have been lost. Also, the “tilt wheels” on the sides of the beam-rider unit are driven into position automatically whenever a change in direction is made. This is a hard-wired change that is dependent only on the polarity of the voltage sent to the main drive motor. A cam-driven bar that is powered by a small unidirectional motor tilts the wheels. The two sides of the beam-rider unit are independently driven so that each side tilts completely into position. All of the circuitry that controls this “tilt” feature is located inside the box that has the mode switch and directional rocker switch mounted on its face. The safety feature is accomplished by using a limit switch with two separate circuits activated by the same switch and a pair of latching relays. The “normally open” (NO) circuit is used to trigger the latching relay circuit. The latching relay circuit (which is located in Box #2 on the rear of the DAC unit) is designed so that only one direction can be “enabled” at a time. The status of these relays is monitored by the DAC unit and signals the host computer when to turn off the motors. The “normally closed” (NC) circuit is used to directly break the power to the motors. Each switch only breaks the power for the direction that is appropriate for it. The other direction is still possible (so that the beam-rider unit can go back to the other end of the beam when the operator is ready). A similar circuit exists for the transverse axis, but no latching relays are used. Instead, the status of the switches is monitored directly by the DAC unit. The motor and switch wiring is connected to the control box on the DAC unit through Cable #2 and Cable #3, both of which use a smaller 14-pin military-specification connector.

The Radio Modem Transceivers

As stated earlier, these transceivers are virtually transparent to the system. They operate over greater distances than are ever likely to be needed in this application. Two items have to be verified to ensure proper operation. The first is that both units are getting adequate power (the red light-emitting diode (LED) on the face of each transceiver indicates whether this is occurring). The second is that they can detect each other (the green LED labeled “connect” indicates whether this is occurring). No field maintenance is required for these units.

Electrical Circuit Diagrams and Schematics

Appendix C of the report includes a series of tables, schematics, and circuit diagrams that completely document the electrical and control systems for the MFL system developed under this study. Table C-1 describes connection details for the 10 Hall-effect sensors (channels 0 through 9 in the National Instrument (NI) environment) along with the connection information for the power requirement. The table also shows the wire color coding at the SCXI-1300 terminal block, wire color coding for Hall sensor interface Cable #1 (connecting the sensor enclosure box to the DAC unit), and pin identification at the end connector of Cable #1. Tables C-2 and C-3 of the appendix show pin identification, wire color coding, and various functions of the wiring for digital/analog Cable #2 and motor control Cable #3, respectively.

Figure C-1 of Appendix C shows a block diagram describing the design concept for developing the data acquisition and conditioning components of the MFL system. Figure C-2 of the appendix shows an overall electrical/control circuit diagram schematic for the MFL system. In the figure, individual circuit diagrams for the longitudinal motion of the beam-rider unit, transverse motion of the sensing-head unit, tilting wheel mechanism, and the influence of various switches is shown. Interfaces of the three cables, Cables #1 through #3, are also shown in the diagram. The figure will help to recognize the interfacing of the various circuits to work as an integral system.

Identification of Primary Components/Parts

The primary components/parts used to fabricate the MFL system are shown in Appendix D of this report. Table D-1 of the appendix shows description, manufacturer information, vendor information, and associated part/model.

CHAPTER 4. SOFTWARE

INTRODUCTION

The software for the magnetic flux leakage (MFL) system is developed using a commercially available platform called LabVIEW (Laboratory Virtual Engineering Workbench). The Lab VIEW platform, by the National Instruments Co., is a graphical programming language that relies on icons and graphical symbols to describe software actions. In general, a front panel is created in any application software that serves as the graphical user interface to the LabVIEW software.

In this study, various graphical user interfaces have been created that would allow easy operation of the mechanical components, electrical components, data acquisition, and data post-processing or interpretation for the MFL system. The software is comprised of two major parts that will be discussed below. It includes the data-acquisition and data analysis parts.

DATA ACQUISITION

The data-acquisition user interface software for the MFL system includes the system control software as well as the data acquisition. The system control capabilities of the software include initiating and stopping the longitudinal motion of the beam-rider unit when it is installed on a concrete beam, initiating and stopping the transverse motion of the sensing-head unit, and monitoring the status of the longitudinal and transverse motions through responses of several limit switches. The data-acquisition capabilities of the software include initiation and stoppage of data acquisition, displaying and recording MFL data during tests, creating recorded data files with given file paths and names, and establishing data display and recording parameters such as data amplitude scales and gain or amplification.

System Control Software

The system control software allows user interaction through a motor control sub-window and a limit or stopper switches sub-window. In the motor control sub-window, software switches are presented to enable the user to indicate the direction of motion and the on/off status for both the longitudinal and transverse motors. The longitudinal motor provides power to drive the beam-rider unit along the length of a concrete test beam and the transverse motor provides motion for the sensing-head unit across the width of the beam. The limit or stopper switch indicators within the software simulate real LEDs to give verification of the direction of the longitudinal motion of the beam-rider unit and of the transverse motion of the sensing-head unit. Figure 6 shows the system control part of the user's interface software with various controllers and indicators that are further defined in table 1.

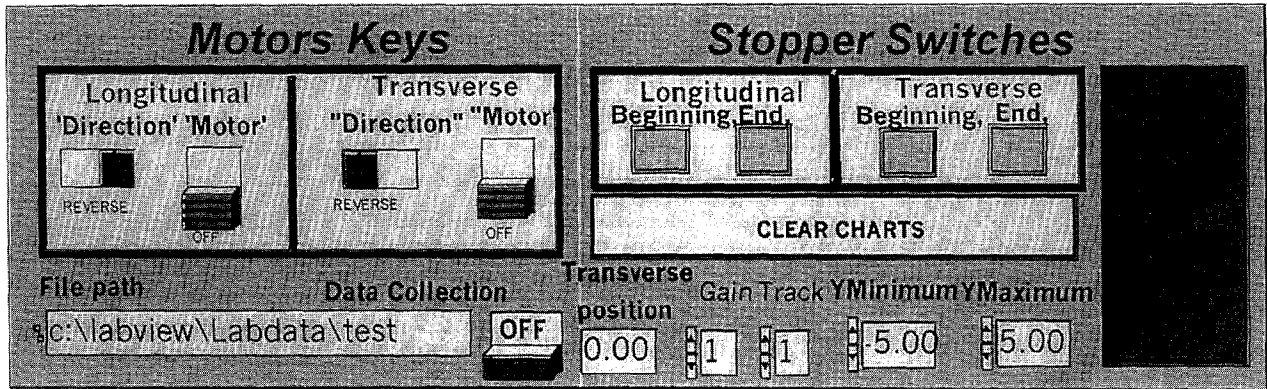


Figure 6. System control part of the user's interface software for the MFL system.

Data-Acquisition Software

The data-acquisition software includes a series of subroutines to facilitate acquiring, organizing, recording, and displaying the MFL data. The user interface software for this part includes a window that allows either any 7 or 10 Hall-effect sensor outputs to be displayed (see figure 7). The horizontal axis of the data display for each channel indicates the distance, in feet, from the point where the test started and the vertical axis indicates the amplitude of the MFL data. Although the entire length of the data for a test beam is recorded, the computer screen display has been restricted to only 3.0 m (10 ft) of data at any time for clarity.

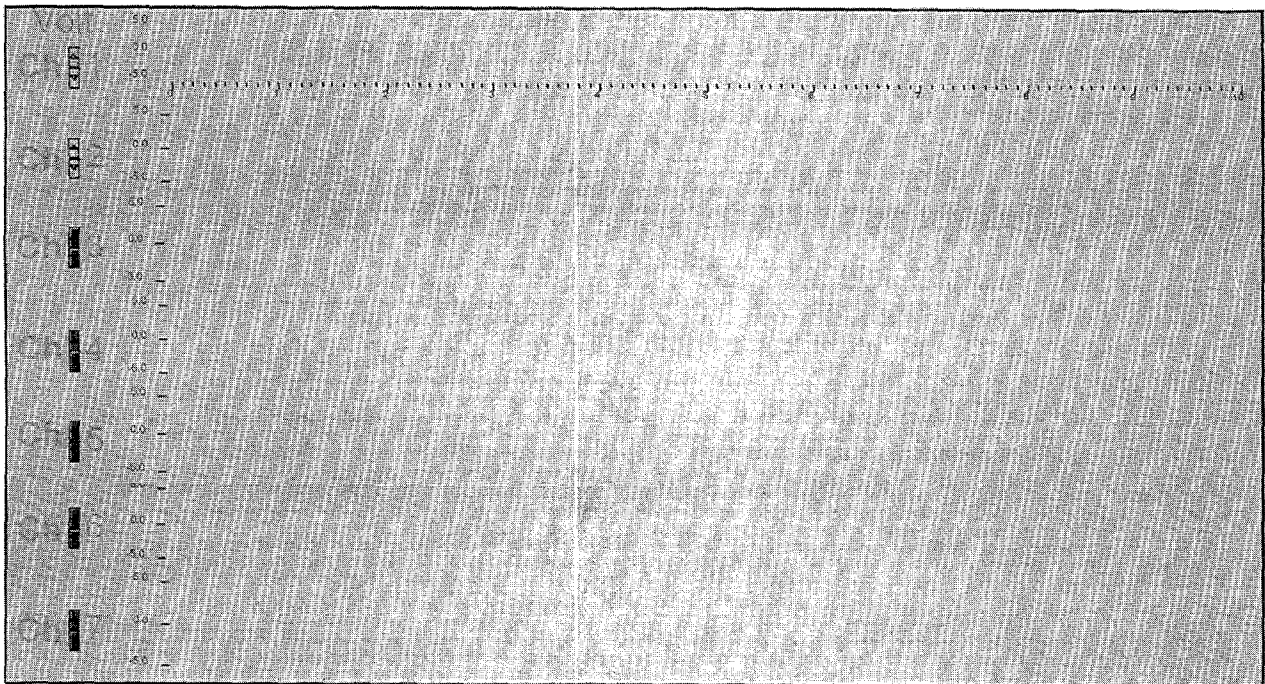


Figure 7. Data-acquisition software for the MFL system.

Table 1. Functional description for the controllers and indicators in the system control software.

Indicator	Function
Longitudinal Direction	Control for the direction of the beam-rider unit's motion
Longitudinal Motor ON/OFF Switch	Control for the motion or stoppage of the beam-rider unit
Transverse Direction	Control for the direction of the sensing-head unit's motion
Transverse Motor ON/OFF Switch	Control for the motion or stoppage of the sensing-head unit
Longitudinal Stopper Switches	Indicator for the position of the beam-rider unit at one end of the beam
Transverse Stopper Switches	Indicator for the position of the sensing-head unit at one side of the test beam
File Path	Indicator for the data file name, including the file path
Data Collection Switch	Control for initiating or stopping data collection
Transverse Position	Indicator for the lateral position of the sensing-head unit
CLEAR CHARTS	Control for clearing displayed data
Gain	User input to amplify the MFL data prior to displaying and recording
Track	User- and software-generated input to identify a specific test path
Y min (min. -5 V)	User input for the lower bound display of the amplitude of the MFL data
Y max (max. +5 V)	User input for the upper bound display of the amplitude of the MFL data
Stop	Control for stopping the data-acquisition software

DATA ANALYSIS (post-processing)

Data analysis and interpretation associated with the MFL system may be accomplished by using different techniques. These include visual examination of the recorded data, the differencing technique, the correlation technique, the two-dimensional profile technique, and the three-dimensional magnetic field disturbance technique. These methods are described briefly in Chapter 6 of this report. One or more of these techniques may need to be used on a set of MFL data to achieve a reliable interpretation of the results of a test under real conditions.

The data analysis software includes a number of subroutines to allow data processing based on the use of the various techniques described above. There are nine analysis options, or subroutine files, available in the data analysis software that may be used, depending on the method of analysis chosen by the operator. The analysis subroutines, as well as the required subroutines for data acquisition, are presented in Appendix E of this report. Each chosen analysis option would create an interface window on the computer screen to allow user's input for required parameters for the data analysis. Generally, the user needs to specify certain information required for data analysis. This includes the name of the recorded data file, desired sensor output, data length, correlation analysis parameters, and data display information. From the displayed user interface window, the operator may execute the analysis software that will result in displayed graphs of the results of the analysis.

The analysis options are chosen from a "Post-Processing Options" user interface window that can be accessed by executing the file "MainMenu.vi" with the file path of Labview\MFD\BeamRider. Figure 8 shows the "Post-Processing Options" window. Each option may be highlighted and executed by double-clicking the mouse button on the highlighted option.

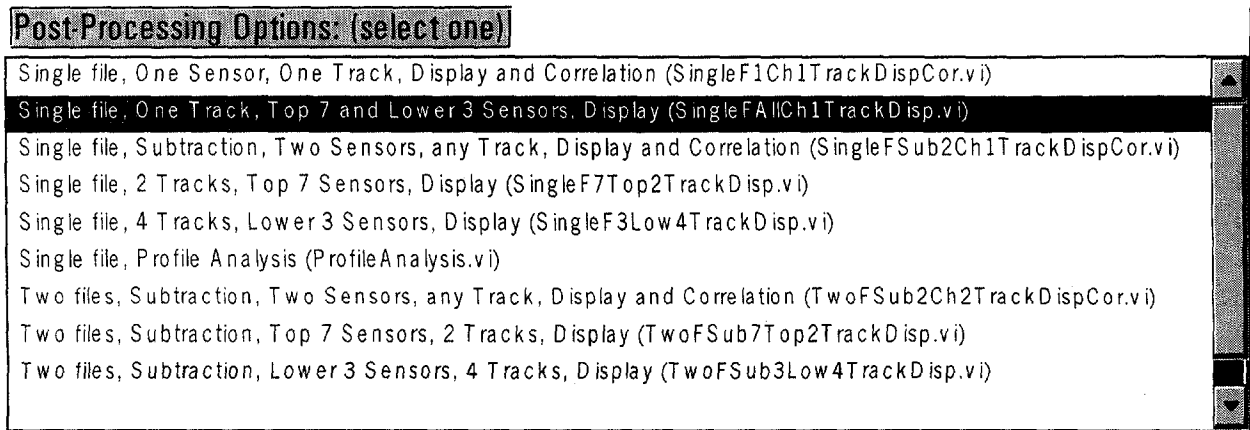


Figure 8. MFL data post-processing options window.

The following is a description of the data analysis options available for the MFL system:

1. Option One:

This data analysis option would allow the user to display recorded data for a desired sensor and a test track along with the results of the correlation analysis. The user input includes the recorded data file name, the track number within the data file, the sensor number, the required correlation analysis parameters, the correlation threshold value for displaying the correlation analysis results above the chosen threshold value, the starting position of the data for the analysis, lower and upper bound amplitude display values, and setting the three-dimensional graph plot switch to either the "Yes" or "No" position. The correlation analysis parameters are shown in figure 38 and include the length, in terms of the total number of points "N" of the basic correlation curve, as well as the peak-to-peak separation distance "B" of the same curve. These parameters are identified as "Number of Points for Correlation (odd number)," and "Peak to Peak Distance," respectively, in the user interface window on the computer screen for this analysis option, as shown in figure 9. After all the required user input parameters are entered within the displayed window, the analysis software may be executed by clicking the mouse button on the right arrow symbol from the tool bar window on the top of the computer screen. Upon execution of the software,

graphs of the sensor output and the results of the correlation analysis are displayed within the analysis option window. The sensor output display shows the MFL data with position along the scan length in feet, against the signal amplitude in volts. On the correlation graph, displayed directly under the sensor output graph, each correlated peak above the specified threshold level is marked with a small square symbol. The numerical values of the correlation peak's "Correlation Factor" and corresponding locations along the scan length "Longitudinal Position (ft)" are also listed at the lower end of the analysis option screen. Figure 9 shows the user interface and data display window for this analysis option.

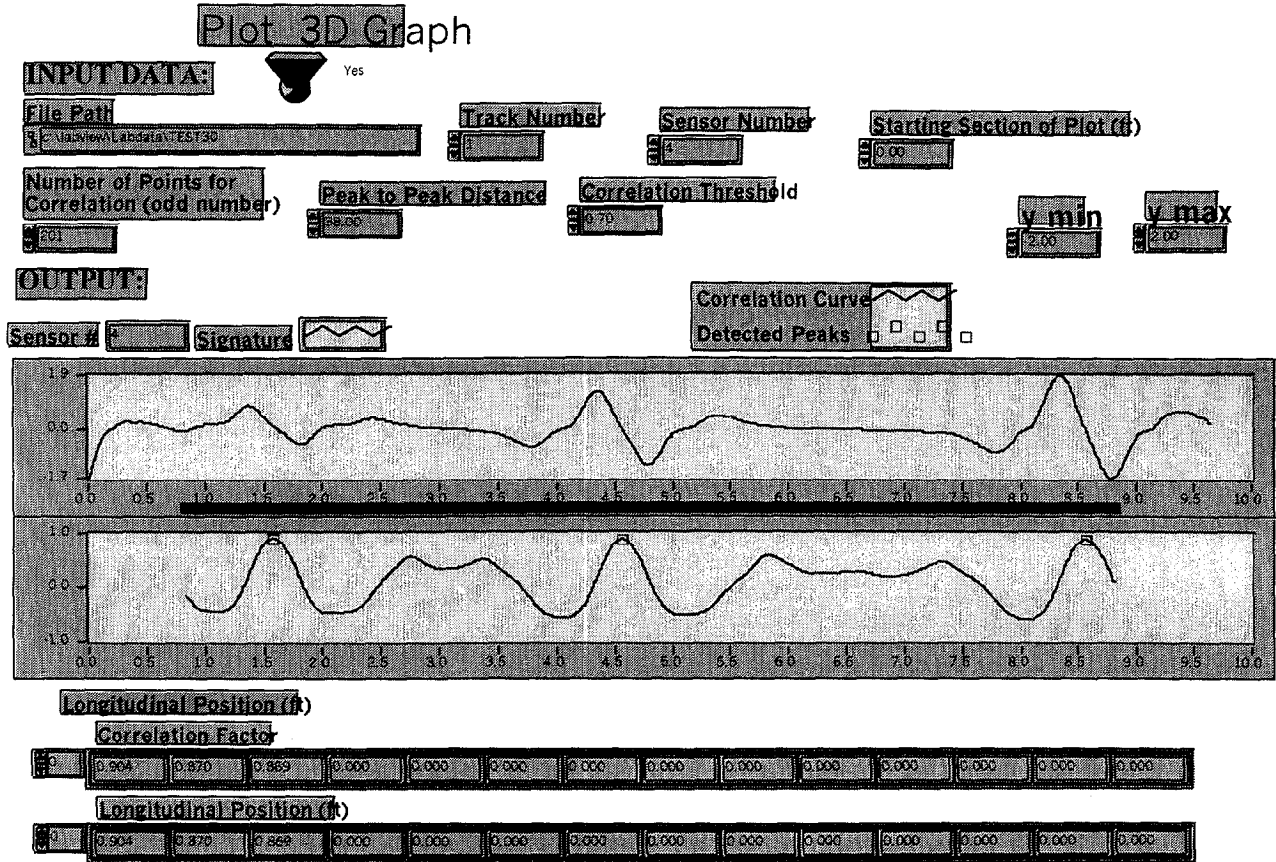


Figure 9. User interface window for MFL data analysis Option One.

2. Option Two:

This data analysis option would allow the user to display recorded data for all 10 Hall-effect sensors. The user input includes the recorded data file name, the track number within the data file, the starting position of the data for the analysis, lower and upper bound amplitude display values, and setting the three-dimensional graph plot switch to either the "Yes" or "No" position. After all the required user input parameters are entered within the displayed window, the analysis software may be executed by clicking the mouse button on the right arrow symbol from the tool bar window on the top of the computer screen. Upon execution of the software, graphs of the sensor outputs are displayed within the analysis option window. The sensor output display shows the MFL data for all sensors, with position along the scan length in feet, against the signal amplitude in volts. Figure 10 shows the user interface window for this analysis option.

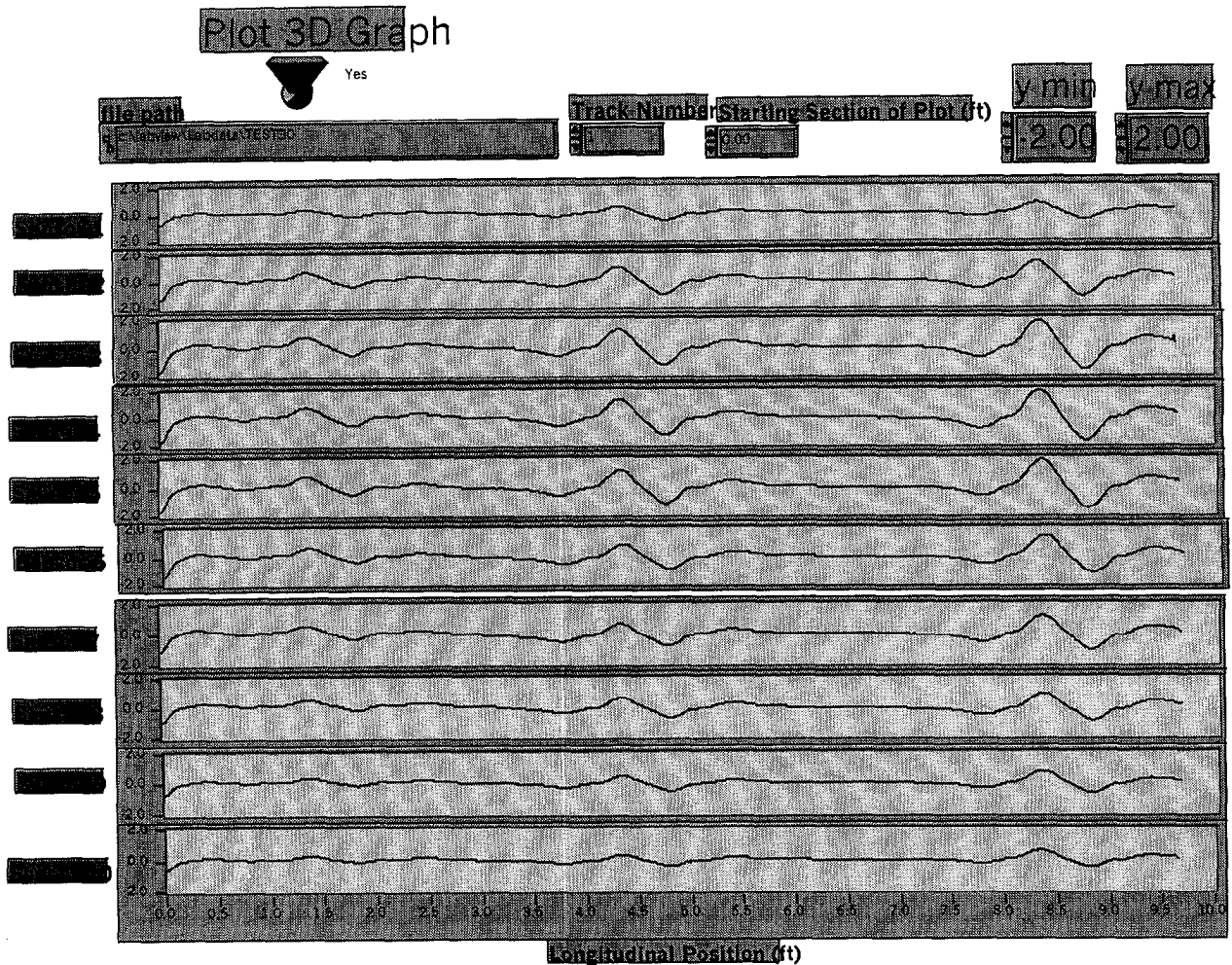


Figure 10. User interface window for MFL data analysis Option Two.

3. Option Three:

This data analysis option would allow the user to display recorded data for two desired sensors from a track within a single file. In addition, the result of subtraction of the two sensor outputs will be calculated and displayed along with the results of the correlation analysis of the subtracted data. The user input includes the recorded data file name, the track number within the data file, the desired sensor numbers, the required correlation analysis parameters (the same as those shown in "Option One"), the correlation threshold value for displaying analysis results above the chosen threshold value, the starting position of the data for the analysis, lower and upper bound amplitude display values, and setting the three-dimensional graph plot switch to either the "Yes" or "No" position. After all the required user input parameters are entered within the displayed window, the analysis software may be executed by clicking the mouse button on the right arrow symbol from the tool bar window on the top of the computer screen. Upon execution of the software, graphs of the two sensor outputs, a graph of the subtracted data, and the results of the correlation analysis are displayed in the order indicated within the analysis option window. On the graph displayed for the correlation results, each correlated peak above the specified threshold level is marked with a small square symbol. The numerical values of the correlation peak's "Correlation Factor" and corresponding locations along the scan length "Longitudinal Position (ft)" are also listed at

the lower end of the analysis option screen. Figure 11 shows the user interface window for this analysis option.

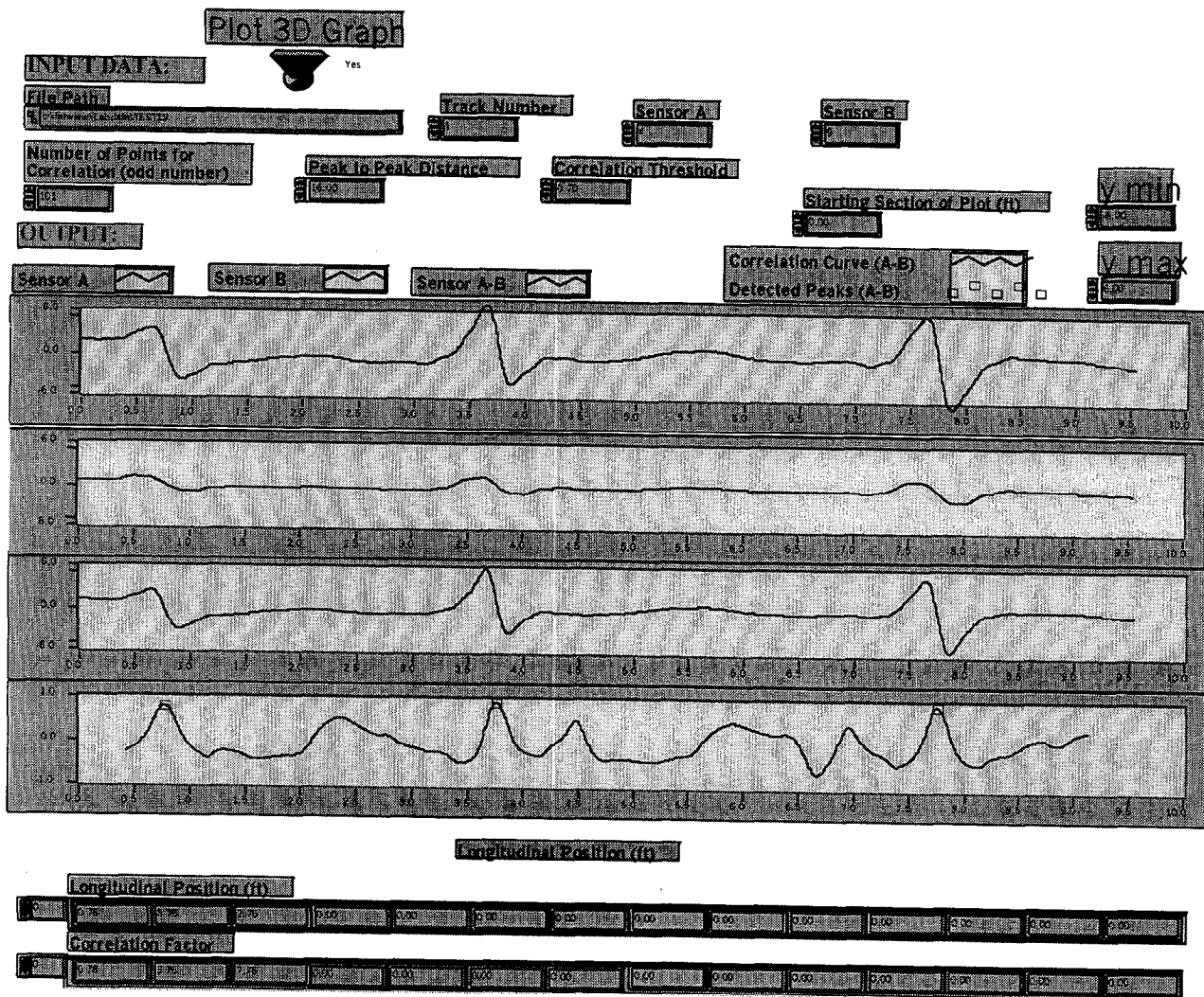


Figure 11. User interface window for MFL data analysis Option Three.

4. Option Four:

This data analysis option would allow the user to display recorded data from two separate tracks within a single file and for the seven sensors located on the top Hall-effect sensor board within the sensor enclosure. The software will align the data from the two tracks and display them without requiring any user instruction. The user input includes the recorded data file name, the two track numbers within the data file, the starting position of the data for the analysis, lower and upper bound amplitude display values, and setting the three-dimensional graph plot switch to either the “Yes” or “No” position. After all the required user input parameters are entered within the displayed window, the analysis software may be executed by clicking the mouse button on the right arrow symbol from the tool bar window on the top of the computer screen. Upon execution of the software, graphs of the sensor outputs are displayed within the analysis option window. Figure 12 shows the user interface window for this analysis option.

5. Option Five:

This data analysis option would allow the user to display recorded data from four separate tracks within a single file and for the three sensors located on the lower Hall-effect sensor board within the sensor enclosure. The software will align the data from the four tracks and display them without requiring any user instruction. The user input includes the recorded data file name, the four track numbers within the data file, the starting position of the data for the analysis, lower and upper bound amplitude display values, and setting the three-dimensional graph plot switch to either the “Yes” or “No” position. After all the required user input parameters are entered within the displayed window, the analysis software may be executed by clicking the mouse button on the right arrow symbol from the tool bar window on the top of the computer screen. Upon execution of the software, graphs of the sensor outputs are displayed within the analysis option window. Figure 13 shows the user interface window for this analysis option.

6. Option Six:

This data analysis option would allow a profile analysis to be performed on one or more tracks of the MFL data within a single file. Performing a profile analysis will result in a line graph that represents data amplitude values along a line in a transverse direction, or the width, of a test beam. The profile analysis results will be calculated for all positions along the length of a test beam and will be displayed for amplitude values above a range defined by the user. The software will align the data laterally from the different tracks prior to performing the profile analysis. The user input includes the recorded data file name, amplitude range (to specify the desired range of data amplitudes in the transverse direction that should be considered for the analysis and display), and the lower and upper bound amplitude display values. After all the required user input parameters are entered within the displayed window, the analysis software may be executed by clicking the mouse button on the right arrow symbol from the tool bar window on the top of the computer screen. Upon execution of the software, graphs of amplitude values in the transverse direction will be constructed for all positions along the scan, or the beam, length. These graphs may be displayed by the operator by entering the track number and the lateral position of interest with respect to the position of the first track. Figure 14 shows the user interface window for this analysis option.

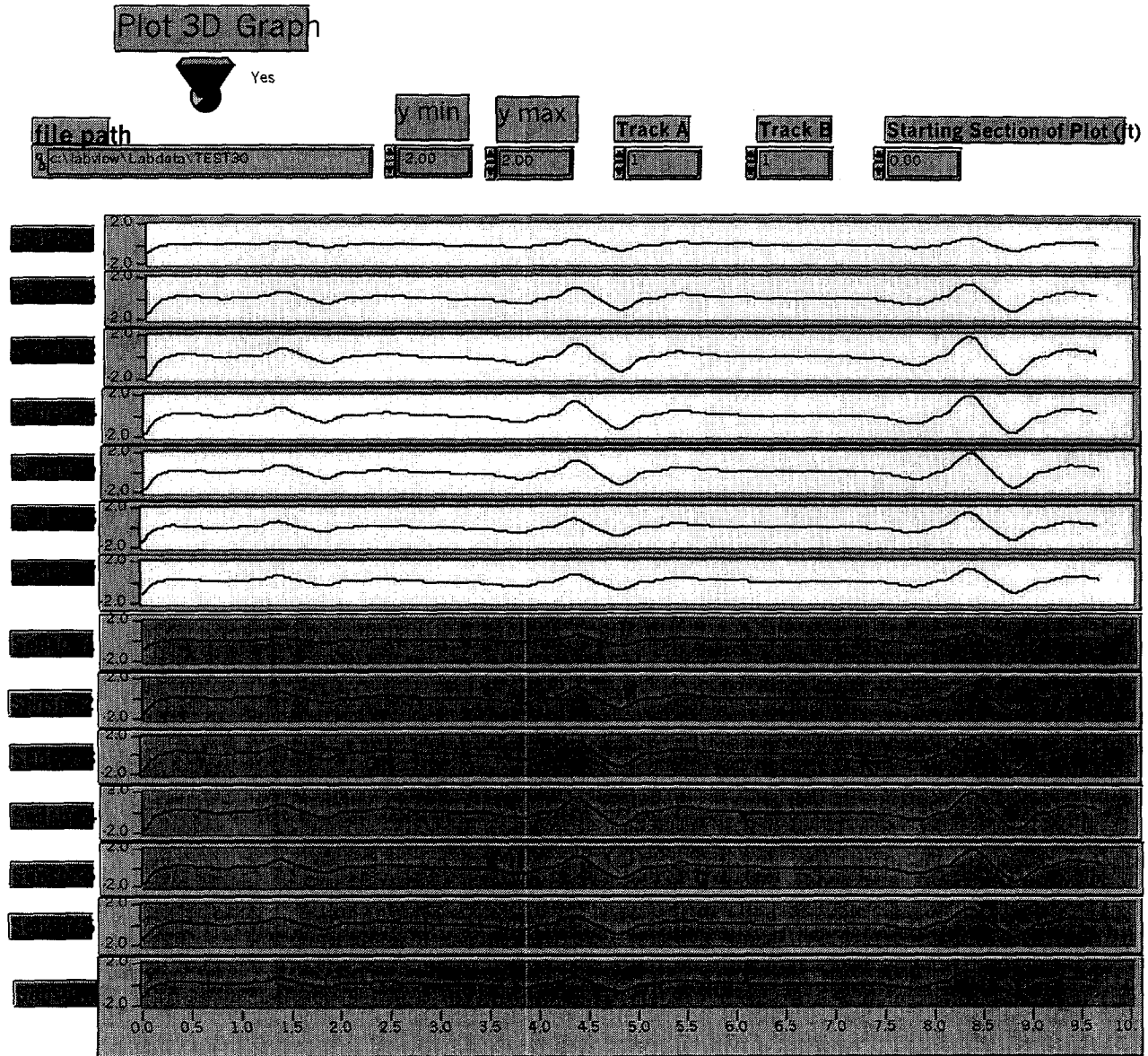


Figure 12. User interface window for MFL data analysis Option Four.

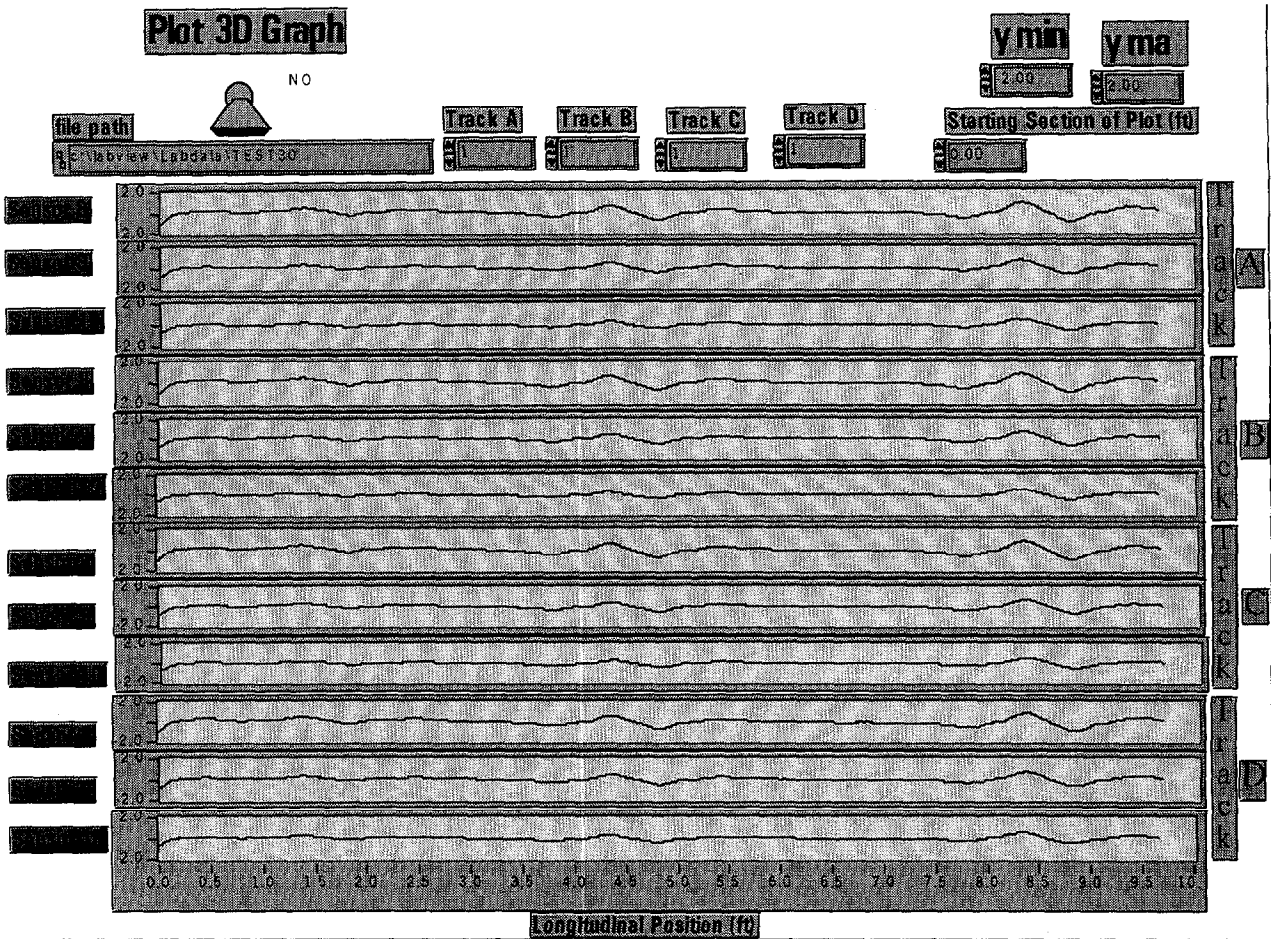


Figure 13. User interface window for MFL data analysis Option Five.

7. Option Seven:

This data analysis option would allow the user to display recorded data for two desired sensors from any two tracks within two different data files. In addition, the result of subtraction, or the difference, of the two sensor outputs will be calculated and displayed along with the results of the correlation analysis of the subtracted data. This analysis option is most effective for periodic inspections of the same test beam to determine if any deterioration, or change, has taken place since the time of an earlier test. The user input includes the names of the recorded data files, the track numbers within the data files, the desired sensor numbers, the required correlation analysis parameters (the same as those in analysis "Option One"), the correlation threshold value for displaying analysis results above the chosen threshold value, the starting position of the data for the analysis, lower and upper bound amplitude display values, and setting the three-dimensional graph plot switch to either the "Yes" or "No" position. After all the required user input parameters are entered within the displayed window, the analysis software may be executed by clicking the mouse button on the right arrow symbol from the tool bar window on the top of the computer screen. Upon executing the software, graphs of the two sensor outputs, a graph of the subtracted data, and the results of the correlation analysis are displayed in the order indicated, within the analysis option screen. On the graph displayed for the correlation results, each correlated peak above the specified

threshold level is marked with a small square symbol. The numerical values of the correlation peak's "Correlation Factor" and corresponding locations along the scan length "Longitudinal Position (ft)" are also listed at the lower end of the analysis option screen. Figure 15 shows the user interface window for this analysis option.

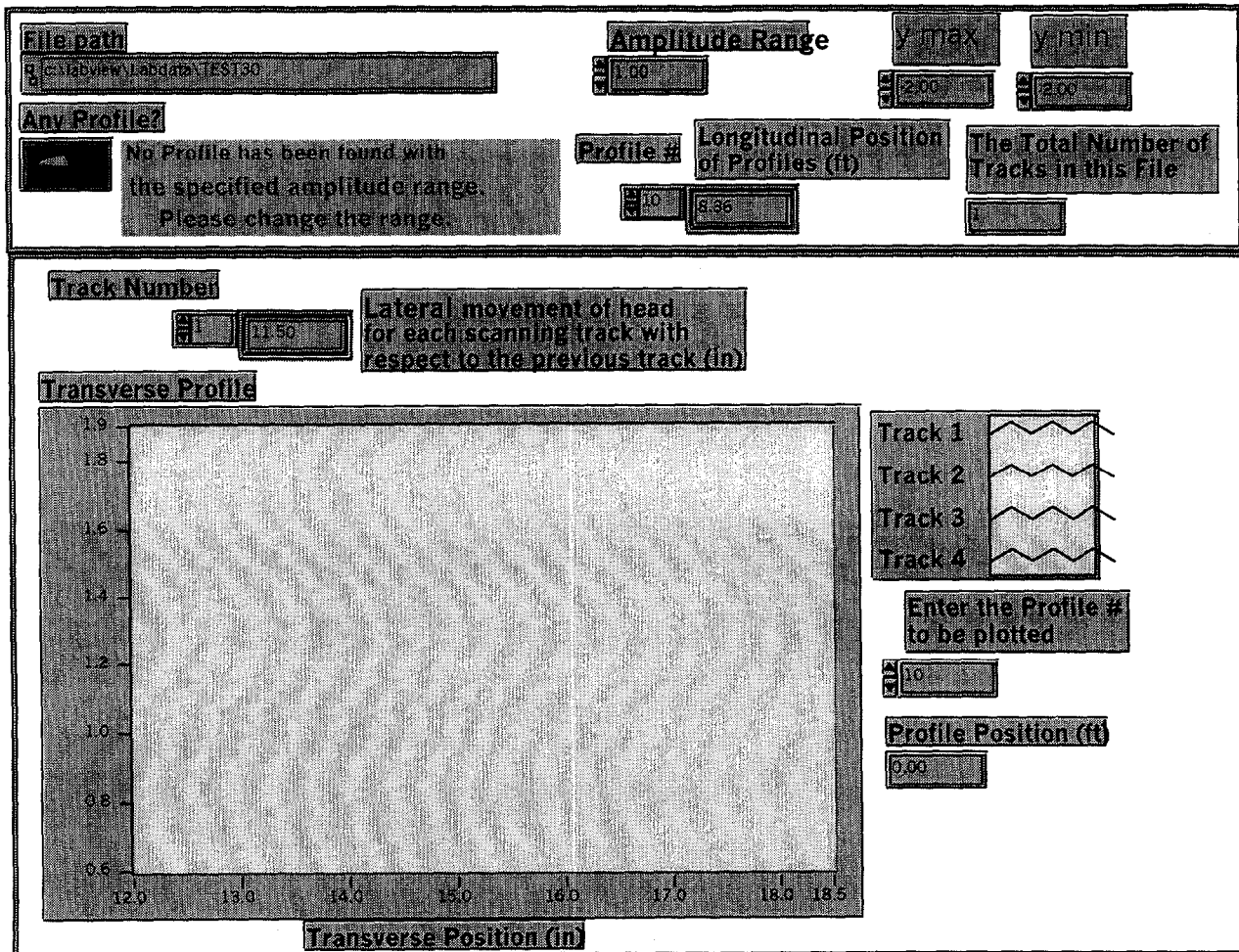


Figure 14. User interface window for MFL data analysis Option Six.

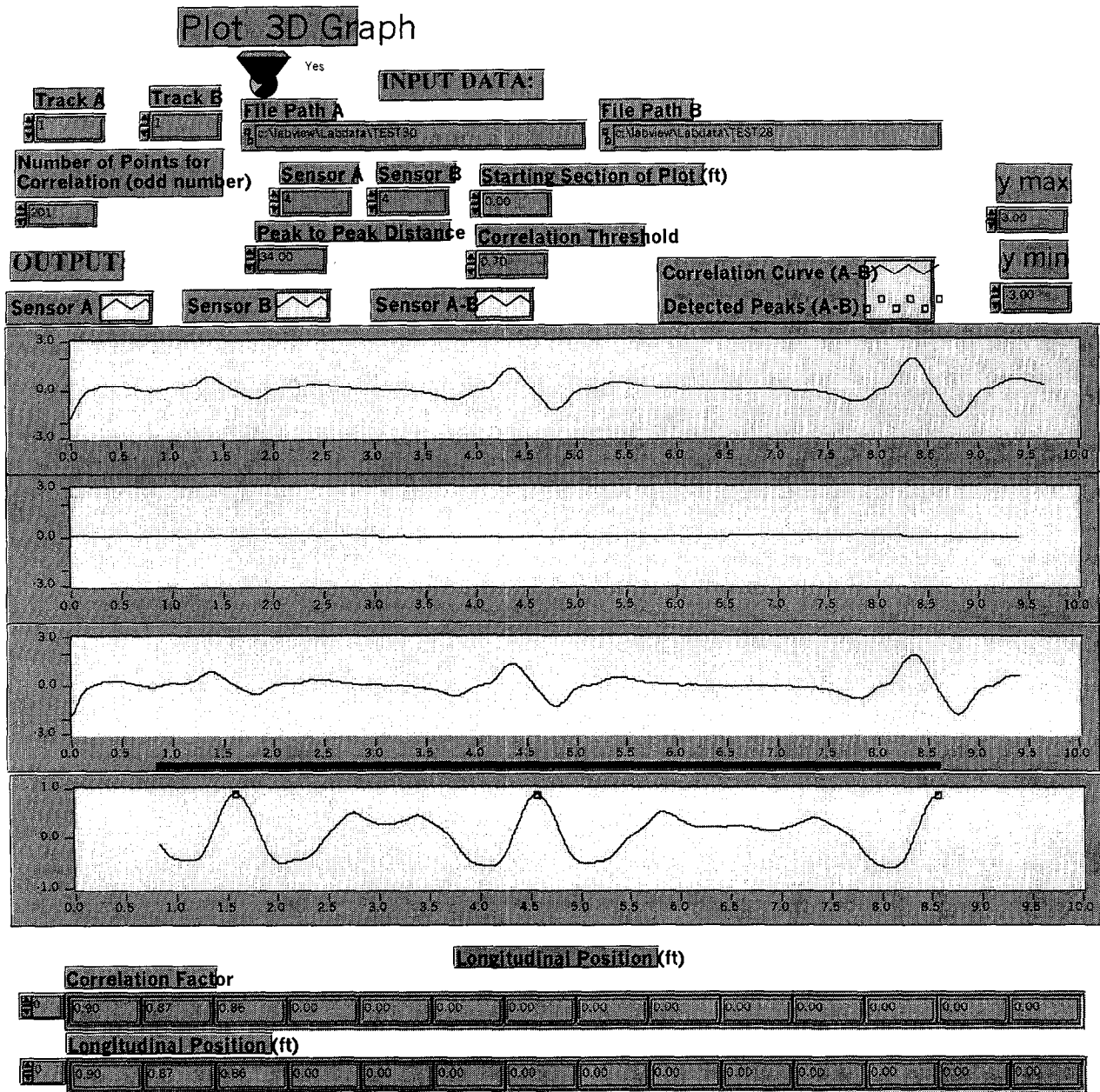


Figure 15. User interface window for MFL data analysis Option Seven.

8. Option Eight:

This data analysis option would allow the user to calculate and display a graph of the difference between the sensor outputs for up to two tracks within two separate data files recorded at different times for the same test beam. The outputs from the seven sensors located on the upper Hall-effect sensor board inside the sensor enclosure are considered in this analysis option. This analysis option is most effective for periodic inspections of the same test beam to determine if any deterioration, or change, has taken place since the time of an earlier test. The user input includes the names of the recorded data files, the track

numbers within the data files, the starting position of the data for the analysis, lower and upper bound amplitude display values, and setting the three-dimensional graph plot switch to either the “Yes” or

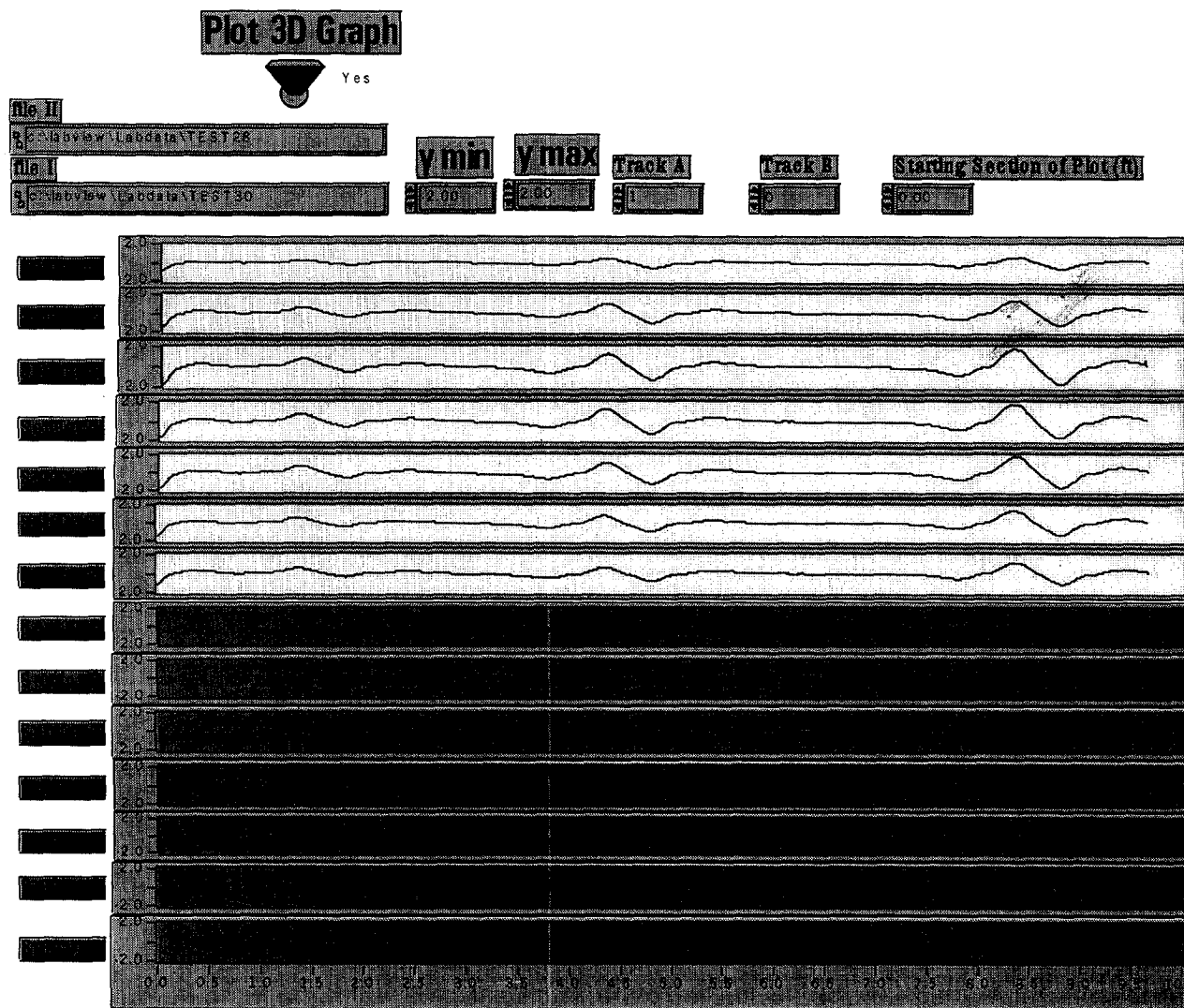


Figure 16. User interface window for MFL data analysis Option Eight.

“No” position. After all the required user input parameters are entered within the displayed window, the analysis software may be executed by clicking the mouse button on the right arrow symbol from the tool bar window on the top of the computer screen. Upon executing the software, the graphs of the difference between the sensor outputs for the two selected tracks of the two different data files are displayed within the analysis option screen. Figure 16 shows the user interface window for this analysis option.

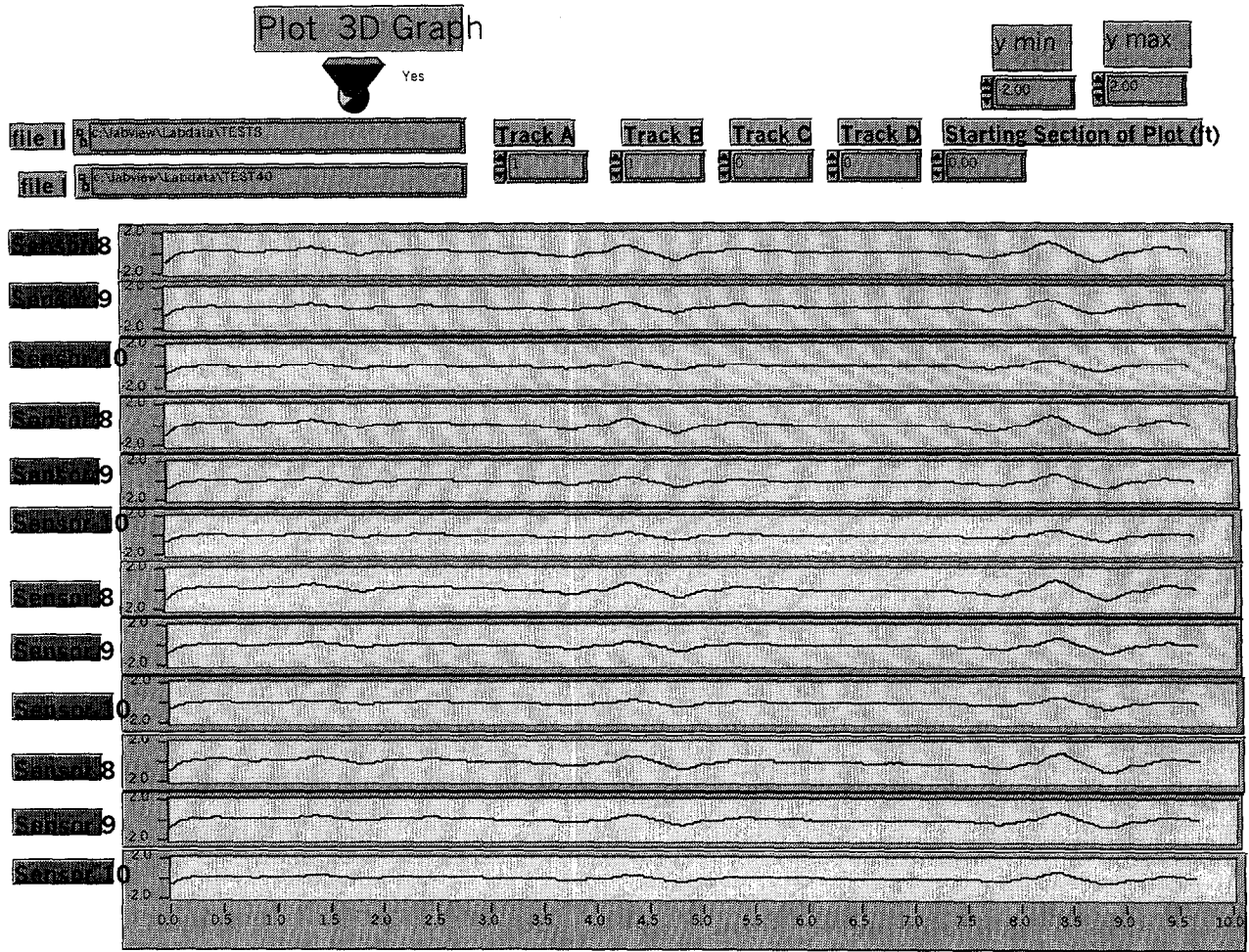


Figure 17. User interface window for MFL data analysis Option Nine.

9. Option Nine:

This data analysis option would allow the user to calculate and display a graph of the difference between the sensor outputs for up to four tracks within two separate data files recorded at different times for the same test beam. The outputs from the three sensors located on the lower Hall-effect sensor board inside the sensor enclosure are considered in this analysis option. This analysis option is most effective for periodic inspections of the same test beam to determine if any deterioration, or change, has taken place since the time of an earlier test. The user input includes the names of the recorded data files, the track numbers within the data files, the starting position of the data for the analysis, lower and upper bound amplitude display values, and setting the three-dimensional graph plot switch to either the “Yes” or “No” position. After all the required user input parameters are entered within the displayed window, the analysis software may be executed by clicking the mouse button on the right arrow symbol from the tool bar window on the top of the computer screen. Upon executing the software, the graphs of the difference between the sensor outputs for the four selected tracks of the two different data files are displayed within the analysis option window. Figure 17 shows the user interface window for this analysis option.

CHAPTER 5. SYSTEM OPERATION

INTRODUCTION

Prior to the installation and operation of the magnetic flux leakage (MFL) system developed under this study, a condition survey should be made on the concrete members of a bridge that are the subject of the testing. This should include a review of available contract documents/shop drawings and a visual inspection of the members. Knowing the location of various reinforcing, prestressing, and post-tensioning steels within a concrete test member can be helpful for reliable data interpretation of the MFL results. This, along with other useful information on the types and locations of other ferromagnetic components (such as stirrups, chairs, tie-down devices, and couplers) can be obtained from the review of available contract drawings. All of these ferromagnetic components will have a significant influence on the MFL data and a prior knowledge of their presence at specific locations can help minimize the difficulties of the data interpretation. The visual site inspection enables the operator to make the necessary adjustments in the structural frame of the MFL system so appropriate spacing between the side wheels on both sides of the device is established. In addition, any significant variation of the width of the test beam along its length should be noted. As described in the earlier parts of this report, the MFL system is maintained on a concrete test beam through frictional forces developed between the side wheels mounted on the system's structural frame. These wheels are spring-loaded and permit approximately 25 mm (1 in) of variation in the width of the test beam. Any variation in the width of the test beam that is found, through the visual inspection, to be in excess of 25 mm (1 in) can cause detachment of the system from the beam.

Using the MFL system as part of an inspection/maintenance program to assess the condition of a bridge on a periodic basis is a valuable means of determining the onset or presence of corrosion problems. The success of periodic inspections depends on the test system's capability of achieving reproducible data under similar conditions. This is possible now through the use of the developed MFL system. Any variations or changes found from the comparison of data obtained at two different times, and under similar conditions, can indicate the presence of defects that have been created since the time of the first test. The operator of the MFL system should perform the tests under similar conditions. These include using the same setup parameters and the same starting and end points for each test.

After installing the MFL system (the beam-rider unit) on a concrete test beam, the operator may install a magnetic marker (such as a small-size ferromagnetic bar) across the width and on the underside of the beam. This is used to produce a sizable peak in the recorded magnetic data. This peak is utilized to define the starting position and to locate other features such as stirrups, other steels, or flaws with respect to the peak. The magnetic marker may be any ferromagnetic material (such as a 1.5-mm- (1/16-in-) to 3-mm- (1/8-in-) diameter steel rod that is the same length as the beam width) or a thin strip of magnetic tape. The marker should be placed such that the beam-rider will cross it shortly after beginning data acquisition and it should be oriented perpendicular to the longitudinal axis of the beam. A recommended location for the magnetic marker is 150 mm (6 in) to 300 mm (12 in) in front of the nearest magnet located on the sensing-head unit. It is important that the operator records the size and exact location of the magnetic marker with reference to some permanent object, such as a pier, abutment, or diaphragm. With the knowledge of the size and position of the magnetic marker for the first test, the second test may be conducted with the same type of magnetic marker placed at the same position as for the first test. This will result in MFL data with the same starting point and length, which makes a comparative evaluation possible.

It is also important to note and record the transverse position of the sensing-head unit across the width of a test beam for each test conducted by the MFL system. Since there are Hall-effect sensors spaced

laterally across the width of the sensor enclosure of the sensing-head unit, it is apparent that deviations in the transverse positioning of the sensing-head unit will result in a variation of the signal amplitude for the corresponding data. The change in the signal amplitude is from the effect of different distances between sensors and steel components within the concrete test beam. This may result in misinterpretation of the MFL data when a comparative evaluation is made for data from two tests performed at two different times. This can, however, be avoided by performing the second test (necessary for a comparative study) with the same position for the sensing head as that for the first test. A recommended test method for scanning an entire beam width is to align the edge of the sensor enclosure with the outside edge of the test beam for the first track of data acquisition. For the second data acquisition track, the sensing-head unit may be moved to a new position that creates no overlap with the first test path. The transverse position for each track (or path) of data acquisition may be read in the user interface window of the data acquisition and system control software and should be documented as a part of the recorded data.

SYSTEM INSTALLATION AND OPERATION

To install the beam-rider unit on a concrete test beam, several steps must be taken. The most important is that the unit be adjusted appropriately for the dimensions of the test beams. Several measurements of the width of the test beam must be taken between the bottom outside edges along the length of the beam. The hardware adjustment entails moving the longitudinal structural frame members, which are those that support the three wheels on each side of the beam-rider unit, to appropriate positions at the locations of the connectors provided on the transverse frame members. It is important to adjust the width of the beam-rider unit appropriately for the concrete beam subjected to testing. If the width of the beam-rider unit is set too narrow for the test beam, the installation will not be possible. If it is set too wide, there will be a risk of detachment of the unit from the test beam.

Steps for Adjusting the Width of the Beam-Rider Unit:

The following steps are recommended for adjustment of the width of the beam-rider unit:

1. Measure the width of the beam that will be tested from the bottom outside edge to the bottom outside edge, including any chamfer at the corners.
2. Measure the distance between the inside faces of the inflatable wheels on the beam-rider unit. This distance should be approximately 38 mm (1.5 in) less than the width of the test beam. Sliding mechanism and spring-loaded devices have been incorporated in the beam-rider unit to allow lateral motion of one of the side-frame members, called the moveable frame member, during the operation of the unit on a concrete test beam. The moveable frame member is the one with three inflatable wheels located on the same side where the spring-loading assemblies are.
3. If the measured dimension is different from that described above, place the beam-rider unit on a workbench or a place that allows convenient disassembly and reassembly of the side-frame members. Note that in most cases where only a small adjustment of the distance between the two side frames is required, only the moveable frame member may need to be adjusted.
4. Remove the spring force clamping knobs by holding the 19-mm (0.75-in) nut with a wrench and loosen the knob by hand.
5. Remove the knob mounting brackets by removing the mounting bolt in each one on the side of the spring-loaded assemblies.

6. Remove the two mounting bolts that connect each end of the wheel mount frame to the transverse frame members of the beam-rider unit.
7. Slide the moveable frame member to a position that results in a cross-distance between the inside faces of the inflatable wheels approximately 38 mm (1.5 in) smaller than the width of the test beam.
8. For test beams with a width of smaller than approximately 500 mm (20 in), both the moveable and fixed-frame members of the beam-rider unit may need to be adjusted.
9. Insert and tighten the frame member mounting bolts, two on each end.
10. Adjust the spring-loaded knob for a 38 mm (1.5 in) smaller fit than the beam's width.

Installing the Beam-Rider Unit on a Concrete Test Beam

The process of installing the beam-rider unit on a test beam should be based on the following step-by-step procedure. The installation should only be undertaken after adjusting the width of the beam-rider unit to the proper dimensions as described in the previous section of this report. Furthermore, it must be made certain that the air pressure in the inflatable wheels of the beam-rider unit is not low. A low air pressure in the tires can cause low frictional forces to be developed between the wheels and the side surfaces of a concrete test beam. This can lead to the detachment of the unit from the test beam. The installation of the beam-rider unit on a concrete test beam may be performed by a two-person crew. An additional assistant may be used to facilitate the operation for added convenience. The step-by-step procedure recommended is listed below:

1. The dc power to the system must be provided through the connectors supplied with the system. The supplied connector prevents reversal of the power polarity which can cause significant damage to the system components. The dc power supply should be adequately charged with an appropriate charger unit prior to initiating a test.
2. Connect the power supply cable emanating from the data-acquisition unit to the 12-V dc battery through the use of the end connectors supplied.
3. Check that Cables #1 through #3 are connected to the data-acquisition unit via the brass military connectors.
4. There are two power switches on the data-acquisition unit that should be turned to the On position.
5. Switch the automatic/manual switch for the control of the motion of the beam-rider unit to the manual position.
6. Press down on the side of the longitudinal-manual drive switch in the direction of the desired travel for the beam-rider unit. This will cause turning of the power drive wheel and adjustment of the toggling wheels so that they are oriented at the appropriate angle to result in pulling the unit up against the bottom surface of the test beam.
7. The operating crew may grasp the longitudinal 25-mm (1-in) round tube handles found on each side of the beam-rider unit.

8. Lift the beam-rider unit to the underside of the beam so the drive wheel is in contact with the lower edge of the test beam.
9. The person on the side of the automatic/manual switch must press and hold the longitudinal manual drive switch down in the direction desired to drive the beam-rider unit while lifting his/her side toward the beam.
10. Continue applying upward force while driving the beam-rider unit with the longitudinal manual switch until all of the wheels are in full contact with the sides of the test beam.
11. Release the longitudinal manual drive switch.
12. Set the automatic/manual switch to the automatic position.
13. Install a flat plate, made of wood or aluminum, at the underside and across the width of the test beam at both ends. Limit switches on the structural frame of the beam-rider unit may be pressed against the installed flat plates at either end of the test beam when the beam-rider unit approaches either end of the test beam.
14. The weight of the various components, such as the sensing head, dc power supply, wireless communication, and data-acquisition units, should be distributed evenly on both sides of the beam-rider unit. An uneven weight distribution on the beam-rider unit can cause difficulties in maintaining the device on a concrete test beam. To balance all weight on the beam-rider unit, it is recommended to laterally move the section of the tube framing that supports the weight of the dc power supply and the data-acquisition units. This part of the frame, called the "carriage," may be slid to one side or the other in order to counter the weight of the sensing-head unit. To slide the "carriage" to a side, loosen the set-screws on the T-connectors installed on the lower cross-tube frames of the beam-rider unit and apply a moderate force in the direction of the desired side. The operator of the MFL system should make certain that all weights on the beam-rider unit are distributed evenly along the sides. This will result in having all contact wheels of the beam-rider unit in full contact with the bottom surface of the test beam during the testing or operation of the unit.
15. The operator should make certain that the path for the motion of the sensing-head unit is free of interference from the data-acquisition and dc power supply units or any other components.
16. The operator should make certain that the path of the beam-rider unit along the length of the test beam is clear and cables, wires, and any other mechanical components will not interfere with the unit during its operation.

Safety Considerations

Safety considerations for the use of the MFL system include working and transporting the permanent magnets as well as securing the beam-rider unit on a test-beam during its operation. Because of the high strength associated with the magnets used in the MFL system, great care should be taken in handling them during transport and operation of the system. When transporting the MFL system, the sensing-head unit should be separated from the beam-rider unit framing and kept in a relatively strong and fully enclosed wooden box that provides approximately 200 mm (8 in) of air space around the magnets. The wooden box will effectively eliminate the possibility of the magnets being in very close proximity to any ferromagnetic materials.

Securing or maintaining the beam-rider unit on a concrete test beam during an inspection operation should be of primary concern to the MFL system operators. Hardware and a functional description for the beam-rider unit is presented in Chapter 3 under "THE MECHANICAL SYSTEM," and its installation procedure is listed in the preceding section. If the recommended installation procedure is followed, the beam-rider unit should be secured safely on a test beam during its operation. However, an additional safety feature has been introduced to prevent dropping of the beam-rider unit if it becomes separated from the test beam for any reason. This will be accomplished by attaching safety cables to the test beam at its ends and by guiding the cables through safety eyes on the frame of the beam-rider unit. The following step-by-step procedure is recommended for the installation of the safety cables.

1. Make certain that access is available to the underside of the test beam at its ends.
2. On each side of the test beam, attach one end of a safety cable to a pipe-clamp installed at one end of the test beam. The free end of each cable should be guided through two safety eyes on each side of the frame of the beam-rider unit. The free end of the cables can be then attached to a second pipe-clamp installed at the other end of the test beam.
3. On the underside and at each end of the test beam, install an aluminum flat plate, in a vertical orientation, by connection through brackets provided with the pipe-clamps. Make certain that the limit switches of the beam-rider unit will contact the flat plates when the unit approaches either end of the test beam.
4. In lieu of the pipe-clamps, safety cables may be guided through the four safety eyes and looped around both bearings at the ends of the test beam.
5. Adequate slack should be provided in the safety cables to allow the beam-rider unit to reach stopping points on the test beam.

Operation of the Beam-Rider Unit

The operation of the beam-rider unit includes remote control of the mechanical and electrical components of the unit through the system's software and via wireless communication. It also includes acquisition of the MFL data with relevant display options and data interpretation. The following step-by-step procedure is recommended for the operation of the beam-rider unit:

1. Supply power to the computer.
2. Connect the radio modem transceiver's communication cable to the serial port of the computer.
3. Supply power to the radio modem transceiver unit.
4. Turn the computer on.
5. Start the data-acquisition user interface computer program file called "7Displays Sensors W control44.vi." This may be done by double-clicking the computer mouse on the file name. The file path is Labview\Emad\Final Design. As described in Chapter 4 of this report, the data-acquisition user interface software includes both the data-acquisition as well as system control software. Upon execution of the software, a display window for the output of the seven Hall-effect sensors, the top row of sensors in the sensor enclosure, will be shown along with a window for the system control.

6. Within the system control window, specify a desired data file name with a chosen file path.
7. Make certain that the longitudinal and transverse motor switches in the system control window are set in the Off position.
8. Using the tool bar shown on the top of the screen, click with the mouse on the right arrow symbol or press "r" while holding the "Ctrl" key on the computer keyboard to execute the data-acquisition software. Actual data acquisition or system control can be accomplished by using the indicators and switches shown in the two windows of the user interface.
9. Select the desired direction for the longitudinal motor, "forward" or "reverse."
10. Move the sensing-head unit to the desired position across the width of the test beam using the switches for the transverse motor in the system control window. Set the direction switch to the "FORWARD" or "REVERSE" position and the motor switch to the On position. The position of the sensing-head unit along the transverse direction will be displayed, in inches, in the indicator space within the control system window under the heading of "Transverse position."
11. Make certain that the "Track" number reads "1". This will indicate the first path for data collection.
12. Use a "Gain" setting of "10" for the data to be recorded. This is a scale factor for magnification of the amplitude of the MFL data. Other settings may be chosen if desired.
13. Set the lower and upper values for the amplitude of the MFL data to be recorded. This is done by choosing appropriate values for the "Y Minimum" and "Y Maximum" indicators within the system control window. Values of -5 and +5 are recommended as initial values.
14. Set the "Data Collection" switch to the On position within the system control window.
15. Set the longitudinal "Motor" switch to the On position within the system control window.
16. The beam-rider unit should start motion in the indicated direction along the length of the test beam and the MFL data should be displayed on the screen.
17. When the beam-rider unit approaches the end of the test beam, a limit switch is activated that stops the motion of the device. The "Track" number should automatically change to "2" within the system control window.
18. The direction of the longitudinal "Motor" within the system control window should change to the opposite direction.
19. The beam-rider unit must be returned to the beginning point of the test beam in order to start the second path of data acquisition for a width of the beam adjacent to the first track. To accomplish this, set the "Data Collection" switch to Off and the longitudinal "Motor" switch to On. The beam-rider unit will travel to the beginning of the test beam and will stop.
20. Move the sensing-head unit to the desired location using the transverse motor direction and On/Off switches.

21. Repeat the data-acquisition procedure as described in the previous steps. Make certain that the "Data Collection" switch is set back to the On position prior to the initiation of the motion of the beam-rider unit for the second track.
22. The recorded data file will be saved automatically under the chosen file name upon stopping the data-acquisition process.
23. If a separate data-acquisition process is required to be initiated, the screen display may be refreshed by clicking the mouse button on the "CLEAR CHARTS" button.



CHAPTER 6. SYSTEM EVALUATION

INTRODUCTION

The evaluation of the magnetic flux leakage (MFL) system included two phases, the laboratory investigation and the field investigation. In both of the two investigations, the primary objective was to determine the system's capabilities, field-worthiness, accuracy of the results produced, reliability of the system and test results, and limitations. During the laboratory investigation, efforts were made to also establish the optimum operational parameters for use of the MFL system. During the field investigation, the beam-rider unit was evaluated for its overall ease of use, including installation, removal, and testing of prestressed concrete girders. It must be noted that during this study, a significant amount of effort was devoted to the development of the new MFL system. Although the system was subjected to some evaluation, the scope was limited due to lack of adequate time and funds. An additional study needs to be initiated that could perform a comprehensive evaluation of the mechanical/control mechanisms, as well as the data collection and analysis capabilities and reliability of the MFL system.

LABORATORY INVESTIGATION

In the laboratory investigation phase of the MFL system, two important objectives were achieved. First, a determination of the reliability of the mechanical components of the system was made. Second, the data-acquisition and analysis capabilities of the system were evaluated by performing a series of tests using prestressing cables with manmade flaws as well as real corrosion. In addition, an extensive database of known magnetic-based flaw signals that existed at the University of Wisconsin-Milwaukee was evaluated to establish operational parameters that would render the MFL system most accurate with respect to its data interpretation.

With numerous mechanical components, reliable operation of the MFL system (the beam-rider unit) was an important concern. Of primary concern was the ability to operate the MFL system without mechanical failure that would disrupt the data-acquisition and testing process. Several parameters influencing the various mechanisms of the MFL system were optimized to achieve the best results. For example, an optimum tilt angle for the tilting wheels of the beam-rider unit was determined through calculations and experimental efforts. This made it possible to maintain the beam-rider unit on the test beam securely and efficiently. Qualities such as functionality and ease of use were also evaluated during the laboratory evaluation phase.

Establishing optimum operational parameters for use in the MFL data analysis was necessary so that reliable interpretation of results from field testing of concrete members could be made. These parameters included the peak-to-peak amplitude range and the overall data length specified for various flaws in prestressing steel or for other ferromagnetic components that influence the MFL data.

To facilitate the laboratory evaluation of the beam-rider unit, a wooden test beam was constructed that emulated an actual reinforced or prestressed concrete beam. Various steel reinforcing bars and prestressing cables with and without flaws were placed at different locations throughout the cross-section of the beam to allow testing under different conditions. The wooden test beam constructed for the laboratory investigation was 4896 mm (192 in) long and 612 mm (24 in) wide. The sides were

constructed with 61-mm x 204-mm (2-in x 8-in) lumber. The bottom of the beam was covered with a 19-mm ($\frac{3}{4}$ -in) plywood sheet that simulated the bottom surface of a concrete beam. This allowed the beam-rider unit to have a planar surface to contact with its contact wheels and longitudinal encoder. The beam's cross-sections, at six locations along its length, were comprised of 25-mm x 204-mm (1-in x 8-in) pine board templates that allowed for the placement of prestressing cables in various patterns. Each template had 3 rows of 13 holes to accept various numbers of prestressing strands. This allowed testing of flawed prestressing cables with the presence of other undamaged cables that had a magnetic masking effect on the flawed cables. In other words, this aided in determining the extent of changes in the shape of the MFL signals from tests on concrete members with heavy reinforcement. The spacing of the prestressing cables accurately emulated in-service prestressed beams by having 50 mm (2 in) of exterior cover as well as adequate tendon-to-tendon spacing of 25 mm (1 in). A photograph of the wooden beam used for the laboratory testing of the beam-rider unit is shown in figure 18.

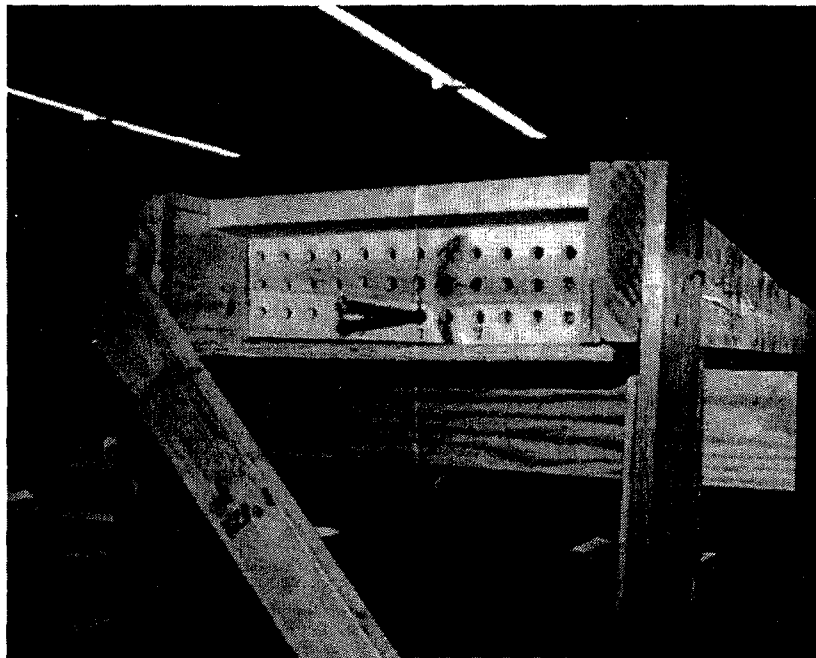


Figure 18. The wooden beam used for laboratory testing of the beam-rider unit.

Flaws in the prestressing cables were introduced with finite reduction in the cross-sectional area at certain locations. The flaw introduction procedure consisted of using a rotary cutting tool to cut out 6-mm- ($\frac{1}{4}$ -in-) long gaps into the wires of new prestressing strands. Careful attention was paid to this process so that only the intended wires would be severed without damaging any of the surrounding wires.

The mechanically flawed test specimens consisted of two 357-mm- (168-in-) long strands with three different size flaws in each one. These two test specimens were named Cable #1 and Cable #2. The percent area reductions, or the size of the flaws, were determined by taking the number of wires cut divided by the total number of wires in the strand (seven). Cable #1 had 7%, 14%, and 29% cross-sectional area reductions spaced at approximately 765 mm (36 in), and consisted of one half-cut, one fully cut, and two fully cut wires. Cable #2 had 43%, 57%, and 71% cross-sectional area losses due to severed wires. A third test specimen, Cable #3, was a fully fractured strand with each severed piece

having different lengths such that they could be differentiated from one another within the recorded MFL data. In addition to the mechanically flawed cables, three corroded cables were used in the laboratory testing. Fifteen undamaged prestressing cables, labeled "Cable 0," were used in the laboratory investigation to provide the effect of magnetic masking for the flawed cables. The 15 undamaged cables were placed around the various flawed cables during some of the tests. These undamaged cables placed in the test template covered a width equivalent to the width of the magnets, causing the maximum possible masking effect. As a result, no additional unflawed cables were required. In addition to the three mechanically flawed strands, three corroded strands were used in the laboratory testing. Figure 19 shows a photograph that includes two prestressing cables with 14% and 71% reductions of cross-sectional area, as well as a cable with real corrosion.

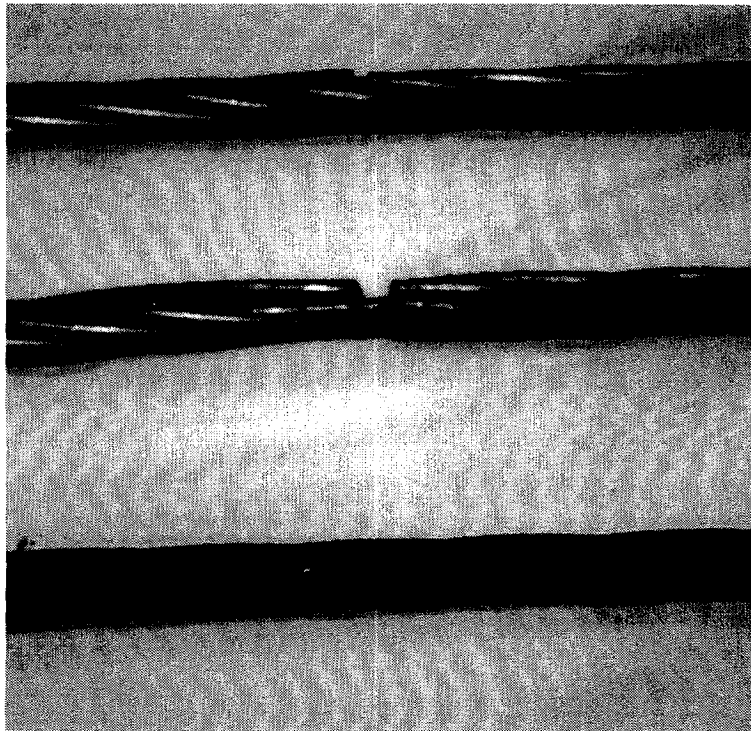


Figure 19. Strands with mechanically introduced flaws and real corrosion.

The corroded strands were taken from a concrete slab that had been used in an accelerated corrosion study under a separate research study. The cables had corrosion pits that were equivalent to a 5% to 15% reduction of cross-sectional area. The corrosion damage was distributed throughout the length of the cables.

A systematic test procedure was used during the laboratory investigation after the test specimens were prepared. To establish a baseline, or benchmark, the first two tests were performed on the wooden beam once, with no prestressing cables, and then with an undamaged cable placed in the lowest row of the wooden beam's templates.

A series of laboratory tests for Cables #1, #2, and #3 were performed with the absence of any other steel cables. It was expected that the MFL signals for these flaws would have the maximum possible

amplitudes compared with those tested with the masking effect of the undamaged cables. The results of these tests were used as control data to deduce the effect that additional steel strands would have on the signal amplitudes for flaws in strands. Test results from these experiments were used to establish basic flaw signal profiles that helped determine various flaw shape parameters that can most accurately describe the flaws.

The tests with Cables #1, #2, and #3 were repeated; however, each time, one undamaged cable was placed next to one of the flawed cables. Both cables were placed in the lowest row of the wooden test beam's templates. Then, the tests were repeated again, but one undamaged cable was placed on each side of one of the flawed tendons while still in the lowest row of the beam's templates. The results of these tests were analyzed to assess the effect of the undamaged cables on the MFL signal amplitude. Finally, the tests were repeated again, but with two undamaged cables placed on each side of one of the same flawed cables.

The above-described test series was performed two additional times, except that the flawed and undamaged cables were placed once in the second row and once in the third row of the wooden test beam's templates. This procedure was utilized to assess the loss of MFL signal amplitude due to the increasing distance between the flawed cables and the magnet/sensor assembly, or the sensing-head unit. To further explore the loss of flawed signal amplitude, a series of tests were undertaken in which the flawed cables were surrounded by 14 undamaged cables. This test was conducted to emulate modern prestressed concrete girders that can have a substantial amount of reinforcement in their cross-sections. As indicated earlier, due to the limited width of the magnets, additional cables would not have been effective in absorbing the magnetic flux. Therefore, no additional unflawed cables were used in the experiment.

A limited number of tests were performed on the cables with mechanical flaws and real corrosion with the presence of steel stirrups placed at different spacing. The presence of stirrups would normally introduce a magnetic masking effect on the signals that would result from the flaws. Special data processing is usually necessary to minimize the effect of the stirrups. One successful method of data analysis has been shown to be the performance of the correlation analysis on data that resulted from the subtraction of the outputs of two Hall-effect sensors when one is located directly above the other at a finite distance. The other successful method is to construct a three-dimensional image of the disturbed magnetic field that can signify the different effects that localized flaws and steel stirrups have on the magnetic field.

Laboratory Evaluation Results

Evaluation of the laboratory test data was centered on ascertaining the most effective values for the correlation parameters, N and B, for various flaw sizes (see figure 38). The first test conducted was based on using a single flawed strand, Cable #1, at a distance of 51 mm (2 in) from the magnet/sensor assembly. No other steel cables were present in close proximity to the flawed cable. The cable contained the three smallest flaws: 7%, 14%, and 29% cross-sectional losses. The amplitude output from a sensor positioned directly under the cable is shown as the upper graph in figure 20. Note the positions of the three flaws from the start of the test at 0.52, 1.40, and 2.62 m (1.7, 4.6, and 8.6 ft), respectively, as shown in the figure. From this figure, it is easy to see the presence of the 14% and 29% cross-sectional losses based on the significant disturbance of the magnetic field at the location of the flaws. Although the disturbance of the field is somewhat evident in the graph at the location of the smallest flaw, the result is not conclusive. The lower graph and the two tables shown below the graph

present the results of the correlation analysis. Each correlation peak has been marked with a small square symbol in the lower graph. Both the correlation factors and associated longitudinal positions for all peaks are shown in the two tables below the lower graph. As shown in the figure, the smallest cross-sectional loss, 7%, could clearly be identified with a correlation factor of 85%. The corresponding position for this flaw is listed in the table as 1.650 ft [0.503m] from the beginning of the test. The correlation factor values for the flaws equivalent to a 14% and 29% loss of cross-section were 98.4% and 99.7%, respectively. The corresponding positions are listed in the table as 4.658 and 8.575 ft [1.420 and 2.614 m], respectively. This indicated a relatively high degree of reliability in detecting these flaws under the given conditions. At a position 7.592 ft [2.314 m] from the start of the test, a correlation factor of -84% is shown in the lower graph and the tables. This should obviously be ignored since it is not relevant to a flaw.

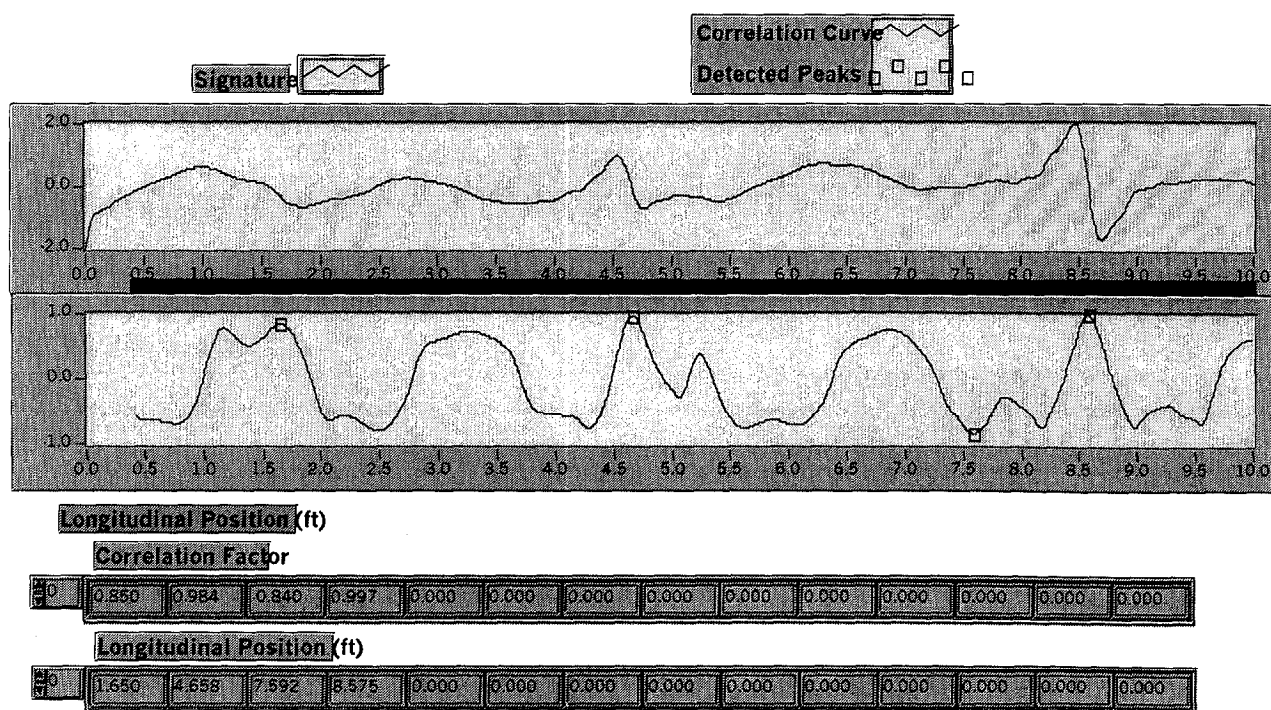


Figure 20. Graphs of a sensor amplitude output and correlation analysis for Cable #1 (distance to magnet/sensor = 51 mm (2 in), no adjacent steel).

The second test was conducted using Cable #2, which included flaws that were equivalent to a 43%, 57%, and 71% loss of cross-section. This cable was placed at a distance of 51 mm (2 in) from the magnet/sensor assembly and no other steel cables were present in close proximity to the cable. Figure 21 shows the results of the amplitude output of a sensor positioned directly under the cable and the corresponding correlation analysis. It can easily be seen that strong indications of the presence of flaws are evident in the graph of the amplitude (at locations 1.633, 4.625, and 8.675 ft [0.498, 1.410, and 2.644 m] from the start of the test) and the correlation factors are very high (approximately 99% for all three flaws). The peak-to-peak amplitude ranges for the three flaws in Cable #2 are approximately 6,

11, and 14 V, respectively. The corresponding values for Cable #1 are approximately 0.6, 1.5, and 4 V. The comparison gives an indication of the effect of the extent of loss of cross-section on the MFL signal strength or amplitude. For the correlation analysis of the data obtained for Cable #2, the optimum values used for the B and N parameters were 28 and 111, respectively. These are the optimum values for B and N, determined experimentally, that result in the highest correlation factors for the considered flaws (see table 3).

The third test was conducted using Cable #3. It contained a complete fracture of the prestressing strands. This cable was placed at a distance of 51 mm (2 in) from the magnet/sensor assembly and no other steel cables were present in close proximity to the cable. Figure 22 shows the results of the amplitude output of a sensor positioned directly under the cable and the corresponding correlation analysis. Again, a very strong indication of the presence of a fracture in the cable is evident in the amplitude graph (at 4.892 ft [1.491 m] from the start of the test and with a peak-to-peak amplitude value of approximately 28 V). The corresponding correlation factor is 99.1%. The optimum values for the B and N parameters used in the analysis were 28 and 141, respectively.

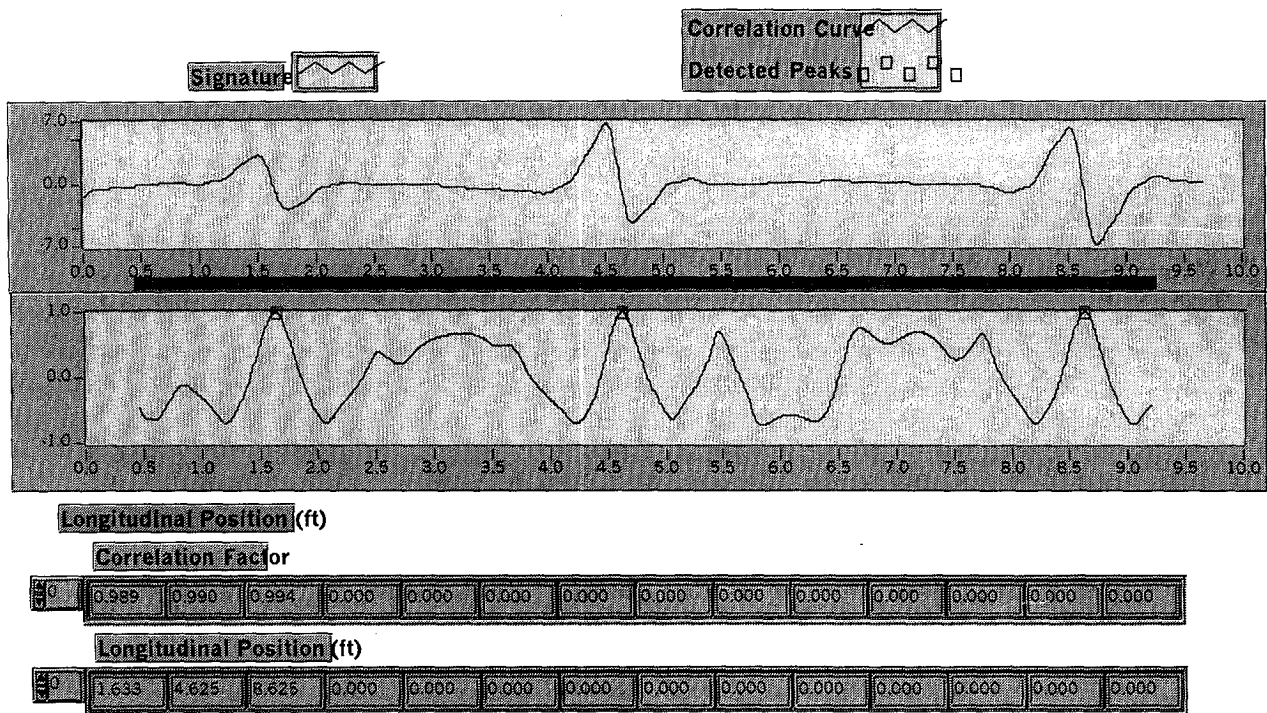


Figure 21. Graphs of a sensor amplitude output and correlation analysis for Cable #2 (Distance to magnet/sensor = 51 mm (2 in), no adjacent steel).

The next series of tests were conducted the same way as described earlier, but the flawed cables were placed in the second row of the templates of the wooden laboratory test beam. In this position, the flawed cables had a distance of 89 mm (3.5 in) to the magnet/sensor assembly. These tests were performed to determine the effect that an additional distance between the flaws and the magnet/sensor assembly would have on the MFL data. As is seen from the results presented here, the MFL signal amplitudes diminish and the signal periods increase with increasing distance between the flawed cables and the magnet/sensor assembly. The immediate observation is that appropriate correlation parameters, namely the B and N factors defined earlier, must be used based on the position of the flawed cables. Figure 23 shows the results of the test conducted with Cable #1 at the above-stated position without the presence of any other

steel cables. It can be seen that with the aid of the correlation analysis, the smallest flaw in the cable (at a location 1.717 ft [0.523 m] from the start of the test) could be detected with good reliability (85.7%). The two larger flaws in the cable were easy to detect by examining the amplitude graph and have yielded correlation factors of 90.2% and 93.3%, respectively. For the correlation analysis, values of 36 and 141 were used for the B and N parameters, respectively, rather than 28 and 101 when the cable had 51 mm (2 in) of distance to the magnet/sensor assembly.

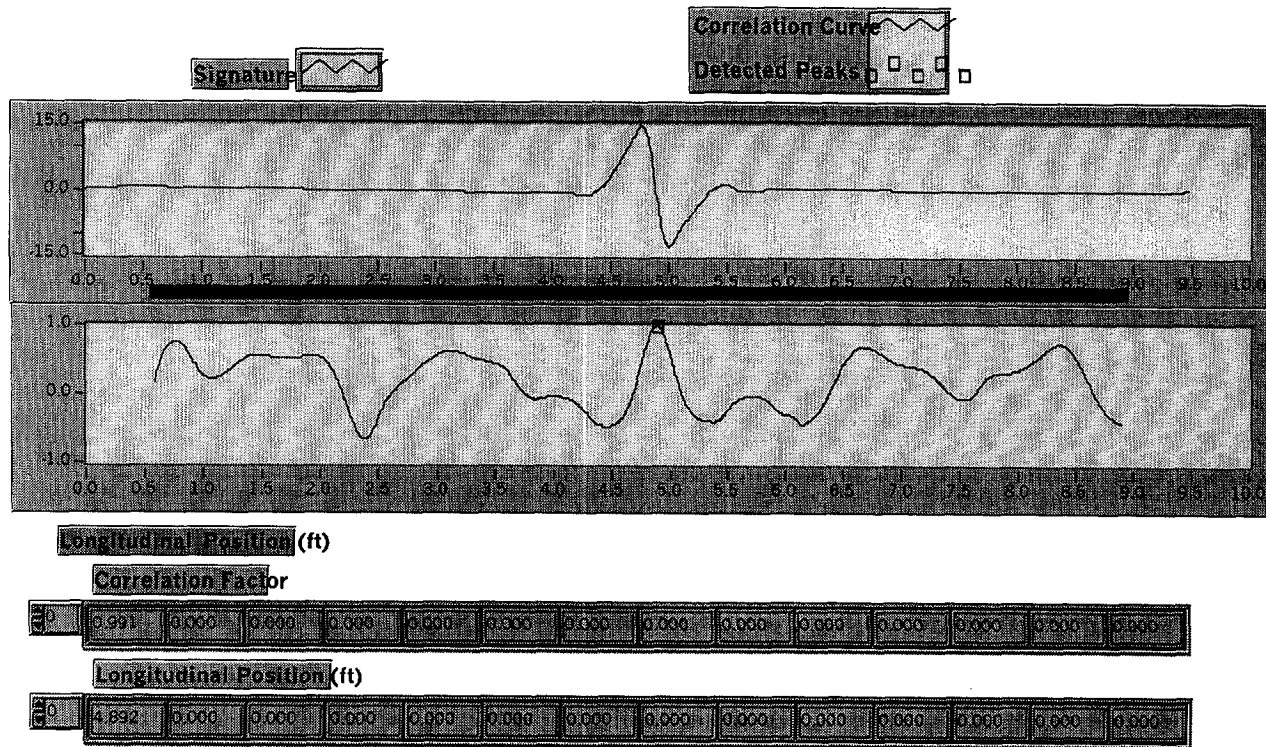


Figure 22. Graphs of a sensor amplitude output and correlation analysis for Cable #3 (distance to magnet/sensor = 51 mm (2 in), no adjacent steel).

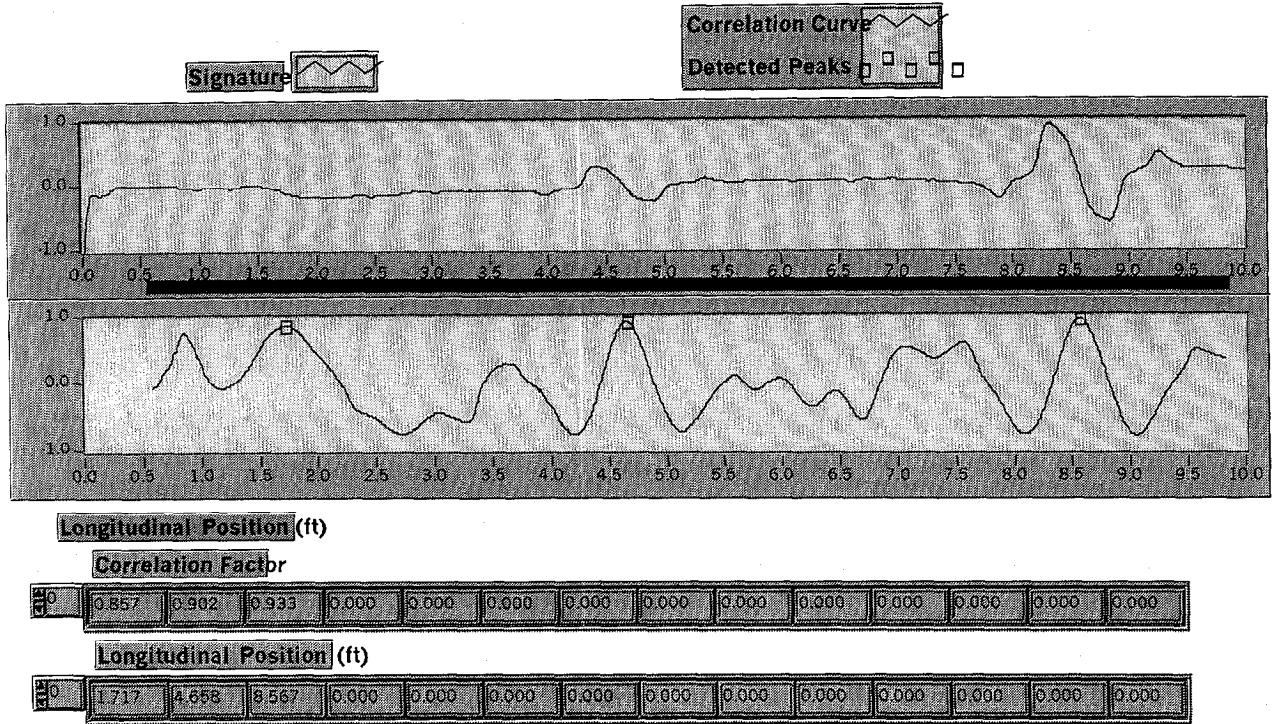


Figure 23. Graphs of a sensor amplitude output and correlation analysis for Cable #1 (distance to magnet/sensor = 89 mm (3.5 in), no adjacent steel).

The test program continued by placing Cable #2 in the second row of the test beam's templates. The results of the test are shown in figure 24. It can be seen from the figure that strong indications of the presence of flaws are evident in the graph of the amplitude, and the correlation factors are high. For the correlation analysis of the data, the values used for the B and N parameters were 36 and 141, respectively.

The test results for Cable #3 in the second row of the test beam's templates are shown in figure 25. It can be seen from the figure that the detection capability for the large flaw in the cable is very good. For the correlation analysis of the data, values used for the B and N parameters were 32 and 141, respectively.

Tests were also performed for the flawed cables placed in the third row of the wooden test beam's templates. At this position, the flawed cables had a distance of 128 mm (5 in) to the magnet/sensor assembly. While the MFL signal amplitudes continued to decrease with the increase in the distance to the magnet/sensor assembly, the signal periods did not change significantly. Therefore, the required parameters for the correlation analysis remained the same as that for the last set of tests.

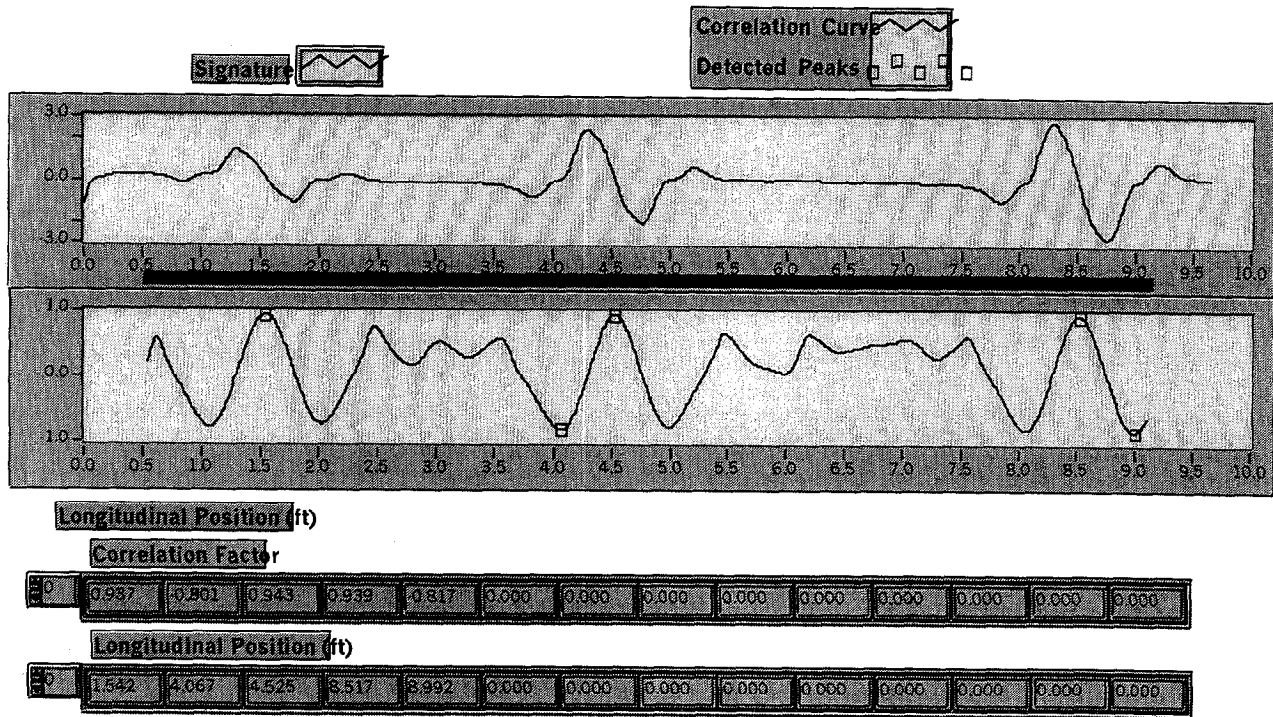


Figure 24. Graphs of a sensor amplitude output and correlation analysis for Cable #2 (Distance to magnet/sensor = 89 mm (3.5 in), no adjacent steel).

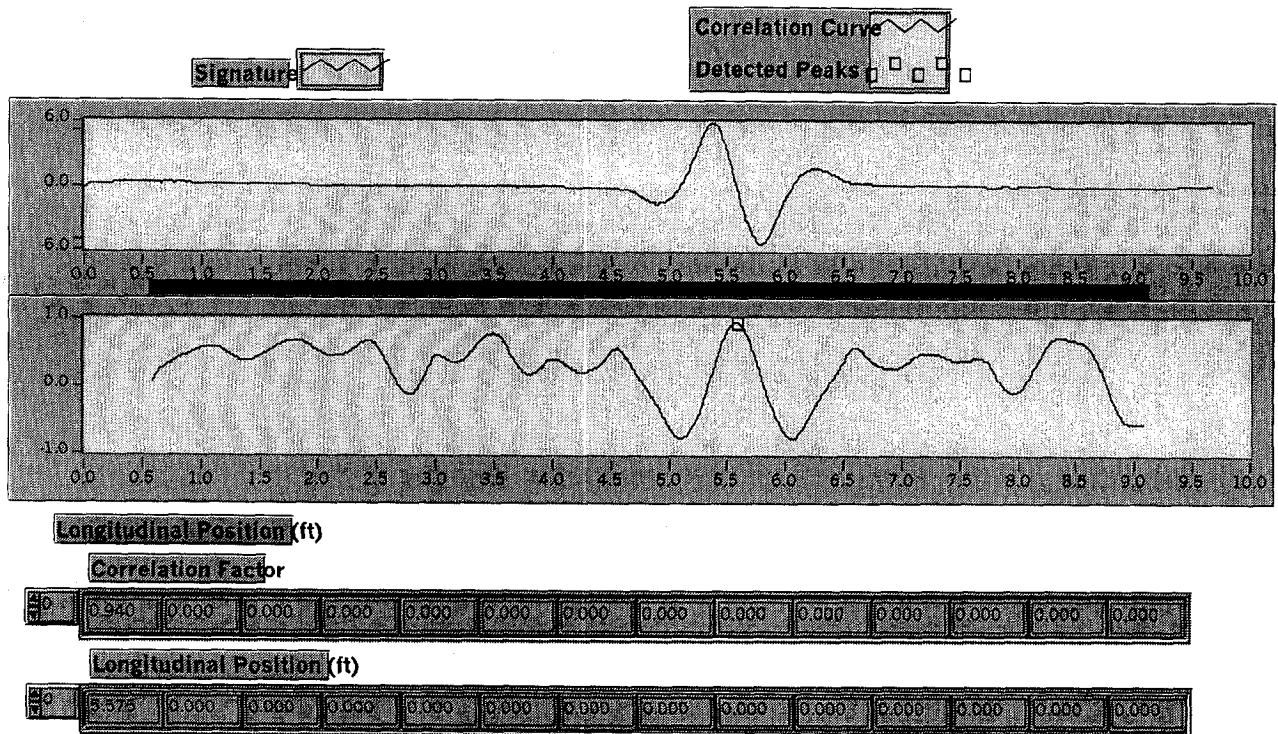


Figure 25. Graphs of a sensor amplitude output and correlation analysis for Cable #3 (distance to magnet/sensor = 89 mm (3.5 in), no adjacent steel).

The results of the test for Cable #1 placed in the third row of the test beam's templates are shown in figure 26. Again, the amplitude graph does not appear to show any evidence of the presence of a flaw at the location of the 7% loss of cross-section (at 1.667 ft [0.508 m] from the start of the test). However, with the use of the correlation analysis, the flaw could be detected with good reliability (89.3%). The two larger flaws in the cable were easy to identify in the amplitude graph and yielded correlation factors of 93.7% and 94.7%, respectively.

Tests were also conducted with Cables #2 and #3 placed in the third row of the test beam's templates. Figures 27 and 28 show the amplitude and correlation analysis results for tests conducted on Cables #2 and #3, respectively. The results showed that the flaws in the cables could easily be detected by both the evaluation of the amplitude graphs and by considering the correlation factors associated with the flaws. For flaws in both cables, the correlation factors were calculated to be higher than 93%. This indicated a relatively high degree of reliability.

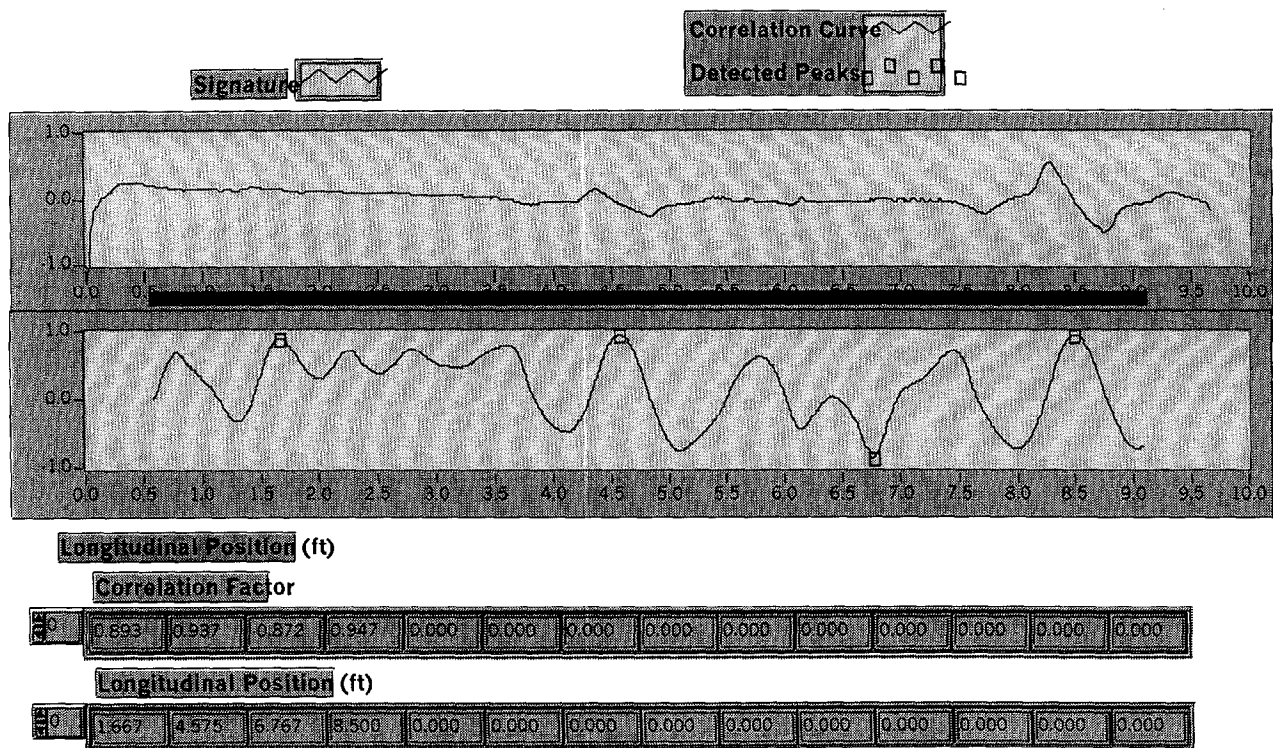


Figure 26. Graphs of a sensor amplitude output and correlation analysis for Cable #1 (distance to magnet/sensor = 128 mm (5 in), no adjacent steel).

To examine the magnetic masking effect of surrounding steel on the cables with flaws, tests were conducted using Cables #1 and #2 with the presence of additional unflawed prestressing cables. The tests included the placement of each of the flawed cables in the first row of the test beam's templates and the positioning of 14 undamaged prestressing cables around the flawed cable. For each flawed cable, there were two undamaged cables on each side and five more in each of the two rows above.

The results of the test conducted with Cable #1 are shown in figure 29. From the graph of the amplitudes, the evidence exists for the presence of flaws associated with the 14% and 29% losses of cross-section. The 7% cross-sectional loss is not clearly indicated in the amplitude graph of the figure. Conducting a correlation analysis (with $B=28$ and $N=101$) for the recorded data revealed that a reasonable correlation index could not be obtained for the 7% cross-sectional loss. The correlation factor was just under 70%. It was decided not to display correlation factors under 70%. It is possible to increase the value of the correlation factor, or the reliability in detecting this small flaw, with additional analysis efforts. This has not been the focus of this study. The correlation factors for the 14% and 29% flaws were 89.5% and 99.1%, respectively.

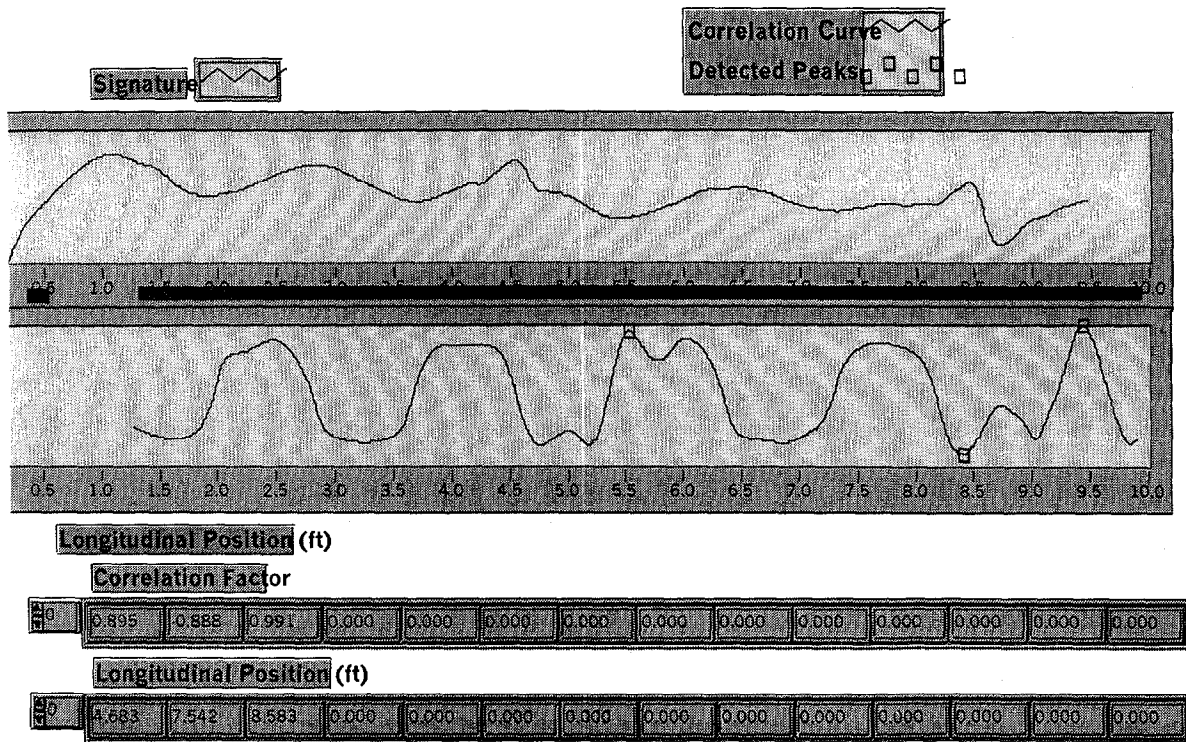


Figure 29. Graphs of a sensor amplitude output and correlation analysis for Cable #1 (distance to magnet/sensor = 51 mm (2 in), 14 adjacent steel cables).

The test conducted with Cable #2 with the additional 14 undamaged prestressing cables was successful. The test results for the amplitudes and the correlation analysis are shown in figure 30. For the correlation analysis, the values of the B and N parameters were 28 and 141, respectively. These values were the same as the values used in the test with Cable #2 in the same position without the additional steel cables. All three flaws were readily distinguishable in the amplitude graph and the correlation factors were at or above 95% for the three flaws.

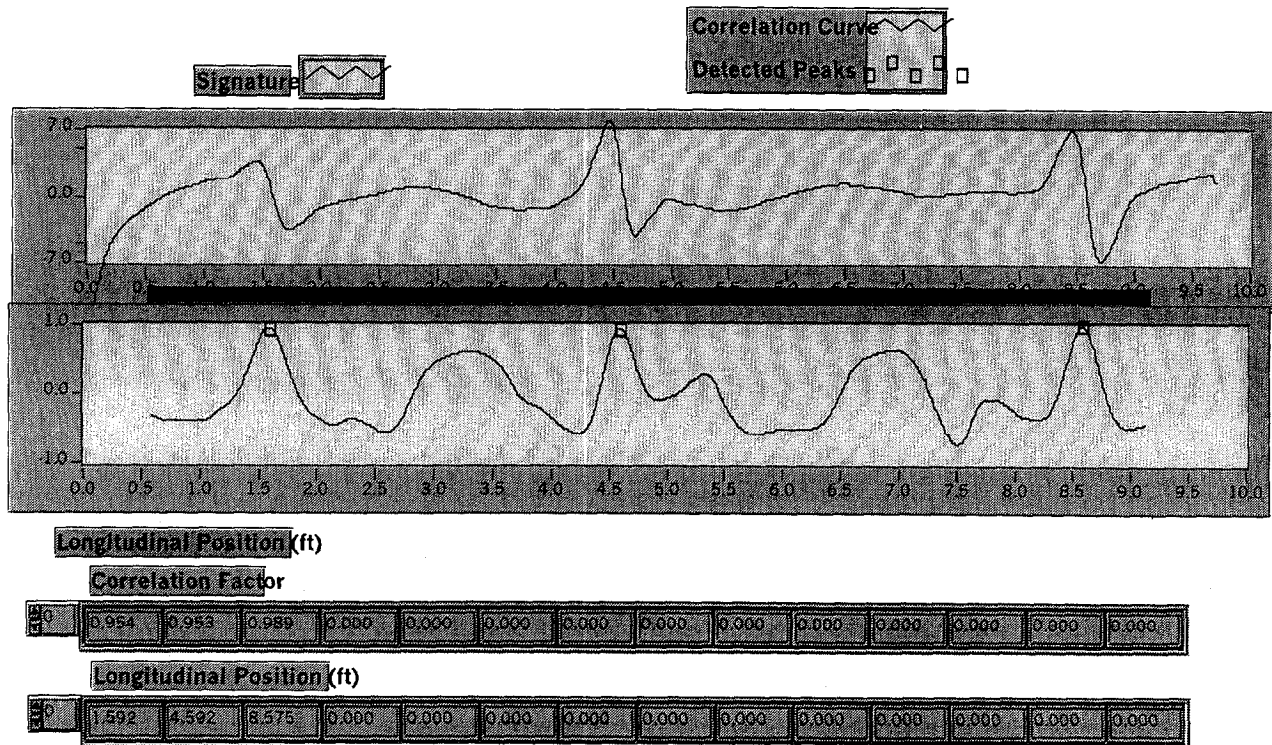


Figure 30. Graphs of a sensor amplitude output and correlation analysis for Cable #2 (distance to magnet/sensor = 51 mm (2 in), 14 adjacent steel cables).

A test was conducted using a prestressing cable with real corrosion (Cable #4). The cable was obtained from a separate study on the corrosion of prestressing steel used for bridge construction. The corrosion of the cable was in the form of pits, causing a cross-sectional loss ranging from 5% to 15%. The cable was placed in the first row of the test beam templates to simulate 51 mm (2 in) of concrete cover. The results of the amplitudes and correlation analysis are shown in figure 31. From the amplitude graph in the figure, the variations of the magnetic field due to the presence of the corrosion pits could easily be seen. A test conducted with an undamaged cable did not show the magnetic field variations observed in figure 31. The results of the correlation analysis showed good agreement with the presence of corrosion pits at the corresponding positions. Corrosion pits equivalent to approximately 10% or more of the cross-sectional area of the cable yielded correlation factors greater than 90%. This is a high correlation value that implies a relatively high degree of reliability in detecting corrosion of prestressing cables under the given condition.

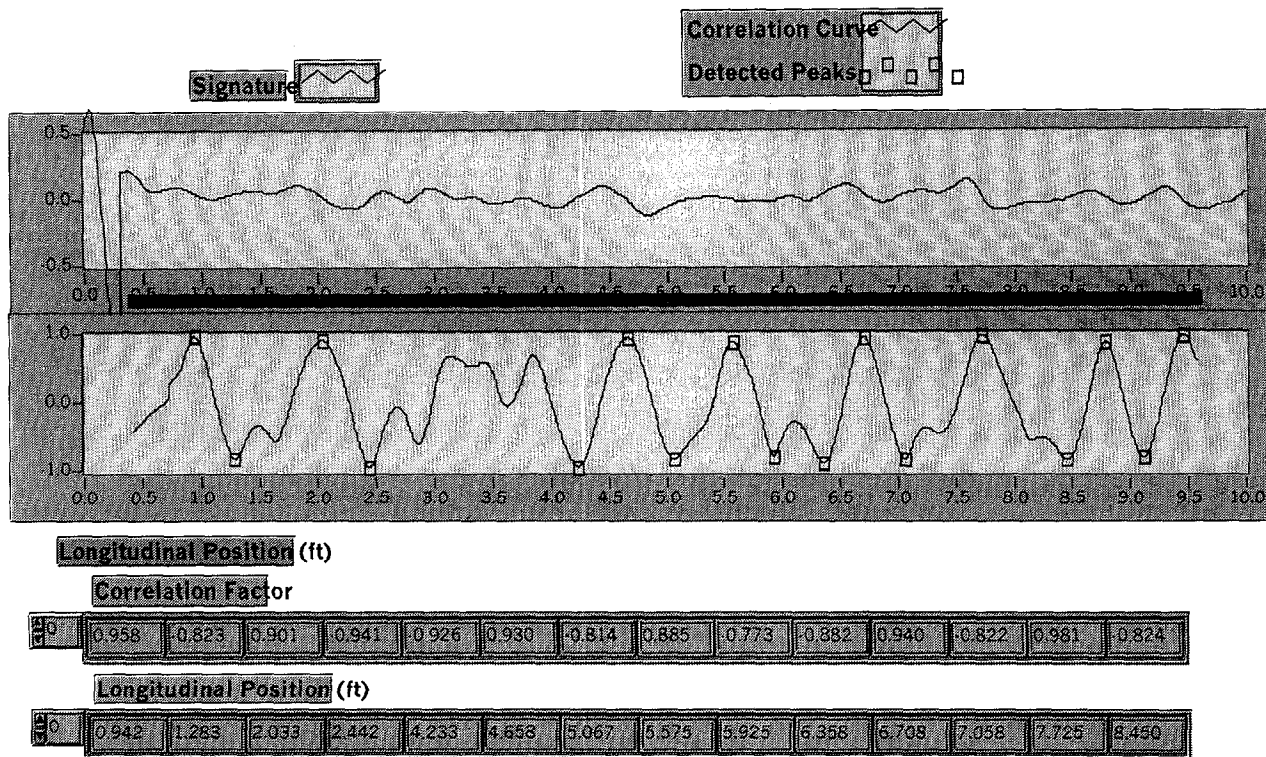


Figure 31. Graphs of a sensor amplitude output and correlation analysis for Cable #4 (distance to magnet/sensor = 51 mm (2 in), no adjacent steel).

FIELD INVESTIGATION

Upon completion of the laboratory investigation, a field study was conducted. The purpose of the field investigation was to evaluate the performance of the beam-rider unit under actual field conditions. The performance of the mechanical, control, and data-acquisition components of the MFL system were assessed in the field. The field test was conducted in the summer of 1998. Representatives from the FHWA (the contracting officer's technical representative), Wisconsin Department of Transportation (DOT), and Construction Technology Laboratories, Inc. were present during the field test. The selected structure for the study was a prestressed I-girder bridge on Interstate I-41 North that crosses over State Street in Milwaukee, Wisconsin. An end span, over a sloped embankment, was chosen for the field test. This provided easy access to the girders and there was no interference with traffic on State Street. The distance between the wheels of the beam-rider unit was adjusted to fit the girders that had a width of 612 mm (24 in). Contract documents for the bridge were obtained from Wisconsin DOT prior to the field test. Structural details for the chosen girders were reviewed to determine the presence and locations of all ferromagnetic materials, including prestressing cables and stirrups, within the girders. A site visit was also made prior to the day of the test to assess all existing conditions and to verify the girder sizes and lengths.

Interior girders with diaphragms on both sides were selected for the test. Figure 32 shows the overall layout of the structural framing for the span used for the MFL test.

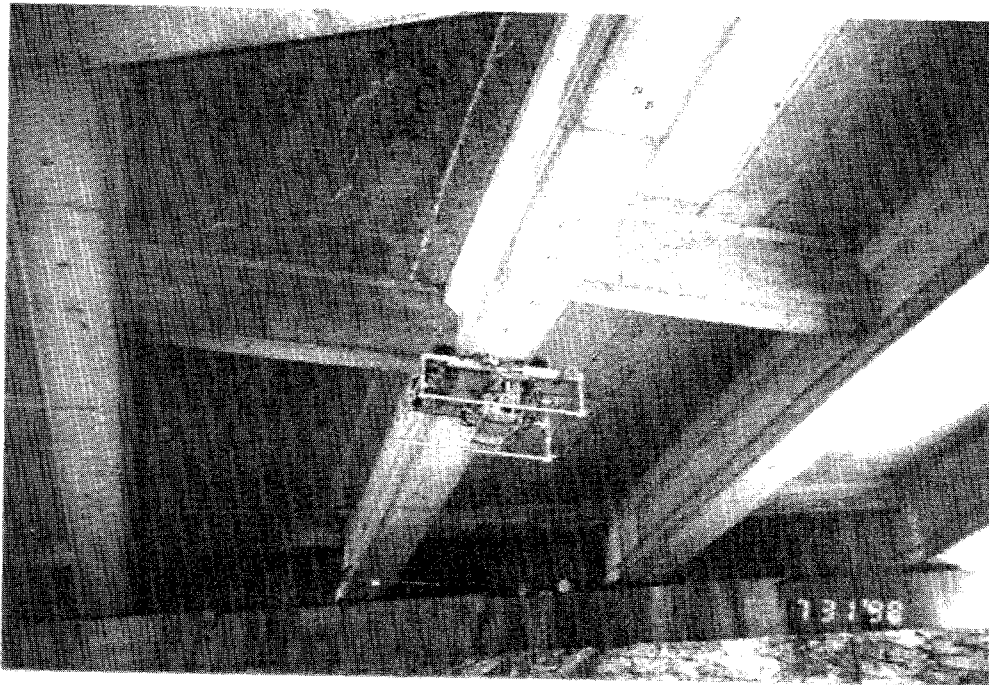


Figure 32. Overall layout of the structural framing of the bridge span tested by the MFL system.

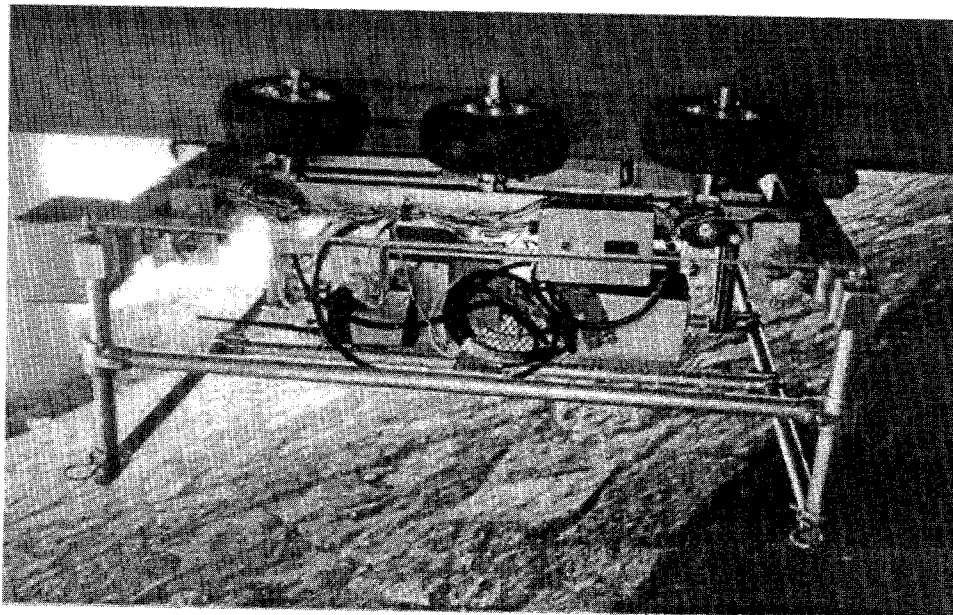


Figure 33. Close-up view of the beam-rider unit on a concrete girder.

One large safety clamp was installed at each end of the test girder. The clamps were used to allow attachment of a set of safety cables that were guided through four safety eye-bars on the beam-rider unit. This provided a measure of assurance to hold the beam-rider unit in the air in case of an unforeseen detachment of the unit from the girder. The stem of each safety clamp was also used for attaching an aluminum plate to provide vertical surfaces with which the limit switches of the beam-rider unit could be in contact. Figures 33 and 34 show a close-up view of the beam-rider unit on the test girder and the details of the safety clamps and safety cables.

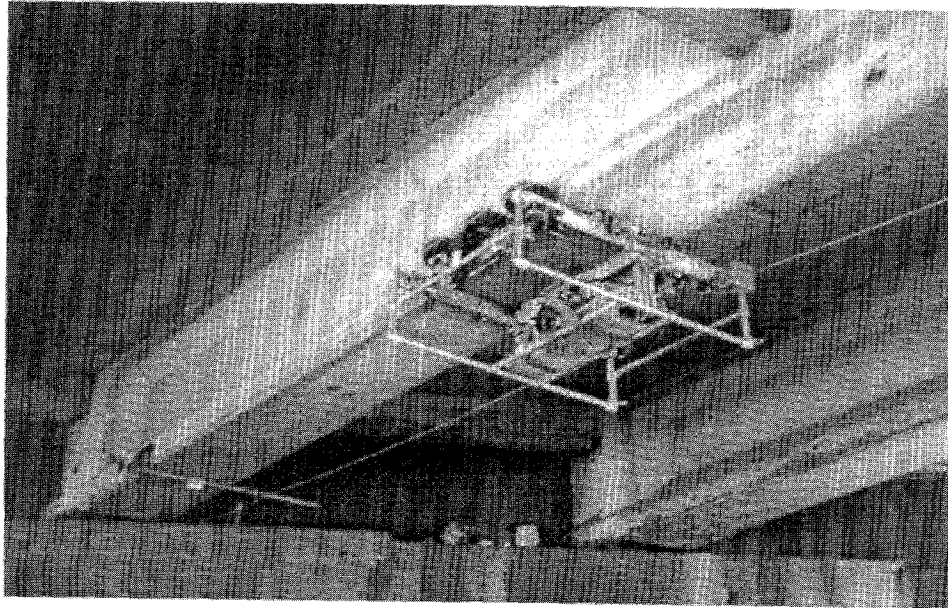


Figure 34. View of the beam-rider unit with the details of the safety clamps and cables.

Tests were conducted for two girders within the same span. For each girder, multiple paths, or tracks, of data needed to be recorded since the width of the bottom flange of the girder was three times the width of the magnet/sensor assembly in the beam-rider unit. The first test was initiated with the edge of the sensing-head unit positioned flush with the edge of the girder. At the completion of this data path, data for the first track was recorded. The test was continued for the second and third tracks by moving the sensing-head unit to the appropriate position across the width of the girder. The data for the three tracks was then placed in a single data file at the conclusion of the girder test. A typical graph of the amplitude output from a single Hall-effect sensor, along with the results of the correlation analysis, is shown in figure 35. Only a 3.0-m (10-ft) length of the data is presented in the figure. In the amplitude graph, repeated magnetic field variations due to the presence of the girder stirrups can be seen. The correlation results are also presented in a graphical form for the data length shown. The high correlation values observed in the data could be attributed to the presence of tie-down devices, other ferromagnetic parts within the girder, or flaws in the prestressing steel. No effort was made to verify the location of the stirrups and the high correlation values from other sources in the girder.

The primary purpose of the field test was to demonstrate the use of the system under field conditions. Due to lack of time and funds, no extensive evaluation of the data and/or verification with the existing

conditions could be made. As recommended earlier, an additional study may be initiated to address a comprehensive system evaluation.

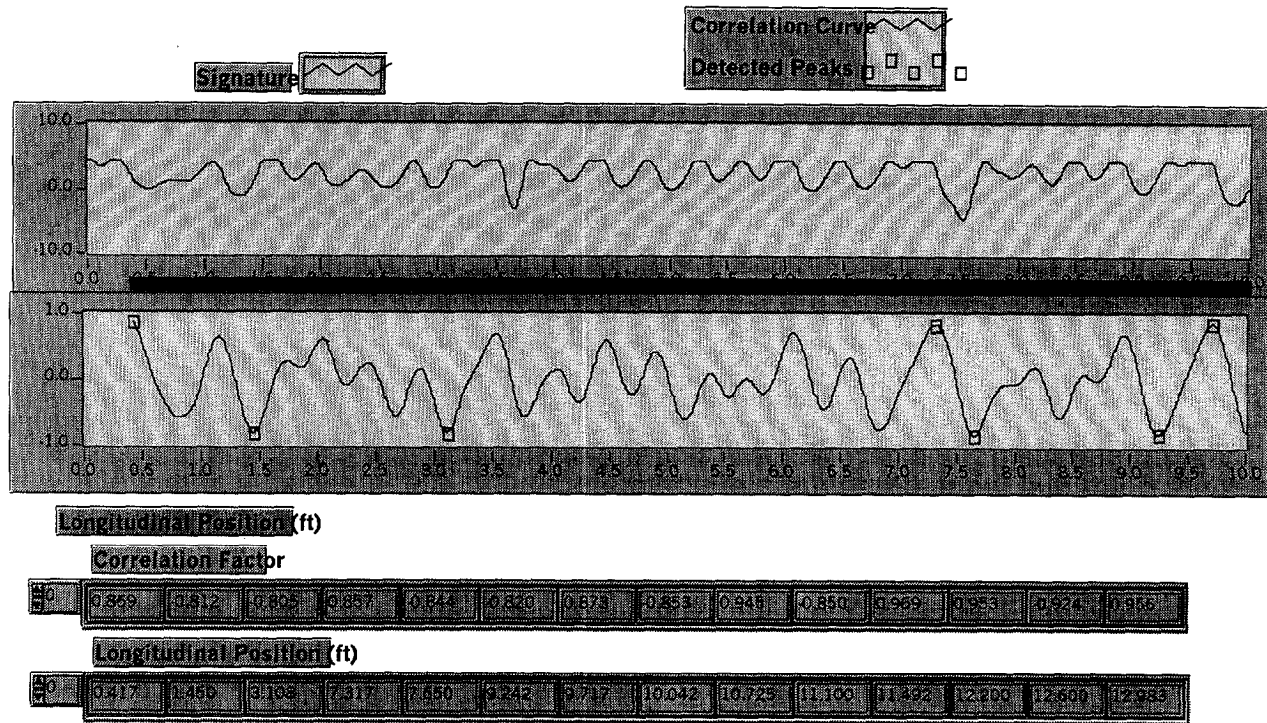


Figure 35. Graphs of a sensor amplitude output and correlation analysis for field test data.

The results of the amplitude outputs for two adjacent tracks from the seven sensors, located on the upper sensor board inside the sensor enclosure of the sensing-head unit, are shown in figure 36. As seen in the figure, the results are for a 9.1-m (30-ft) length of the girder tested. Variations of the magnetic field shown in the figure indicate the presence of the stirrups and their spacing at various locations along the length of the girder.

Figure 37 shows a three-dimensional graph for a 3.0-m (10-ft) section of the girder and for two adjacent tracks. Compared with the graph in figure 35 or 36, it can be seen that the evaluation of the three-dimensional view of the magnetic field is a more advantageous approach for interpreting the recorded data under real conditions. The presence of the stirrups is evident in the graph in the form of regularly spaced peaks along the length of the girder. Irregular individual peaks stand out in the graph and could be indicators of flaws or some discontinuities (such as tie-down devices or other ferromagnetic artifacts) in the girder at their associated locations. These irregular peaks within the graph must be investigated further through examination of contract drawings and/or additional signal analysis to determine if they are related to the presence of some ferromagnetic components within the girder or to flaws. Additional investigation of MFL data based on three-dimensional magnetic field construction must be performed to fully realize the potential of the approach.

Field test/track 1&2/30ft

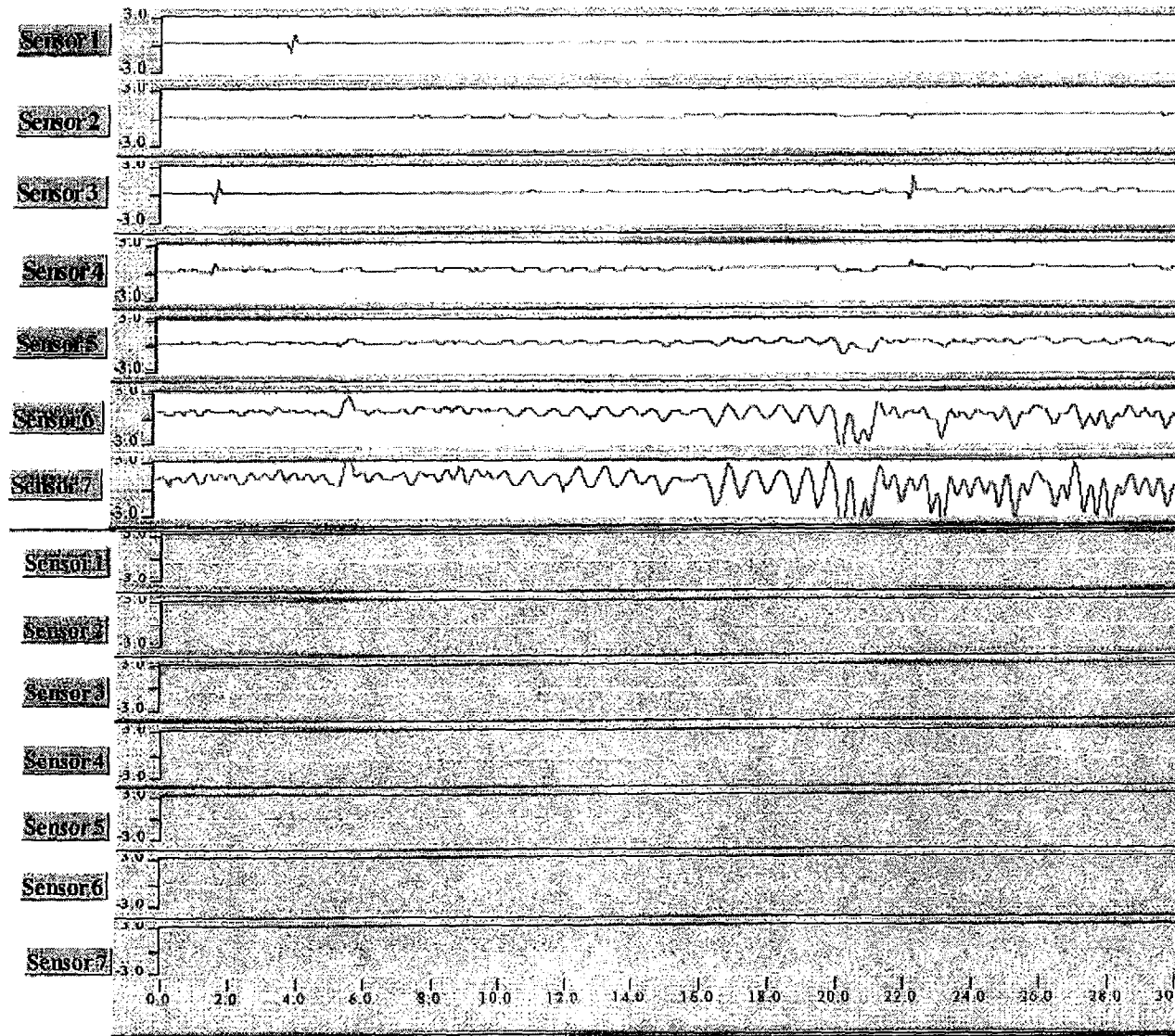


Figure 36. Amplitude data for tracks 1 and 2 of a girder during field testing.

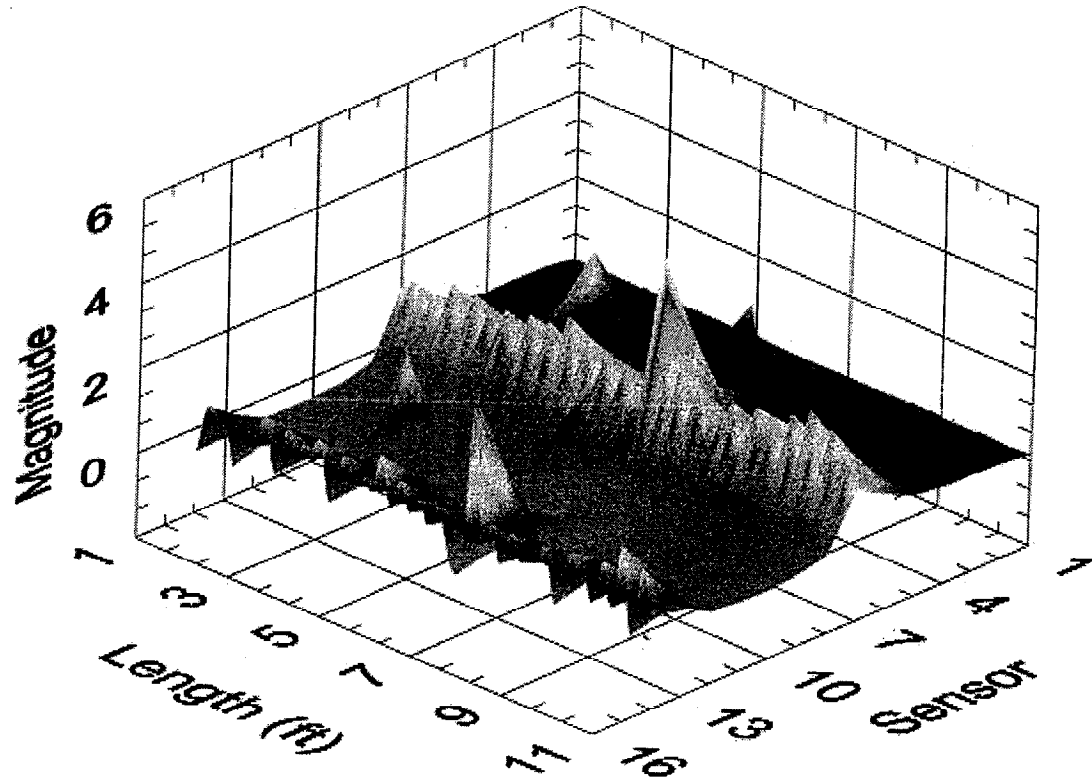


Figure 37. Three-dimensional graph for tracks 1 and 2 of a girder during field testing (only 3.0m (10 ft) of data is shown for clarity).

Two separate tests were intentionally conducted along the same track on a girder to assess the reproducibility of the data recorded. The results of the sensor outputs were later compared and it was found that they were identical. This, as it was expected, showed the capability of the system to yield reproducible data for the same girder under similar conditions. This capability is essential for the system since it would make it possible to perform periodic inspection of concrete members over time. If test conditions are kept the same for two separate MFL tests at different times, which is possible, a difference in the results of the two tests could lead to the conclusion that a flaw was created since the time of the first test.

ANALYSIS METHODS AND SUMMARY OF FINDINGS

Data Interpretation

During and after the completion of the laboratory evaluation of the MFL system, efforts were made to assess and improve the data interpretation capability of the system. The data interpretation methods used included visual examination of the acquired data; performing other data-processing procedures, such as the correlation and profile analysis; and determining the optimum values for the necessary analysis parameters that affect the accuracy of the results. The process of visual examination included assessing the characteristic shape of the flaw signals. Post-processing procedures used in the study included using the appropriate post-processing software to ascertain needed information from data files that were recorded during a test. For example, to minimize the magnetic masking effect of stirrups on a flaw signal, the operator may utilize a post-processing file that subtracts the outputs of two sensors located along a vertical line of a known distance.

Post-Processing Methods for the Recorded Data

The most common, and straightforward, data evaluation method is the visual analysis of recorded data through the use of a graph of sensor amplitude output. This method of interpretation utilizes the operator's knowledge of flaw signal attributes to locate potential flaws. This procedure is most useful in areas of low secondary reinforcement or when the flaws are large (greater than approximately 14% loss of section). Signals from secondary reinforcement such as stirrups and chairs can mask the flaw signal or make it appear that flaws are present where there are none.

Correlation analysis is a method of post-processing data whereby flaws are identified based on using mathematical models for them. This is done by utilizing a mathematical curve that represents the ideal shape of a flaw signal. These models are constructed based on the results of experiments from different flaw sizes and shapes. The mathematical flaw signal is compared with various segments of the recorded data over the entire length of the data file. The correlation process determines the degree with which the two curves match in terms of a correlation percentage. The user must determine and specify the parameters that describe the flaw of interest. The parameters for the flaw model that need to be pre-determined and specified are the overall length, N , and the peak-to-peak separation, B . The mathematical relationship defining the flaw model is given by the following relationship:

$$Y = \frac{-AX}{(X^2+B^2)^{\frac{5}{2}}}$$

Where Y is the signal amplitude as a function of position (X), B is the peak-to-peak separation distance, and A is the peak-to-peak signal amplitude. These parameters are described in figure 38. Note that X varies from $-(N-1)/2$ to $(N-1)/2$ points, which defines the length of the signal. After the correlation analysis is performed, the values of the correlation factors are plotted as a function of the position. A perfect match of the mathematical model with a segment of the recorded data will yield a correlation factor, or index, of 1.0 or 100%. An exact inverse of the mathematical signal will yield a correlation index of -1.0 or -100%.

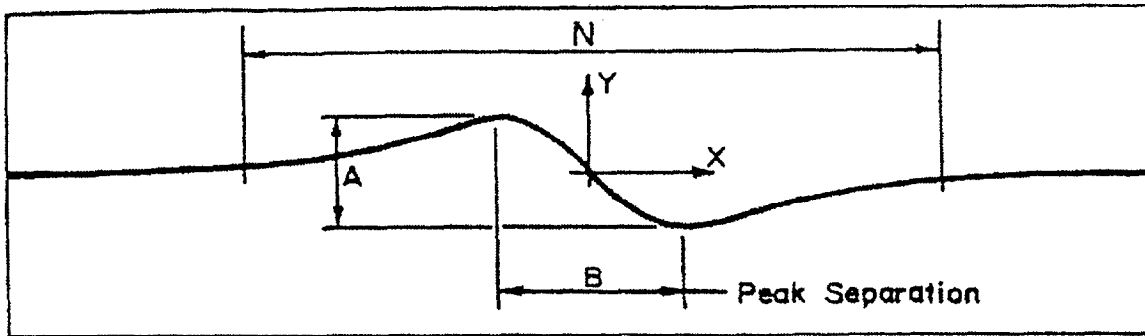


Figure 38. Required parameters for the correlation analysis.

Another valuable post-processing tool is the use of subtracted data. This process utilizes the data from two sensors located above and below one another. The data output from the lower sensor is subtracted from the data output of the upper sensor. The advantage to this procedure is that the user can minimize the influence of strong signals resulting from stirrups.

A two-dimensional profile analysis procedure can be used to develop a two-dimensional curve representing the amplitude of the MFL across the width of a girder for any point along the length of the girder. This is useful in determining whether or not a signal may be from a stirrup or a flaw. Since stirrups usually span the entire width of the flange of a girder, the outputs from all sensors in the array across the width will be of nearly the same amplitude. In contrast, the signal amplitude from a flaw will be strongest at the sensor located directly below the flaw. It will be weaker at the sensors located on either side of the flaw. Therefore, in profile, the signals produced from a stirrup should create a relatively flat horizontal line, whereas the signal from a flaw should have a distinct peak at the transverse flaw location.

The use of a graph showing the three-dimensional magnetic field variations is a useful method of post-processing for the MFL data. It combines the capabilities of the visual examination method along the data length with the two-dimensional profile analysis technique. The method makes it easy to identify stirrups or other discontinuities in a concrete girder.

The amplitude of a flaw signal is measured in volts. The voltage is a function of the amount of flux that fringes or leaves the magnetized reinforcing steel. The Hall-effect sensors detect the fringing flux. The total amplitude is an indicator of the size of the flaw if the relative location of the steel is known. From

the MFL test data, and depending on the amount of concrete cover and the location of the steel, the user may make an estimate of the flaw size. Examples of the change in the MFL signal amplitude can be seen in table 2. The results shown in the table are for a specific instrumentation gain setting.

It is important to understand the effect that additional steel has on the signals received from a flawed tendon. Additional steel can be thought of as masking steel. Therefore, the additional steel absorbs some of the magnetic flux. It, therefore, lowers the amount of flux traveling in the flawed tendon. Lower magnetic field levels reduce the amount of flux that will leave the steel when it encounters a flaw in the form of a corrosion pit or fracture.

Table 2. Signal amplitudes for a single prestressing tendon at different cover depths.

Single Prestressing Tendon Test		
Concrete Cover mm (in)	% Section Loss	Signal Amplitude (volt)
51 (2)	7	1.5
51 (2)	14	2
51 (2)	29	4
51 (2)	43	6
51 (2)	57	11
51 (2)	71	13
51 (2)	100	28
89 (3.5)	7	0.25
89 (3.5)	14	0.5
89 (3.5)	29	1.5
89 (3.5)	43	2.5
89 (3.5)	57	4.5
89 (3.5)	71	5.5
89 (3.5)	100	11.5
128 (5)	7	0
128 (5)	14	0.4
128 (5)	29	1
128 (5)	43	1.5
128 (5)	57	2.5
128 (5)	71	3.5
128 (5)	100	7.5

Correlation Parameters Based on Test Results

The correlation analysis parameters, B and N, were evaluated during the laboratory investigation phase of the study. Optimum values for B and N parameters were obtained through experimentation. Optimum values of B and N are defined as values that result in the highest possible correlation factor for a specific flaw. A systematic approach was used to examine every possible combination of B and N values. The determined optimum values were grouped together such that the values in the group would cover a small range of flaw sizes. The optimum B and N values found in the laboratory study are shown in table 3. The optimum B and N values were taken from the results of 18 specific tests of cables with known flaw

conditions. Each test result was evaluated using the post-processing software for the MFL system. Approximately 25 combinations of B and N were used for each test to achieve the optimum values.

The optimum values of B and N may be used for post-processing of the MFL data obtained from field testing of prestressed concrete members. By using B and N values from the given data, one could arrive at an estimate for the extent of loss of section in the prestressing steel used in prestressed concrete members. Additional studies will be required to construct predictive graphs to facilitate the use of the proposed approach.

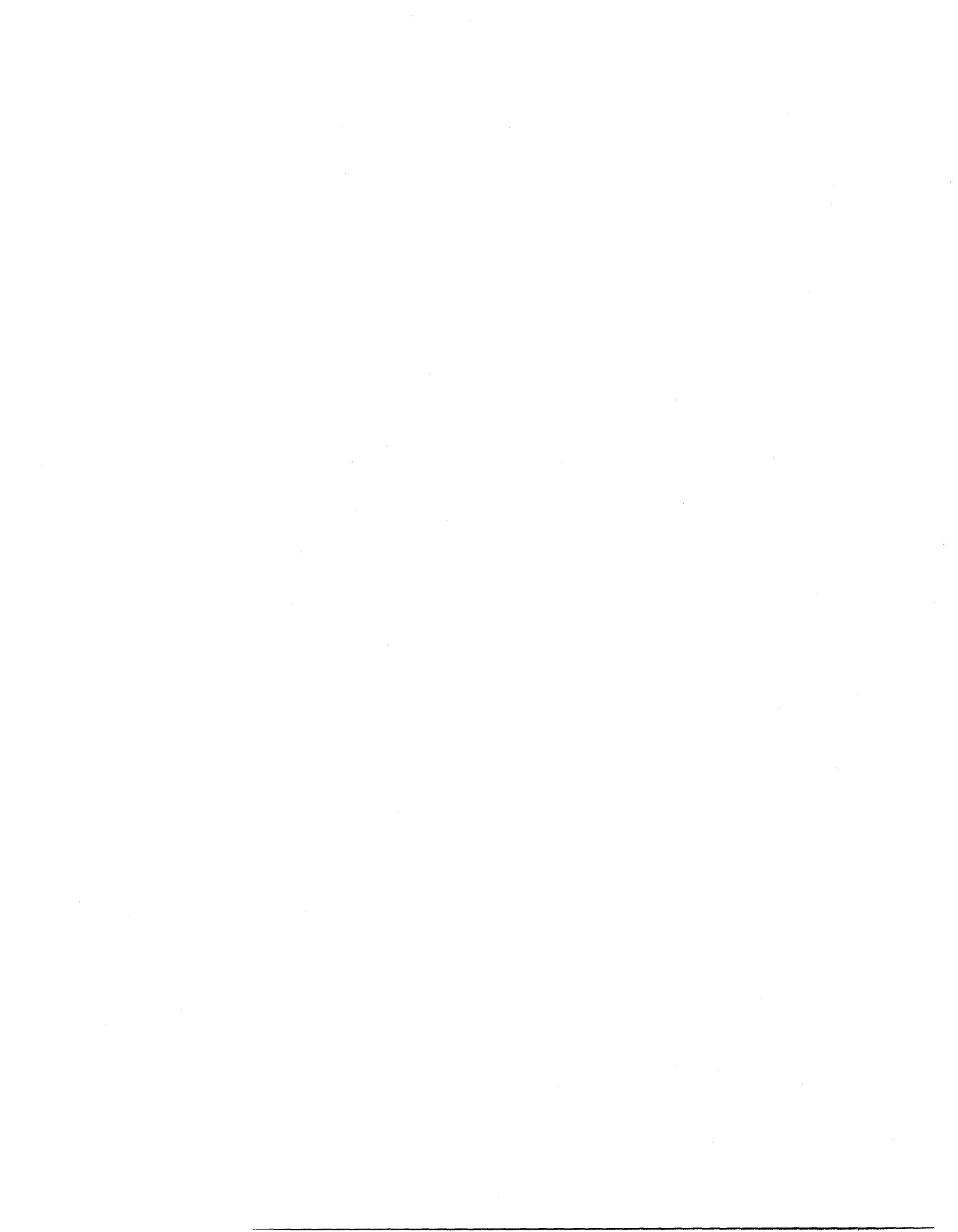
Table 3. Optimum B and N values for post-processing of MFL data.

% Area Loss for a Single Cable Test

Concrete Cover	7%, 14%, 29%	43%, 57%, 71%	100%
51 mm (2 in)	B=28, N=101	B=28, N=111	B=28, N=141
89 mm (3.5 in)	B=36, N=141	B=32, N=131	B=32, N=141
128 mm (5 in)	B=36, N=141	B=32, N=131	B=32, N=141

% Area Loss for a Cable with a 14 Masking Cables Test

Concrete Cover	7%, 14%, 29%	43%, 57%, 71%	100%
51 mm (2 in)	B=28, N=101	B=28, N=141	B=28, N=141
89 mm (3.5 in)	B=28, N=101	B=32, N=141	B=32, N=141
128 mm (5 in)	B=28, N=101	B=36, N=141	B=36, N=141



CHAPTER 7. CONCLUSIONS

This report summarizes the results of findings and details of the development of a new nondestructive evaluation system based on the concept of magnetic flux leakage (MFL). The basic methodology is based on introducing a dc magnetic field in close proximity of the prestressing or post-tensioning steel and monitoring the variations of the field due to loss of cross-sectional area of steel from corrosion or fracture.

Two strong permanent magnets are used to provide the required magnetic field for the MFL system. A set of 10 Hall-effect sensors are used in the system to measure the variations in the magnetic field due to the presence of flaws in prestressing or post-tensioning steel. Software was developed to acquire and analyze the MFL data as well as to control all hardware, including mechanical and electrical components of the system. The system is designed and fabricated to offer ease of use during the field operation. The operation of the system includes attaching the structural frame to a test beam and conducting a test by controlling the frame by a notebook computer from a remote site via wireless communication.

During both the laboratory and field investigations, it was demonstrated that the installation and operation of the MFL system were successful. System installation on a test beam may be accomplished easily and in a time period not longer than a few minutes. During the laboratory study, steel prestressing strands with partial localized cross-sectional area losses from 7% to 71% were used as test specimens. Also, prestressing strands with real corrosion were used for the same purpose. It was found that the MFL system is capable of detecting a 7% reduction in the cross-sectional area of the strands. This capability was demonstrated for the strands that were placed at a distance of up to 128 mm (5 in) from the magnet and sensor assembly of the system. A field demonstration was conducted that showed that installation and operation of the MFL system were successful.

It is recommended that additional laboratory and field investigations, beyond this study, be conducted with the use of the new MFL system in order to fully evaluate its capabilities and limitations. This would also facilitate the establishment of a more comprehensive database that can enhance the data interpretation capability and the overall reliability of the system.



Specifications for the Permanent Magnets

DAN3 HELMHOLTZ MAGNETIC PROPERTY EVALUATION 7-05-88
 Feb 4 1987-Excel version PC calculation precision improved
 & Normal Bd*Hd corrected. RES/RAW

Customer: University of Wisconsin

Tested by: RAW
 Test date: 2/15/87
 Part Number: PMW96-1206-4
 Inventory #: P383HRR0260B

Small PC coil HCC .22362 Amps/gauss
 Large PC coil HCC .09887 Amps/gauss
 24" Chair Coil" HCC 0.02275 Amps/Gauss

Coil Constant conversions
 CC coil Number Use this constant in sheet

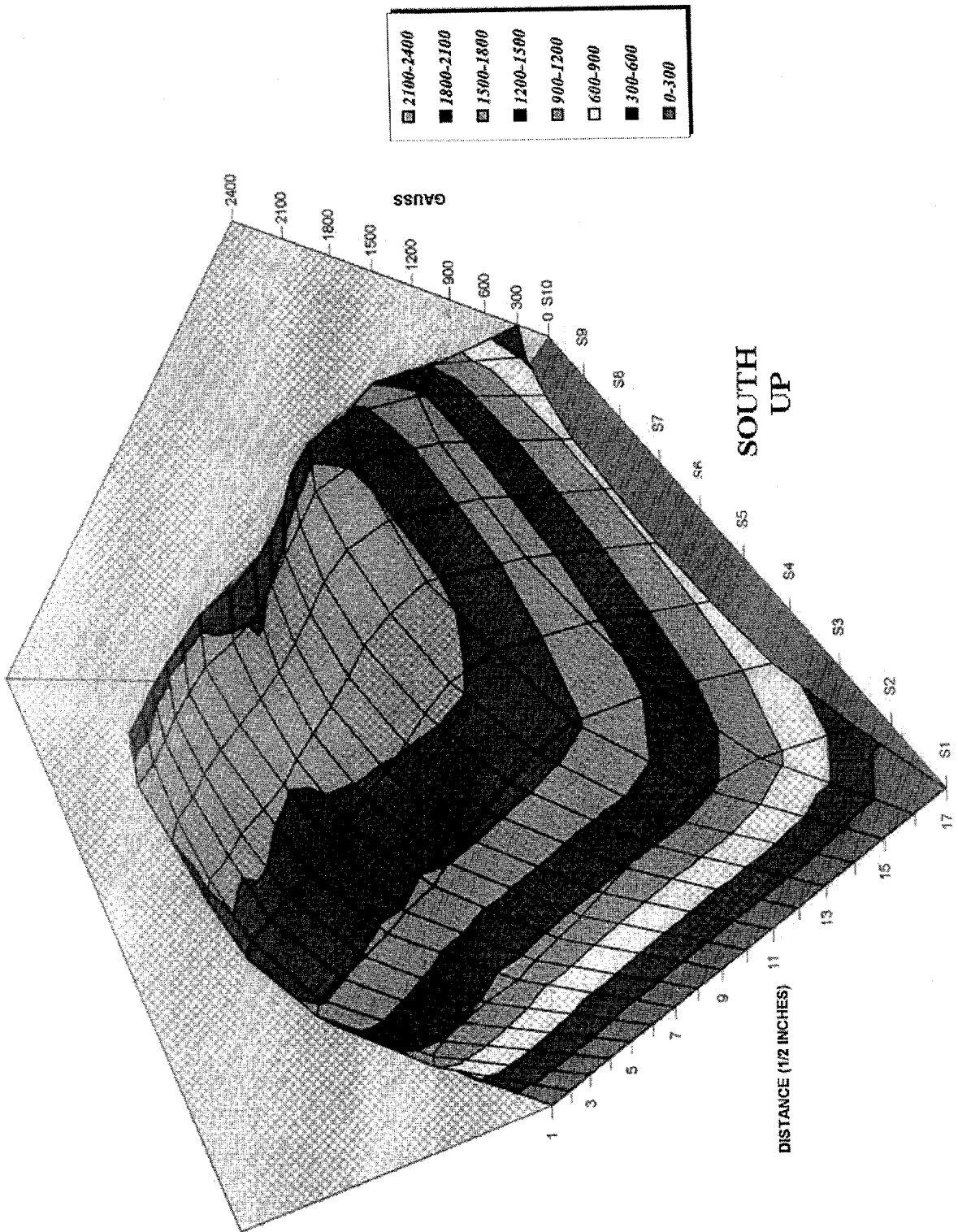
26.081 0.00518 0.1350996 Amps/gauss

Enter dimensions in inches:

	1	2	3	4	5	6	7	8	9	10	11	12	13	14	15	16
If Rectangle (ie Dia = 0):																
WIDTH =	1.89	1.89	1.89	1.99	1.99	1.99	1.99	1.99	1.99	1.99	1.99	1.99	1.99	1.99	1.99	1.99
THICKNESS =	1.89	1.89	1.89	1.99	1.99	1.99	1.99	1.99	1.99	1.99	1.99	1.99	1.99	1.99	1.99	1.99
	1.00	1.00	1.00	1.00	1.00	1.00	1.00	1.00	1.00	1.00	1.00	1.00	1.00	1.00	1.00	1.00
If Cylindrical (ie W & H = 0):																
DIAMETER =	5	0.50	0.50	0.50	0.50	0.50	0.50	0.50	0.50	0.50	0.50	0.50	0.50	0.50	0.50	0.50
LENGTH #/HT=	2	1.498	1.498	1.498	1.498	1.498	1.498	1.498	1.498	1.498	1.498	1.498	1.498	1.498	1.498	1.498
L factor =	1	1	1	1	1	1	1	1	1	1	1	1	1	1	1	1
(L factor = .7 for Alnicos, 1.0 for BaFe & RECo)																
Ur =	1.1	1.05	1.05	1.05	1.05	1.05	1.05	1.05	1.05	1.05	1.05	1.05	1.05	1.05	1.05	1.05
HCC (A/g) =	0.09887	0.09887	0.09887	0.09887	0.09887	0.09887	0.09887	0.09887	0.09887	0.09887	0.09887	0.09887	0.09887	0.09887	0.09887	0.09887
(HCC is Helmholtz Coil Constant in Amps/gauss.)																
2 X Mom =	70.665835	19.84428	19.84428	19.84428	19.84428	19.84428	19.84428	19.84428	19.84428	19.84428	19.84428	19.84428	19.84428	19.84428	19.84428	19.84428
Scale 10*(X)	6	5	5	5	5	5	5	5	5	5	5	5	5	5	5	5
(Scale is Fluxmeter multiplier power)																
Area =	19.635	3.960	3.960	3.960	3.960	3.960	3.960	3.960	3.960	3.960	3.960	3.960	3.960	3.960	3.960	3.960
Magnet vol =	39.270	5.932	5.932	5.932	5.932	5.932	5.932	5.932	5.932	5.932	5.932	5.932	5.932	5.932	5.932	5.932
P.C. =	1.073	2.112	2.112	2.112	2.112	2.112	2.112	2.112	2.112	2.112	2.112	2.112	2.112	2.112	2.112	2.112
Intrinsic properties:																
Bdi =	8516	12429	12519	12602	12691	12744	12834	12834	12563	12525	12500	12480	12634	12672	12480	12749
Br =	8830	12629	12720	12804	12895	12874	12837	12837	12765	12726	12700	12681	12681	12837	12876	12681
Hc (SL) =	6209	12028	12114	12195	12281	12071	12225	12225	12157	12120	12096	12077	12225	12263	12077	12337
B*H Max =	10.603	37.974	38.523	39.036	39.592	38.248	39.234	39.234	38.798	38.562	38.405	38.287	39.234	39.472	38.287	39.951
Normal properties:																
Bd =	3373	8435	8496	8552	8613	8466	8574	8574	8526	8500	8483	8470	8574	8600	8470	8652
Hd =	3143	3994	4023	4049	4078	4008	4060	4060	4037	4025	4017	4010	4060	4072	4010	4087
Bd*Hd Max =	10.602	33.691	34.177	34.632	35.126	33.934	34.808	34.808	34.422	34.212	34.073	33.968	34.808	35.020	33.968	35.445
Equiv R =	2.5	1.1227373	1.1227373	1.1227373	1.1227373	1.1227373	1.1227373	1.1227373	1.1227373	1.1227373	1.1227373	1.1227373	1.1227373	1.1227373	1.1227373	1.1227373
PC on Steel=	2.147	4.224	4.224	4.224	4.224	4.224	4.224	4.224	4.224	4.224	4.224	4.224	4.224	4.224	4.224	4.224
	4516.1527	10114.606	10187.41	10255.014	10327.818	10151.008	10281.015	10281.015	10223.812	10192.61	10171.809	10156.208	10281.015	10312.217	10156.208	10374.621
Lbs pull =	231.080	233.760	237.140	240.300	243.720	235.450	241.520	241.520	238.840	237.380	236.410	235.690	241.520	242.980	235.690	245.930
Efficiency =	5.884	39.405	39.975	40.508	41.084	39.690	40.713	40.713	40.261	40.015	39.852	39.730	40.713	40.959	39.730	41.457
(Eff = Lbs of pull/cu. in. of magnet)																

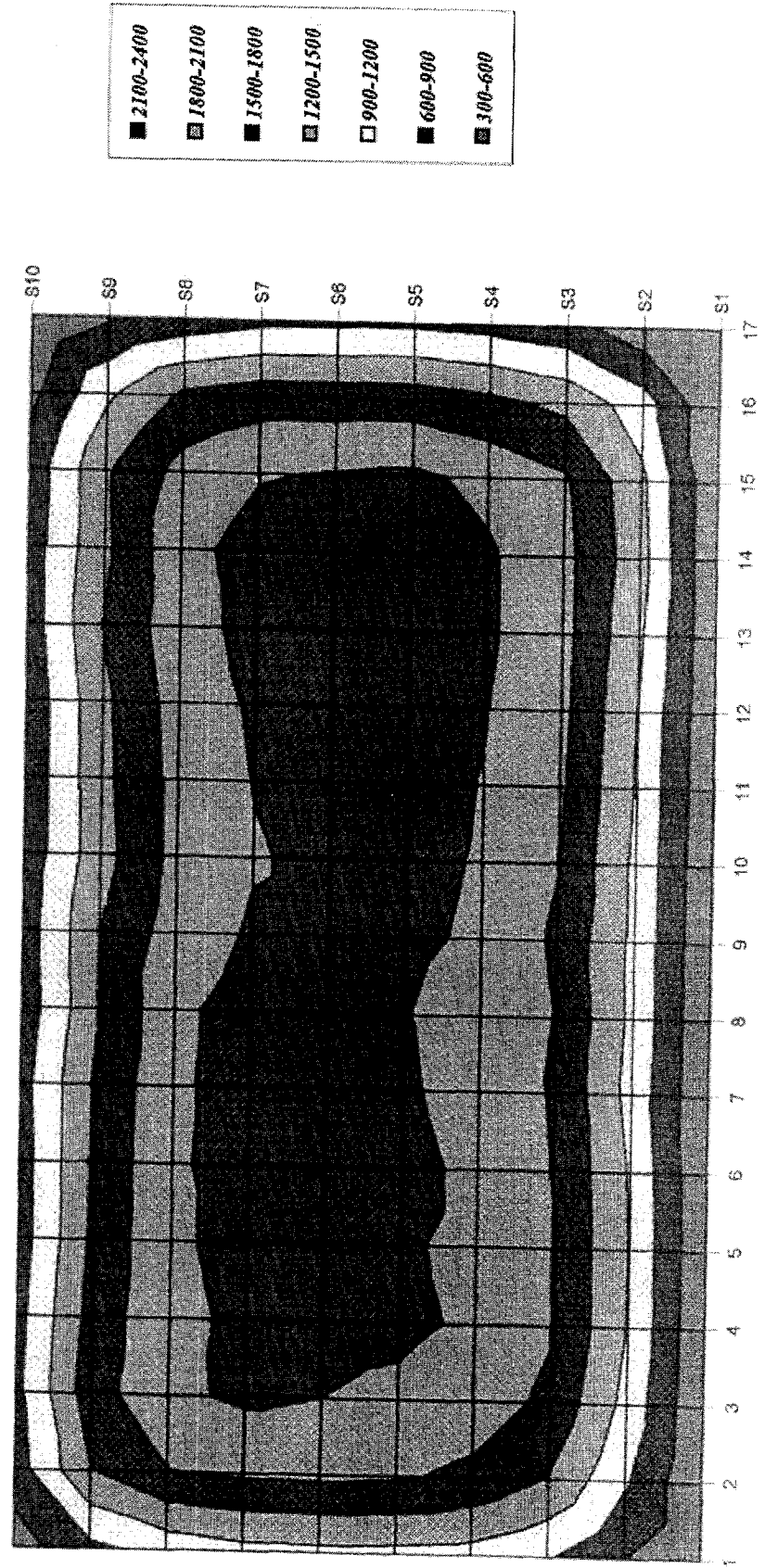
APPENDIX A. TECHNICAL DATA FOR PERMANENT MAGNETS

Gauss Readings at a Plane 0.4675" From Top of Magnet



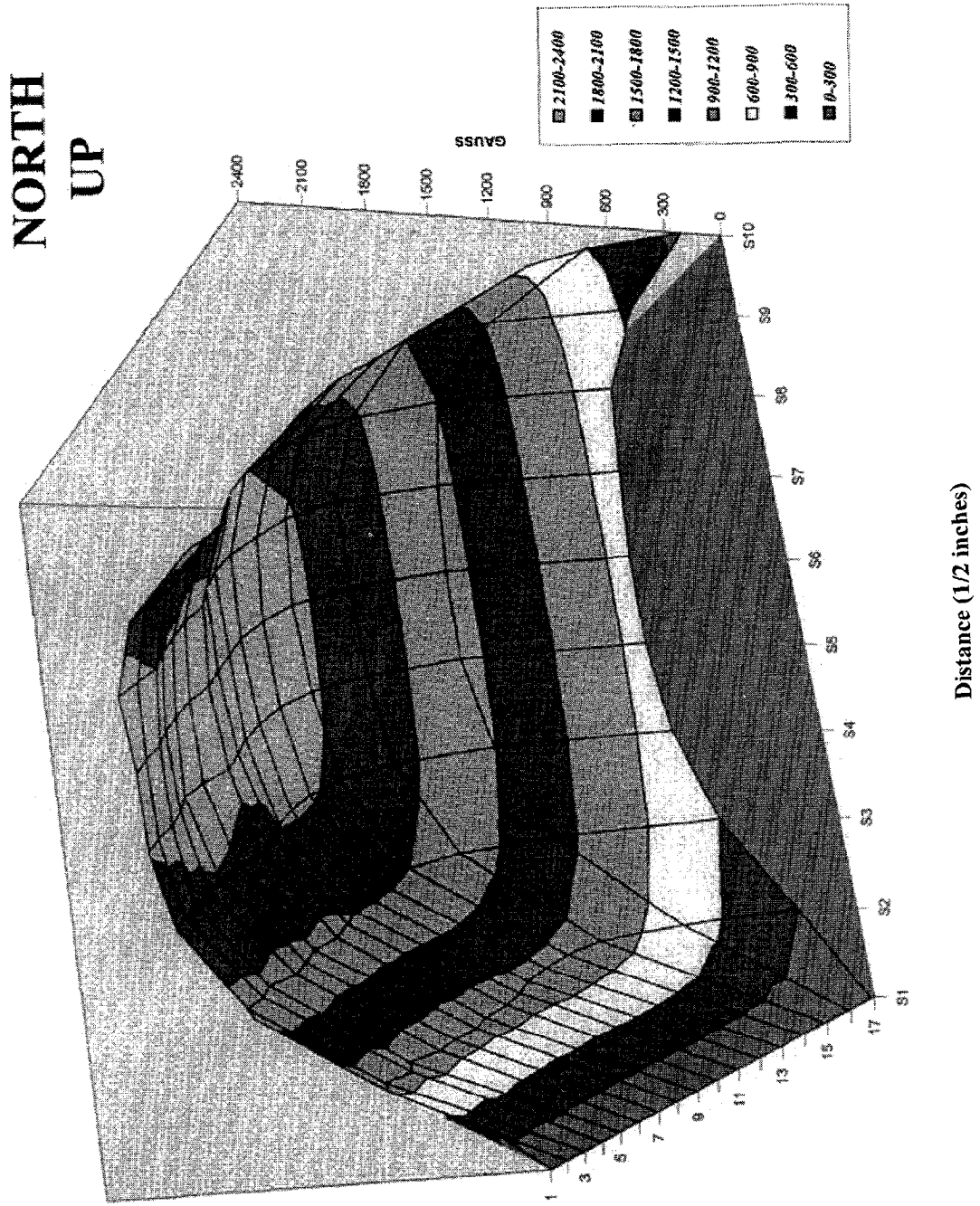
Overhead View of Gauss Readings at a Plane 0.4675" From the Top of the Magnet

SOUTH
UP



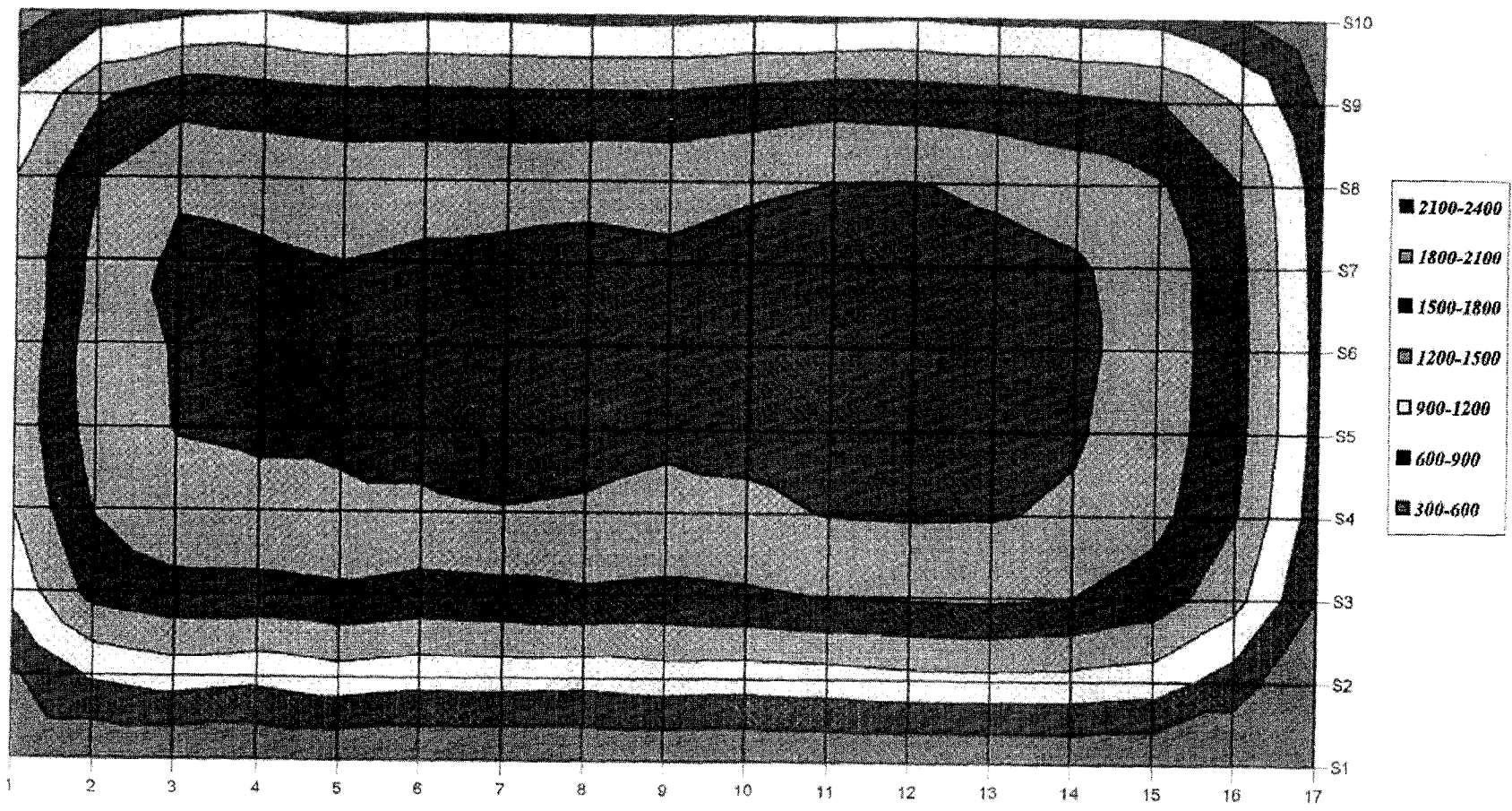
Distance (1/2 inches)

BOX II - Gauss at a Plane 0.4675" From the Top of the Magnet



BOX II - Overhead View of Gauss Readings at a Plane 0.4675" From the Top of the Magnet

**NORTH
UP**



71

Distance (1/2 inches)



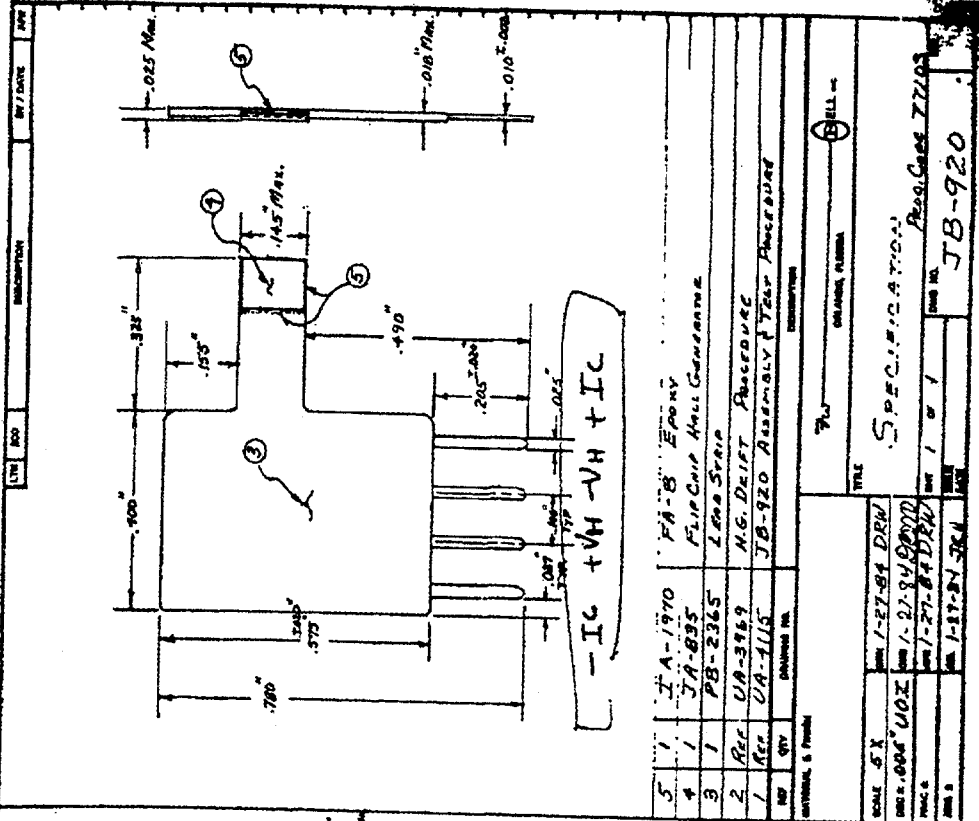
APPENDIX B. TECHNICAL DATA FOR HALL-EFFECT SENSORS

Hall-Effect Sensor Schematic and Specification

Electrical

- R_{in} (Input Resistance) 30 Ω - 120 Ω
- R_{out} (Output Resistance) 70 Ω - 300 Ω
- V_{DD} (Measurement Voltage) (20.0 to 10mA) 4 mV MAX.
- V_{E} (Magnetic Sensitivity) 8-13mV/10mA-KG
- I_{max} (Maximum Continuous Output Current) 70mA
- BT (Near Temperature Coefficient of V_H) (mV/°C) max. -0.07%/°C
- o_c (Near Temperature Coefficient of Resistance) (20 to 100°C) 0.10%/°C
- R_{G} (Gatekeeper Resistance, Measured at Ambient) 0.8°C/mW
- R_{B} (Minimum Resistance, Measured at Ambient) 0.09°C/mW
- Operating Temperature Range... -55°C to +100°C
- Storage Temperature Range... -55°C to +120°C

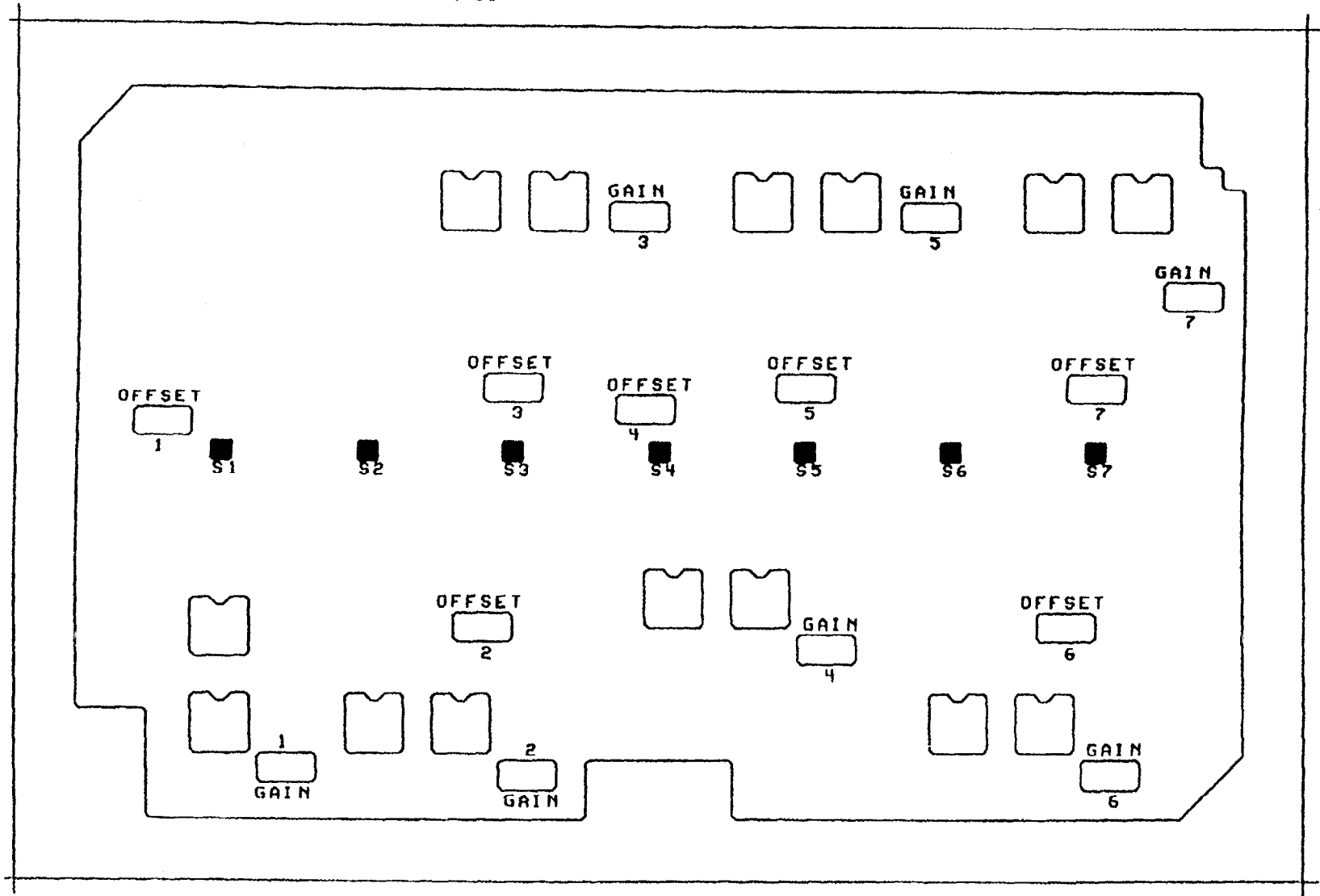
DRIFT TEST PER UA-3969 (U.G. DRIFT TEST PROCEDURE)



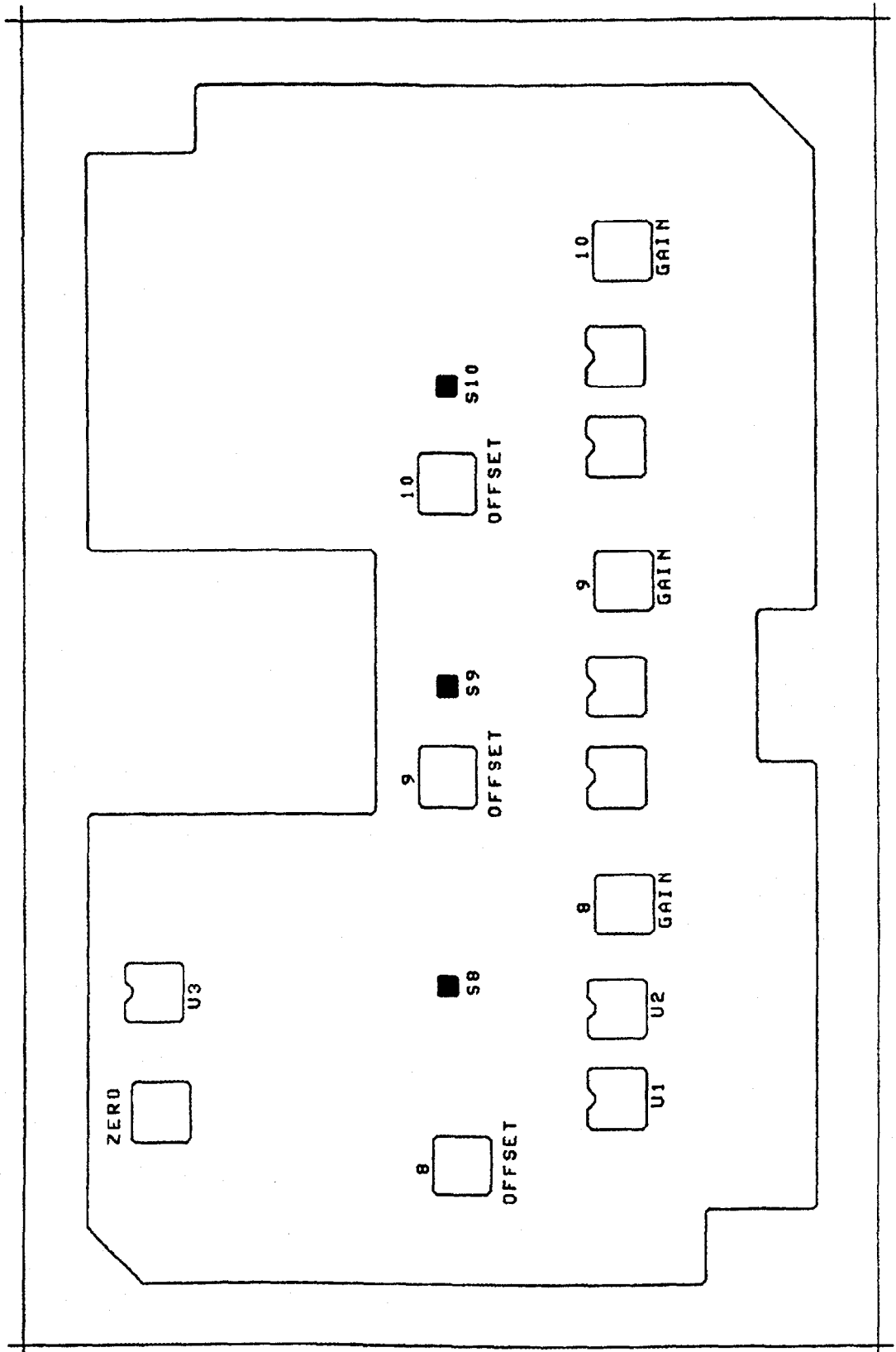
5	1	JA-1970	FA-B Epoxy
4	1	JA-895	Flip Chip Hall Generator
3	1	PB-2365	Lead Strip
2	Rev	UA-3969	M.G. DRIFT PROCEDURE
1	Rev	UA-1115	JB-920 Assembly & Test Procedure

DATE: 1-27-84
 SCALE: 5X
 DRAWN: UOZ
 CHECKED: UOZ
 TITLE: SPECIFICATION
 PART NO: JB-920
 REV: 1 of 1
 PROJ: 77108
 DESIGNED BY: 1-27-84 JRM
 DRAWN BY: 1-27-84 DRW
 CHECKED BY: 1-27-84 DRW
 APPROVED BY: 1-27-84 DRW

**Printed Circuit Board Layout for the Hall-Effect Sensors
(Upper Board Inside of the Sensor Enclosure)**



**Printed Circuit Board Layout for the Hall-Effect Sensors
(Lower Board Inside of the Sensor Enclosure)**



APPENDIC C. TECHNICAL DATA FOR ELECTRICAL AND CONTROL SYSTEMS

Table C-1. Hall-effect sensor and power connection data (Cable #1)

J1	CABLE	SENSOR#	WIRE	CHANNEL
A	1-BLK	1	ORG/BLK	0
B	1-WHT	2	GRN/BLK	1
C	2-BLK	4	RED/BLK	3
D	2-WHT	6	GRN	5
E	3-BLK	7	BLU/BLK	6
F	3-WHT	5	WHT/BLK	4
G	4-BLK	3	BLU	2
H	4-WHT	8	WHT	7
J	5-BLK	9	RED	8
K	5-WHT	10	ORG	9
L	6-BLK	GROUND	BLK	
M	7-BOTH	(+) 12 V dc	RED	
N	6-WHT	SHIELD	BLK	
P	8-BOTH	(-) 12 V dc	GRN	

Table C-2. Pin identification and function description for digital/analog Cable #2.

J2	CABLE	WIRE	BOARD	FUNCTION
A	1-BLK	RED	(+) 5 V (49)/1302	
B	1-WHT	GRAY	32/1302	LE
C	2-BLK	ORG	33/1302	TB
D	2-WHT	WHT	34/1302	TE
E	3-BLK	GRN	31	LB
F	3-WHT	GRN/WHT	CH11/1300	TRV.POT
G	4-BLK	BLU/WHT	CH10/1300	ENCODER
H	4-WHT	BLK/WHT	GROUND	GROUND
I	5-BLK			
J	5-WHT			
K	6-BLK			
L	6-WHT			
M	7-BLK	BLK	GROUND	
N	7-WHT	RED	(+) 12 V	

Table C-3. Pin identification and function description for motor control Cable #3.

J3	CABLE	FUNCTION	
A	1-BLK	M1	Long M
B	1-WHT	M1	Long M
C	2-BLK	M2	Trans M
D	2-WHT	M2	Trans M
E	3-BLK	TB	
F	3-WHT	TB	
G	4-BLK	TE	
H	4-WHT	TE	
I	5-BLK	TE	
J	5-WHT	TE	
K	6-BLK	TB	
L	6-WHT	TB	
M	7-BLK	GROUND	
N	7-WHT	(+) 12 V	

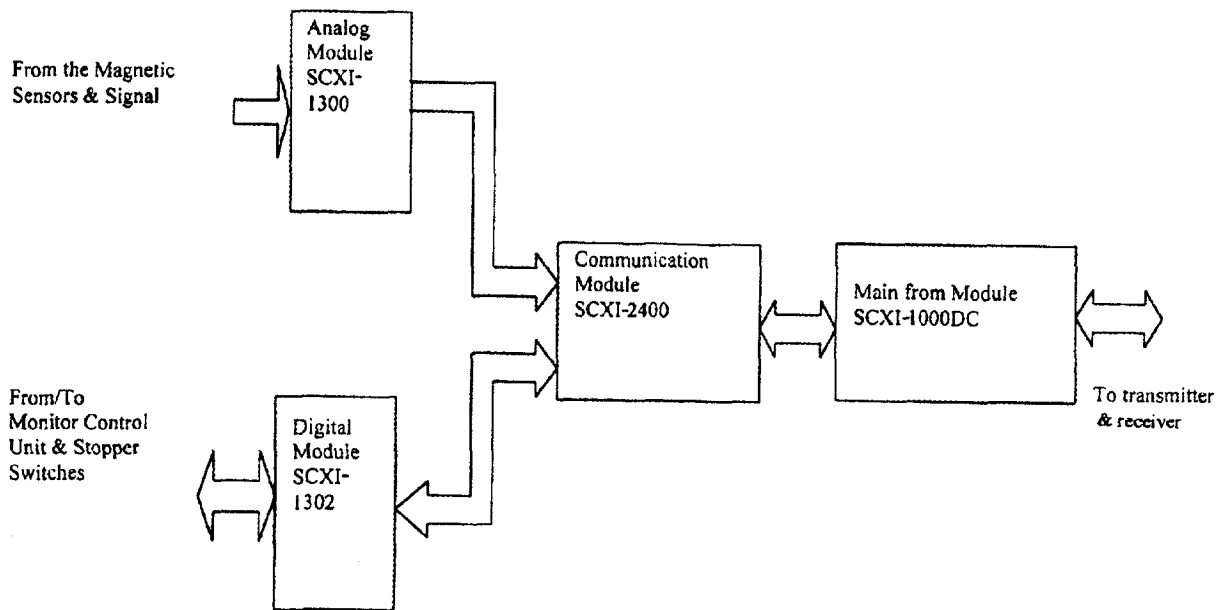


Figure C-1. Block diagram describing data acquisition and conditioning.

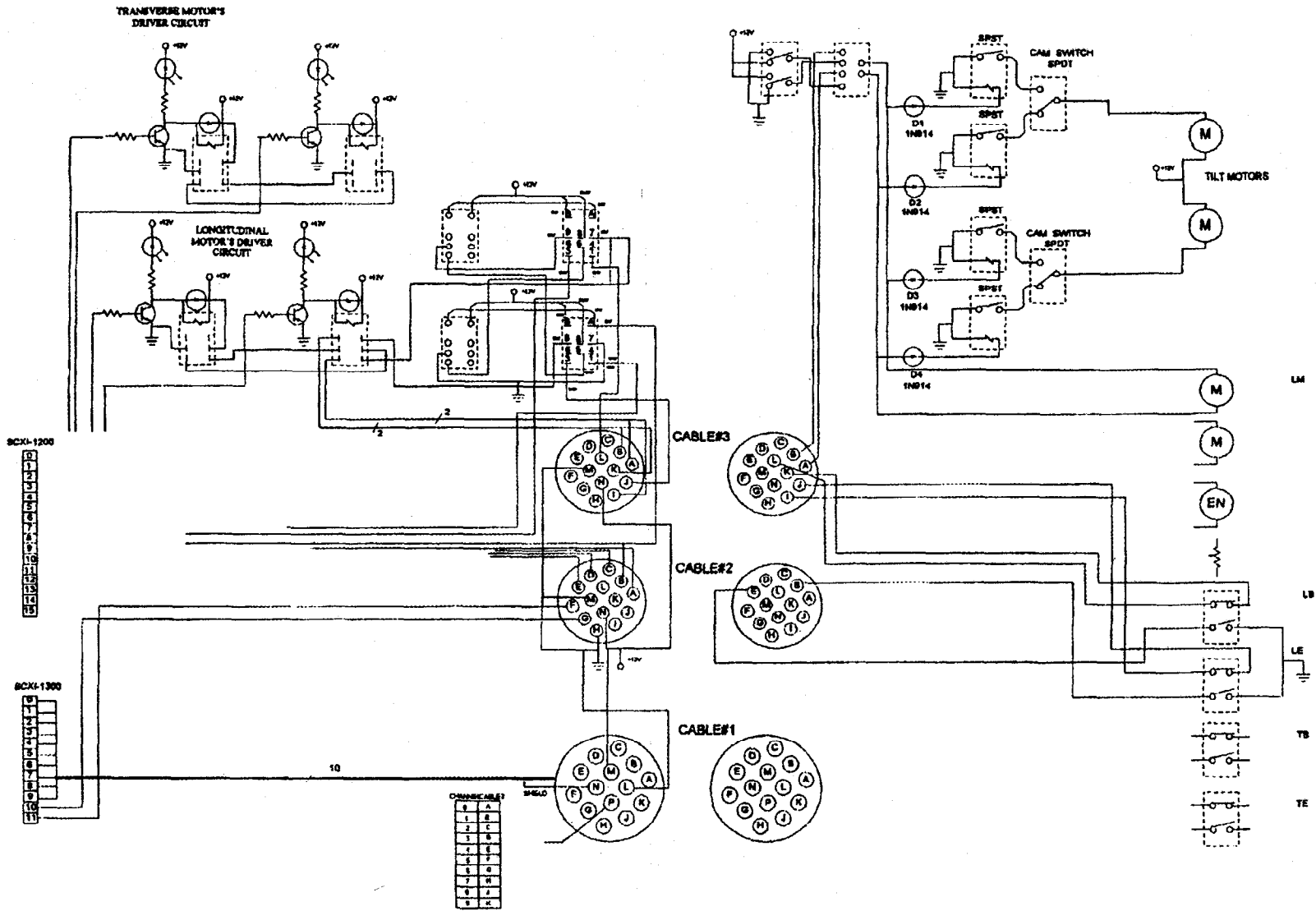


Figure C-2. Circuit diagram for overall electrical control for the MFL system.

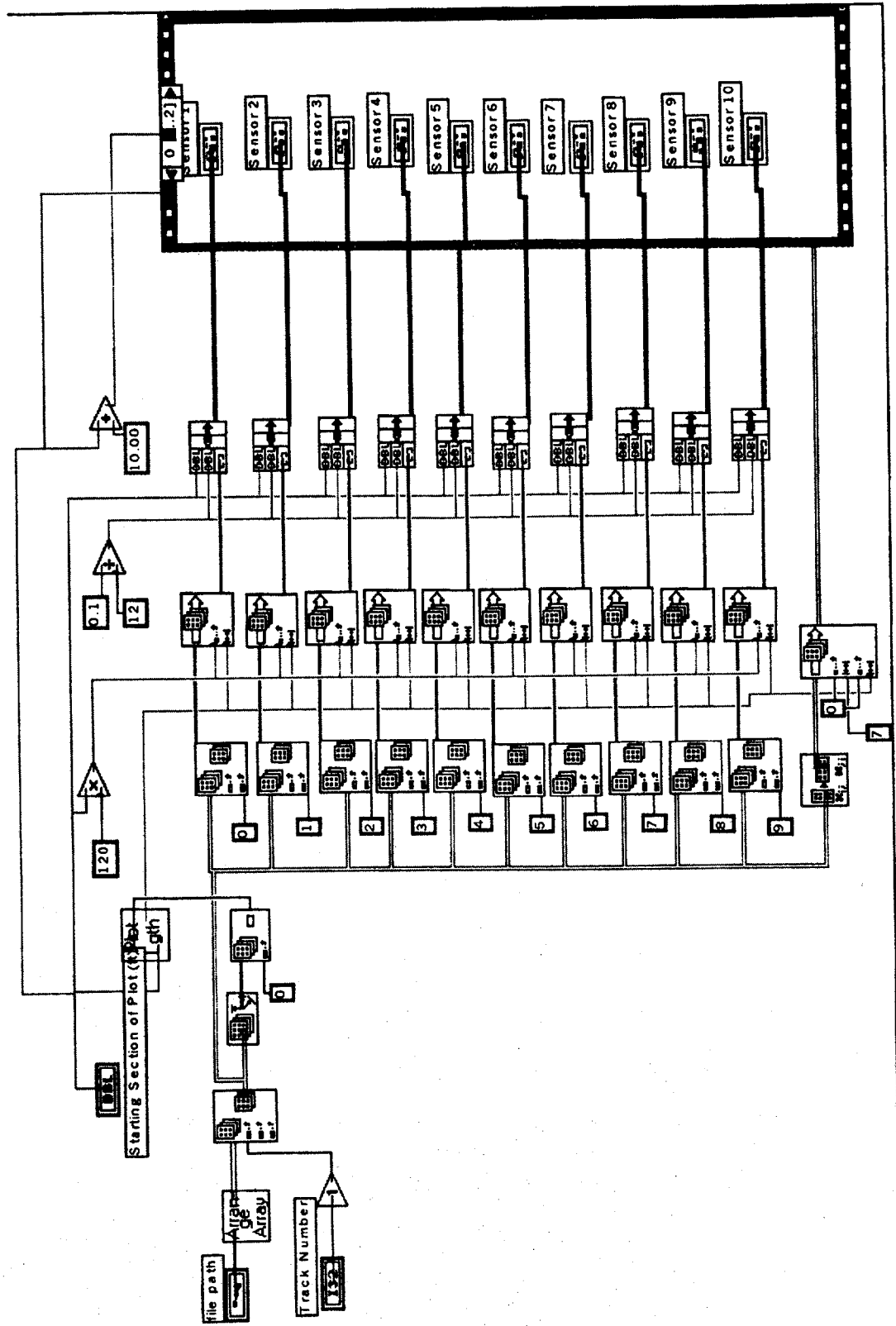
APENDIX D. PRIMARY COMPONENTS/PARTS DESCRIPTION

Table D-1 Primary components/parts data for the MFL system.

Part	Quantity	Part Description	Manufacturer	Vendor	Part Number
1	1	Permanent Magnets	Dexter Magnetic Materials	Dexter Magnetic Materials	PMW96-1206
2	10	Hall Sensors	F. W. Bell	F. W. Bell	JB-970
3	1	Magnet Sensor Assembly Encoder Wheel	BEI Sensors and Systems	BEI Sensors and Systems	94-01039-2095
4	6	Inflatable Contact Wheels	Cheng	M&M Supply	13-037-2P-2P-3/4 BB
5	1	12-Volt dc Drive Motor	Dayton	Granger	1LA74
6	1	2.974" OD 1/2" Pitch Drive Motor Gear	US Tsubaki	Granger	1L131
7	1	1.839" OD 1/2" Pitch Drive Motor Gear	US Tsubaki	Granger	1L106
8	8	Prelubricated Self-Aligning Machined Ball-Bearing Pillow Block	Browning	Granger	5X707
9	2	Toggle Motor	Dayton	Granger	4Z837
10	2	Adjustable Toggle Cam			
11	2	Toggle Switch	Honeywell Micro Switch	Stock Products	A 3Y 1-110
12	1	12-Volt dc Transverse Motor	Dayton	Newark Electronics	311SM6 T
13	2	Transverse Drive Linear Slide Rail	SKF Specialty Products Co	Granger	2L005
14	2	Transverse Drive Stopper Switches	SKF Specialty Products Co	SKF Specialty Products Co	LLEHS 23LCL-860M2
15	2	Longitudinal Limit Switch	Telemecanique	Granger	XCK-P110
16	1	Longitudinal Encoder (Model H20DB-25-F3-SS-120-ABZC-7272SM18-24)	Square D	Granger	C54GD
17	1	Transverse Potentiometer	BEI Sensors	BEI Sensors	924-01039-2095
18	4	10-Amp Toggling Relays	Bourns	Newark Electronics	3540S-1-202
19	1	Transmitter/Receiver	Ontron	Digi-Key	G6B-1147P-US-DC12
20	1	All-Weather Transmitter/Receiver	Wireless Scientific	Wireless Scientific	CK 232
			Wireless Scientific	Wireless Scientific	CK 232aw

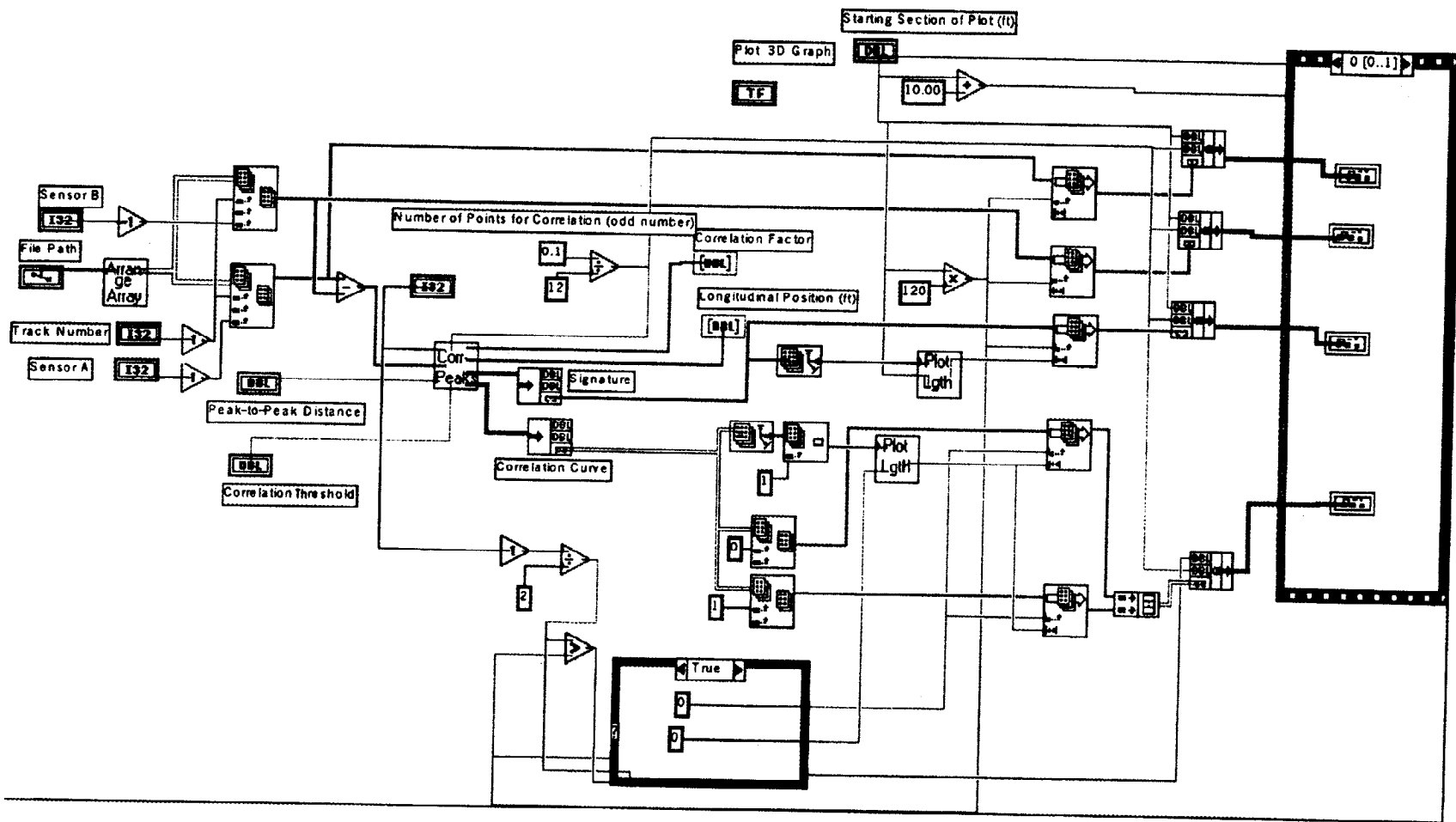


Subroutine for Post-Processing Option 2

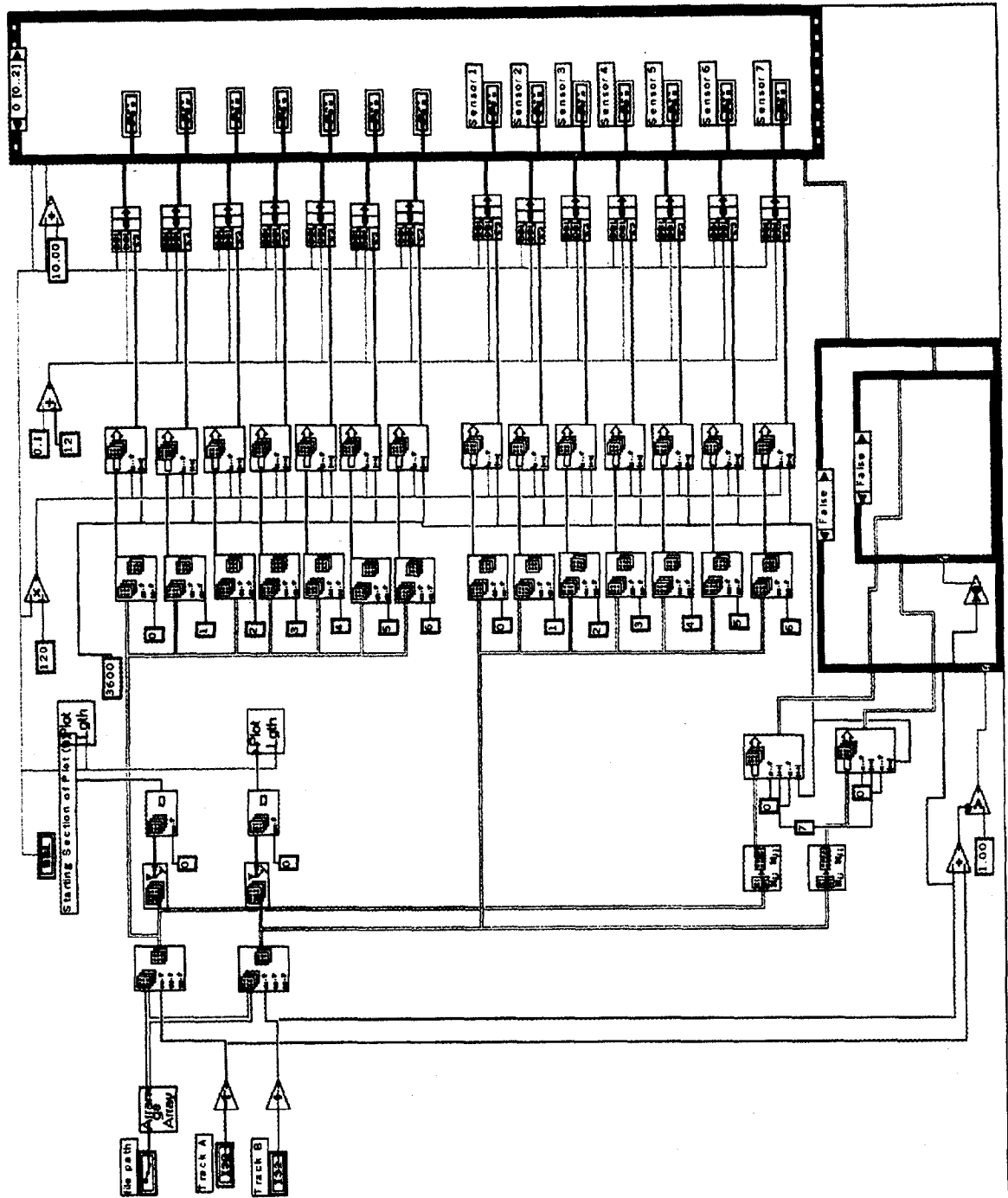


Subroutine for Post-Processing Option 3

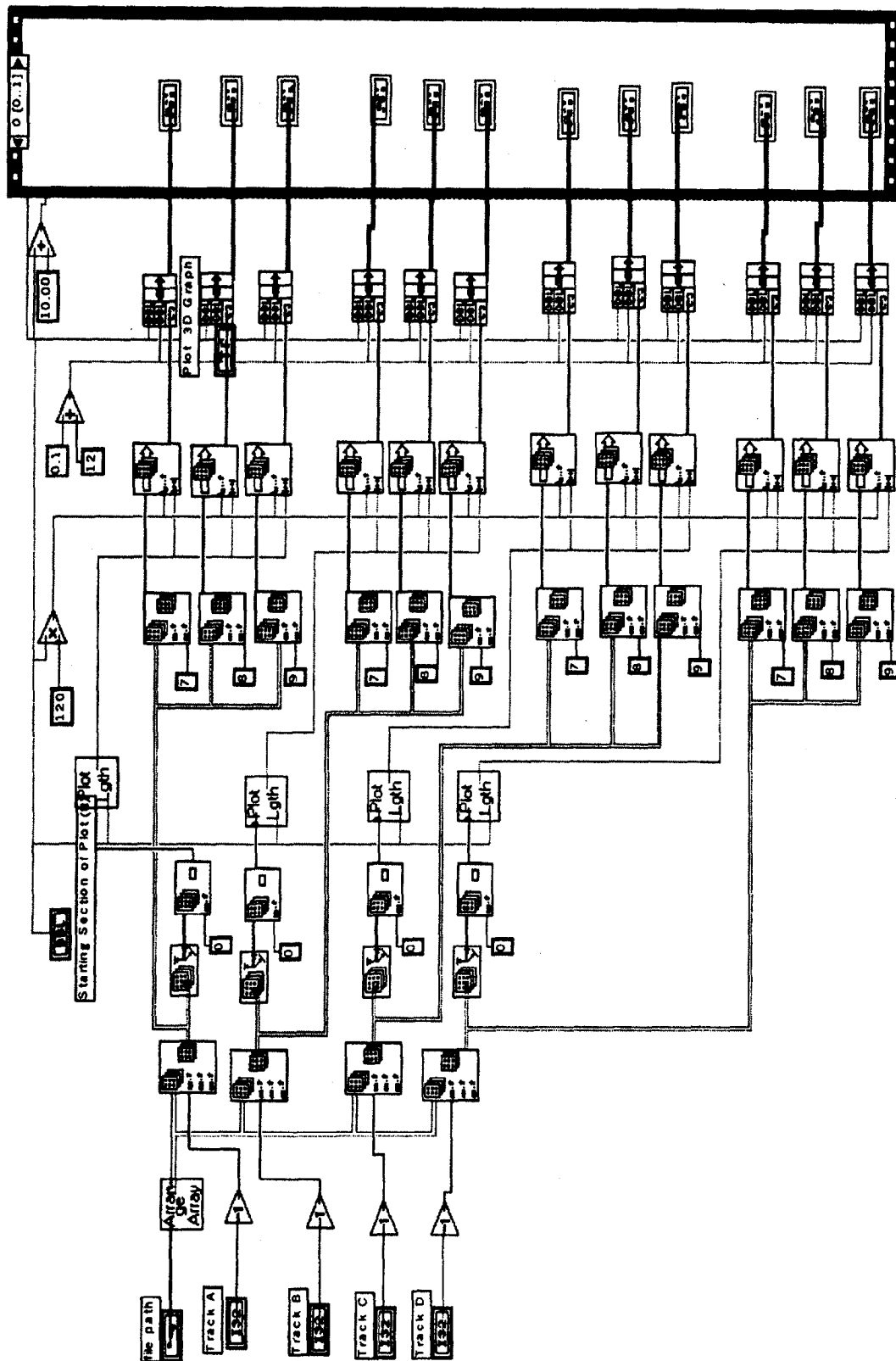
85



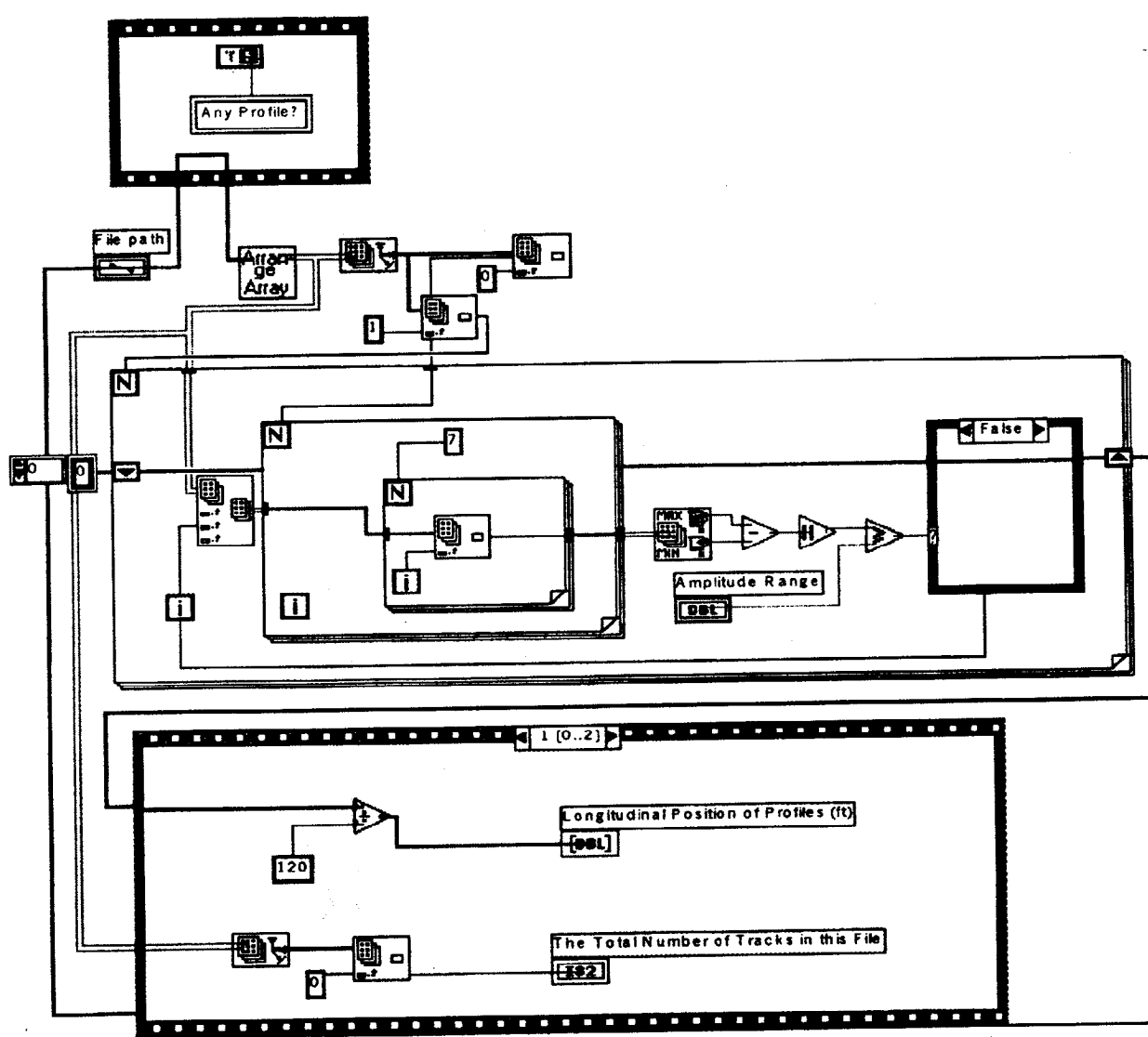
Subroutine for Post-Processing Option 4



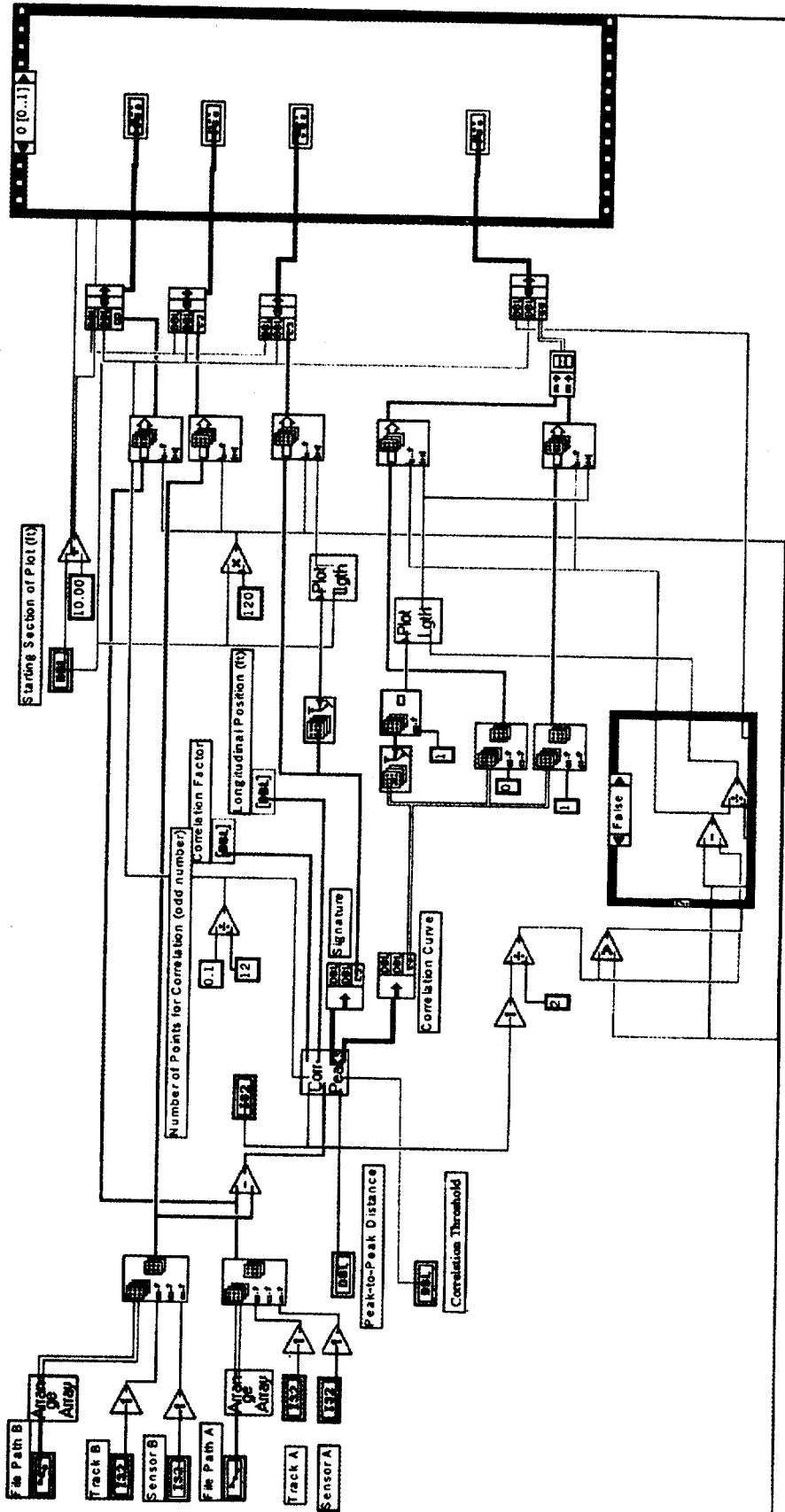
Subroutine for Post-Processing Option 5



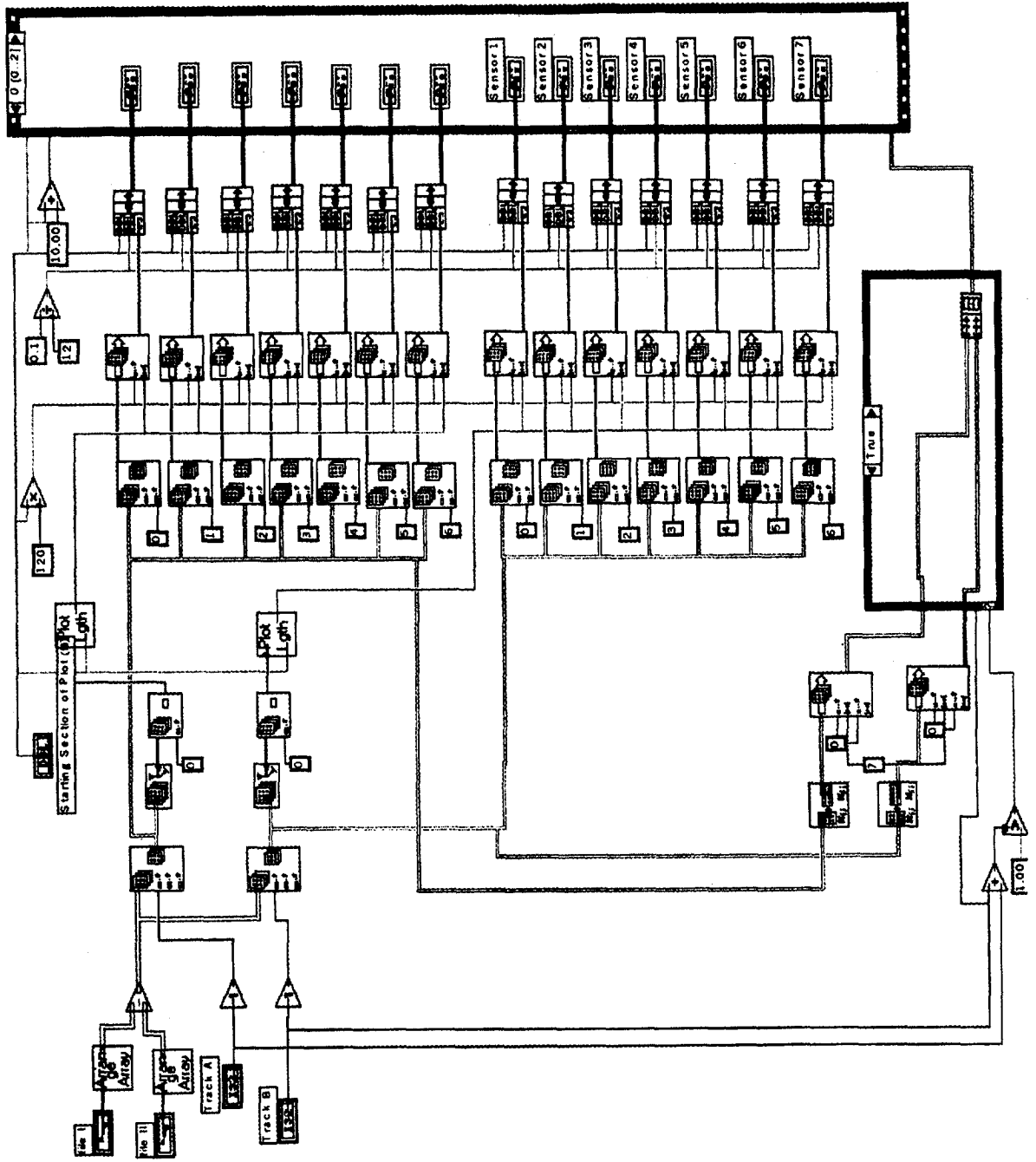
Subroutine for Post-Processing Option 6



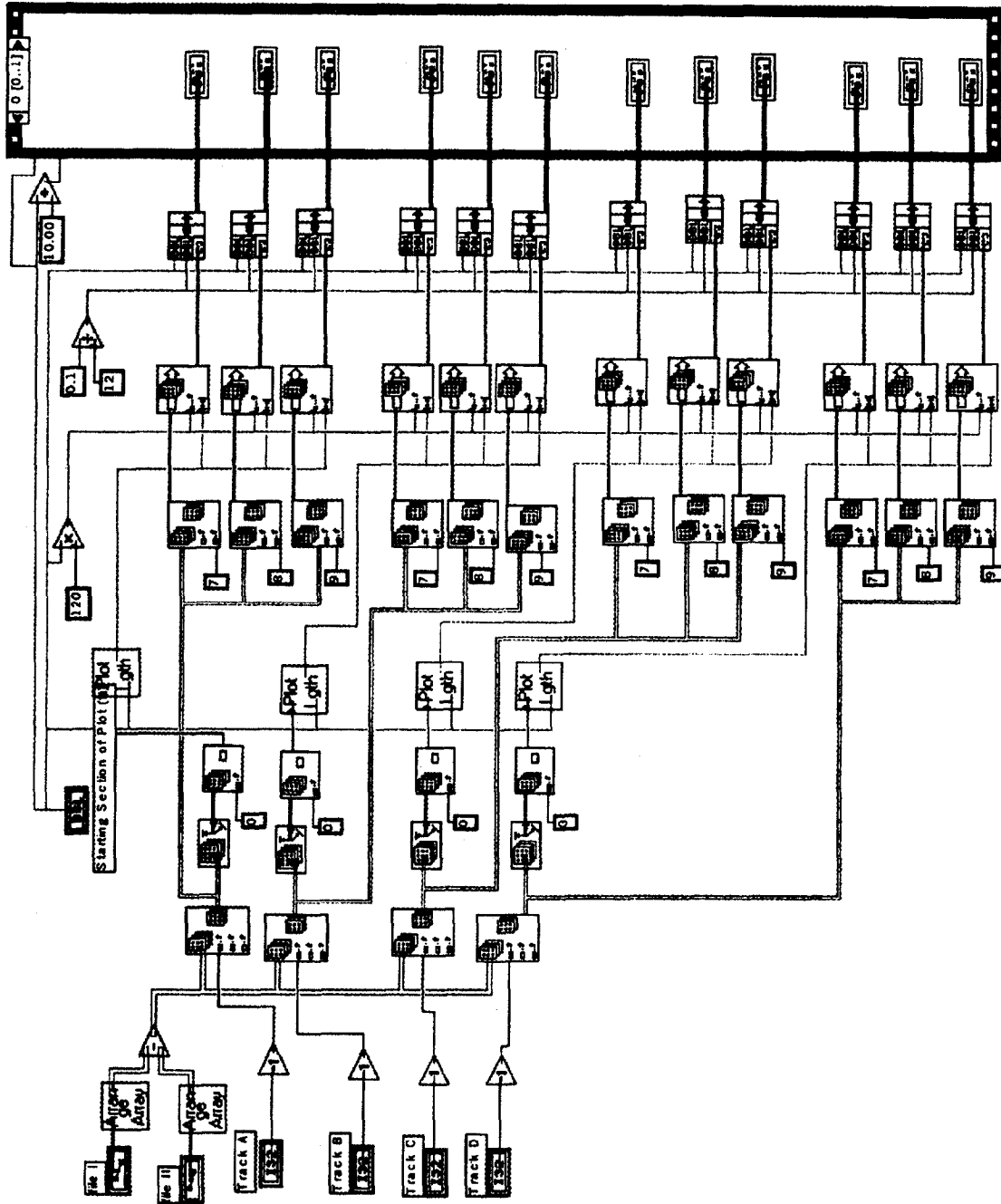
Subroutine for Post-Processing Option 7



Subroutine for Post-Processing Option 8

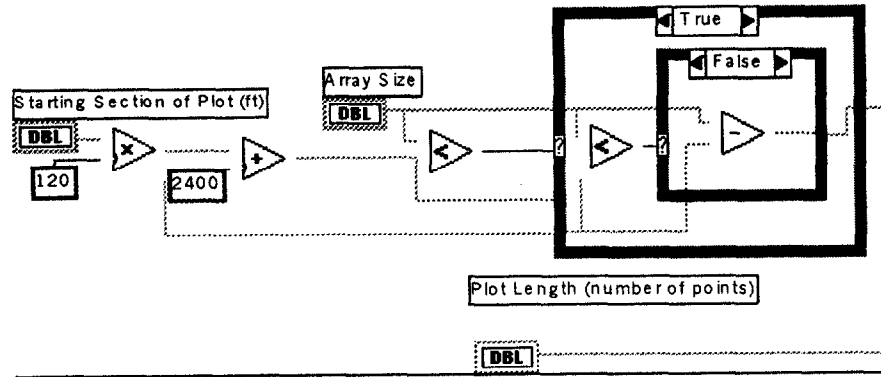


Subroutine for Post-Processing Option 9



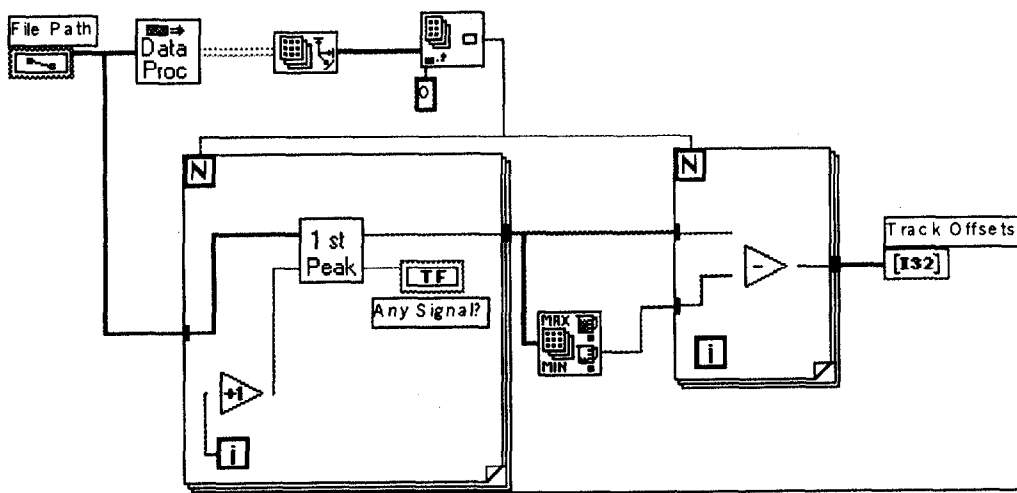
Data Display Length Subroutine:

The function of this subroutine is to measure the length of the data file being processed and to give the user the option to choose the starting point for displaying the data on the computer screen.



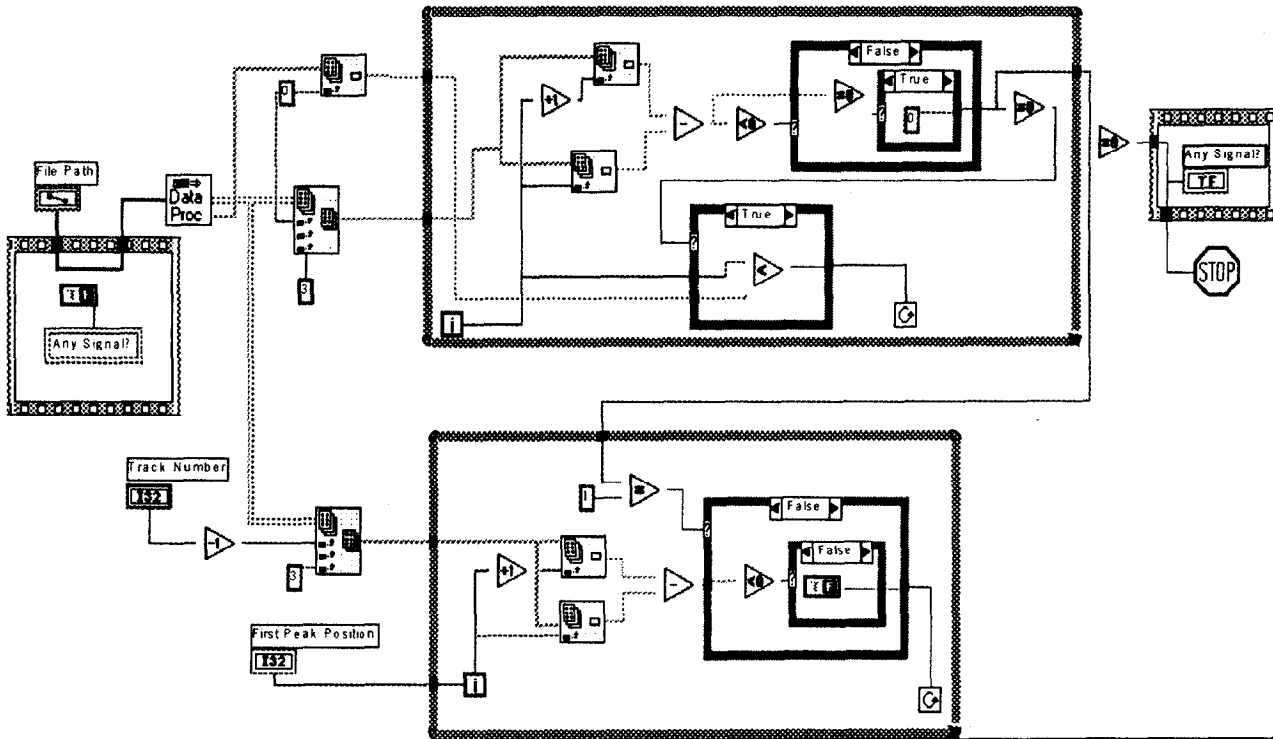
Data Offset Subroutine:

The function of this subroutine is to make adjustment in the data length for two tracks so they become equal lengths. At each end of a test beam, a magnetic marker the beam structure, there is a reference bar that gives a known peak signal that serves as a reference for the track length. The subroutine adjusts the length of the tracks according to the distance between the reference wires. The block diagram of the subroutine is shown in figure A.5.



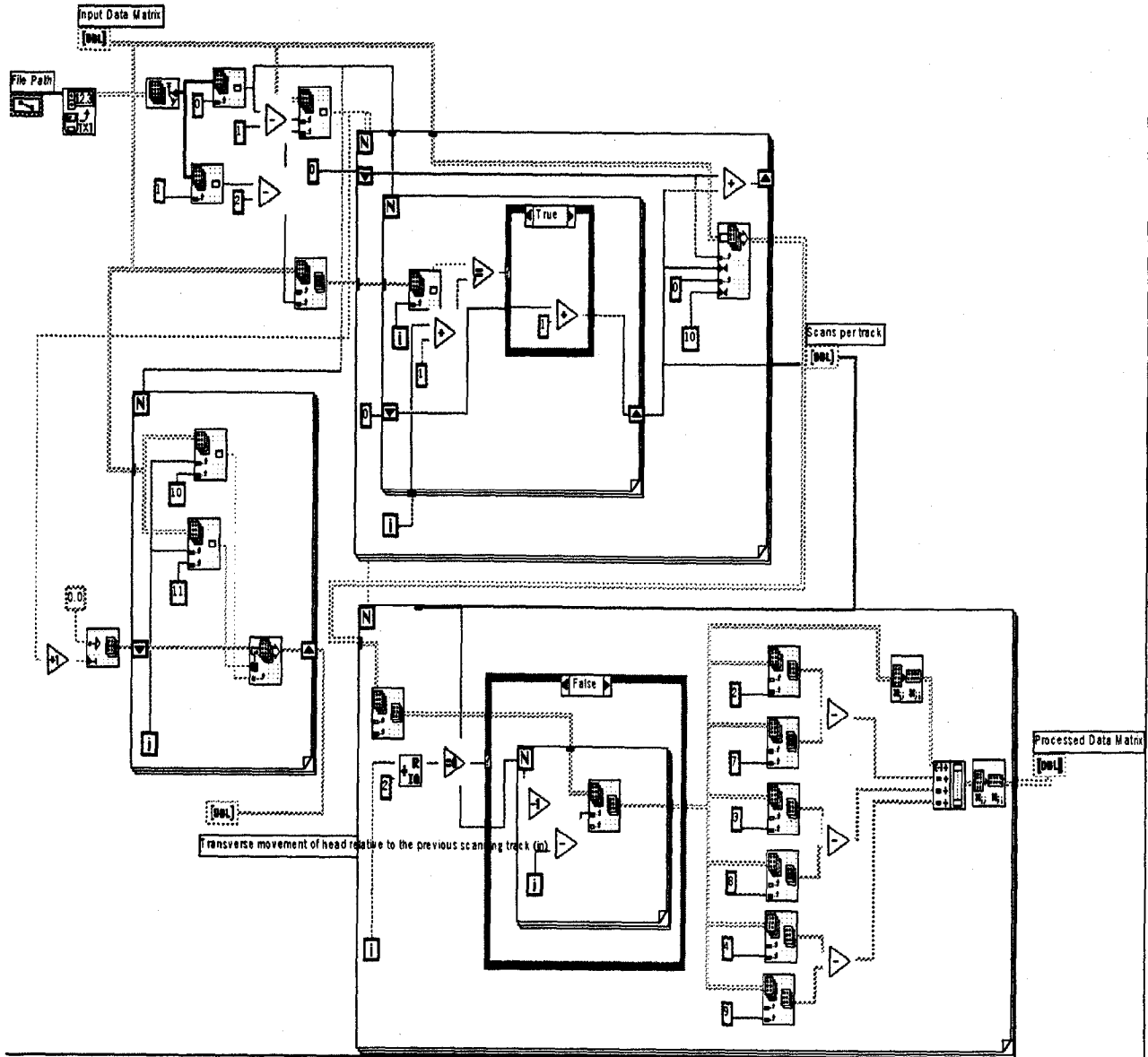
First Peak Subroutine:

The function of this subroutine is to identify the position of the first peak in recorded MFL data for each sensor within any track. The data offset subroutine described in the appendix will utilize this information to make adjustments in the length of the recorded data for the sensors of different tracks.



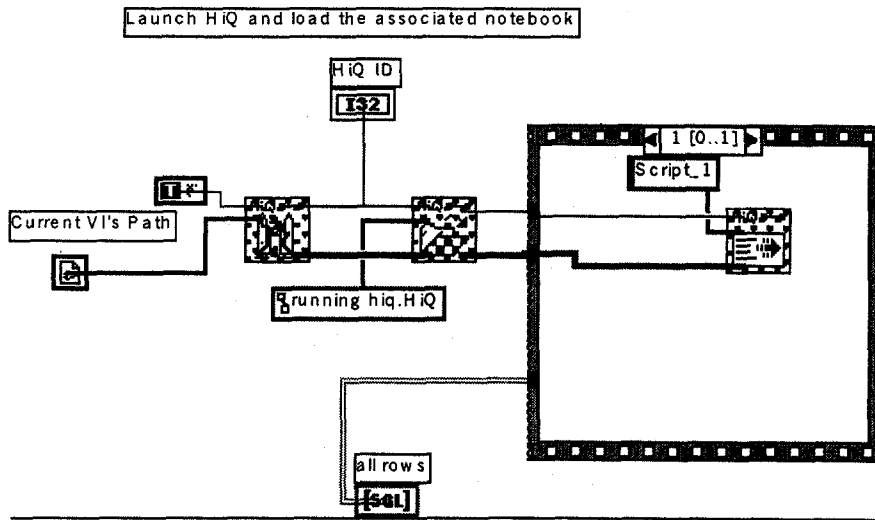
Data Processing Subroutine:

The function of this subroutine is to arrange the recorded data in a file with multiple tracks so that there is no overlapping of sensor outputs across the width of a test beam. Sensor output overlaps will occur if the sensing-head unit is positioned such that a new track or path overlaps with the previous one. The subroutine keeps track of the transverse position of the sensing-head unit and constructs a corrected data file without sensor output overlap.



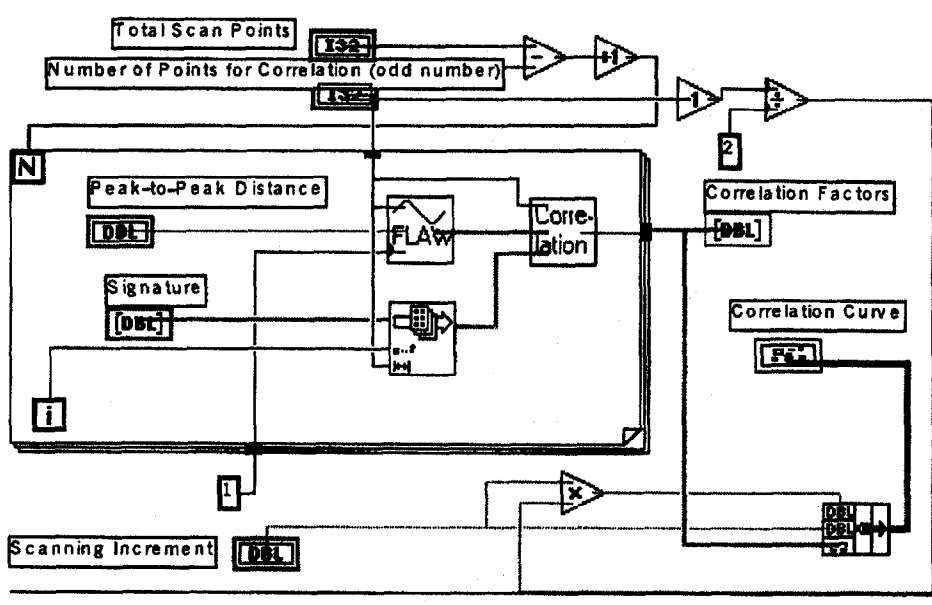
Three-Dimensional Graph Subroutine:

The function of this subroutine is to construct and display a three-dimensional graph of the MFL data from the seven Hall-effect sensors that are located on the upper sensor board inside of the sensor enclosure. The subroutine executes National Instrument's "HiQ" program as well as a data display subroutine. Any number of data tracks can be used here.



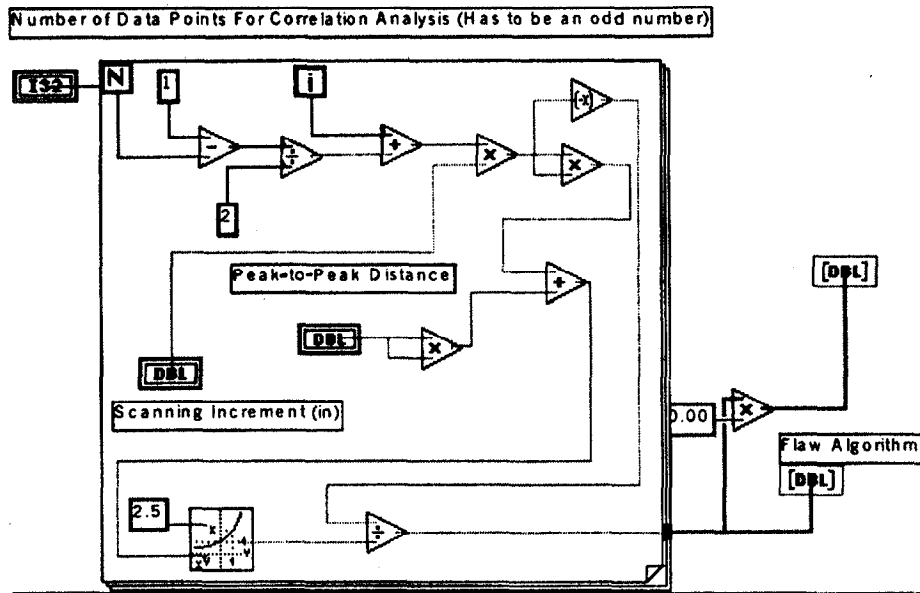
Correlation Analysis and Display Subroutine:

The function of this subroutine is to perform a correlation analysis between the recorded MFL data and a predefined signal template. The subroutine calculates the corresponding correlation factors and displays a graph of the correlation factors along the test path.



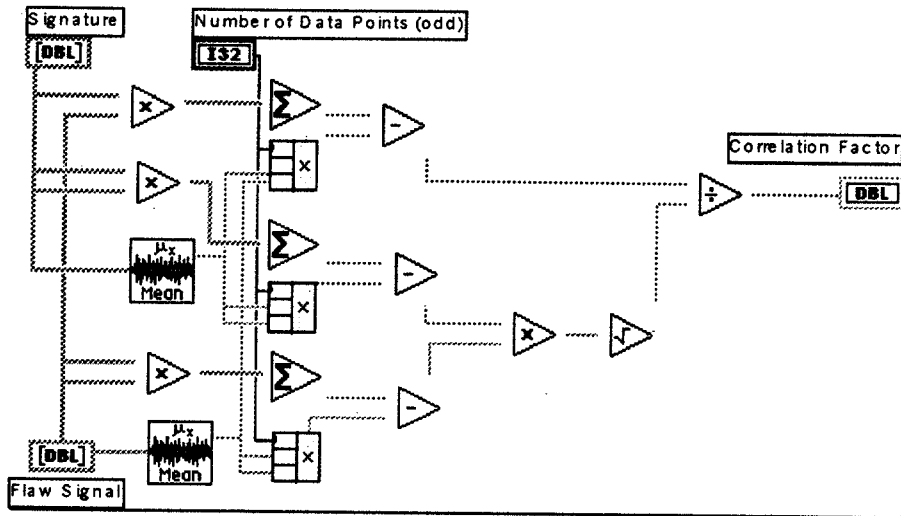
Flaw Signal Definition Subroutine:

The function of this subroutine is to define and construct a theoretical flaw signal template that will be used in the correlation analysis.



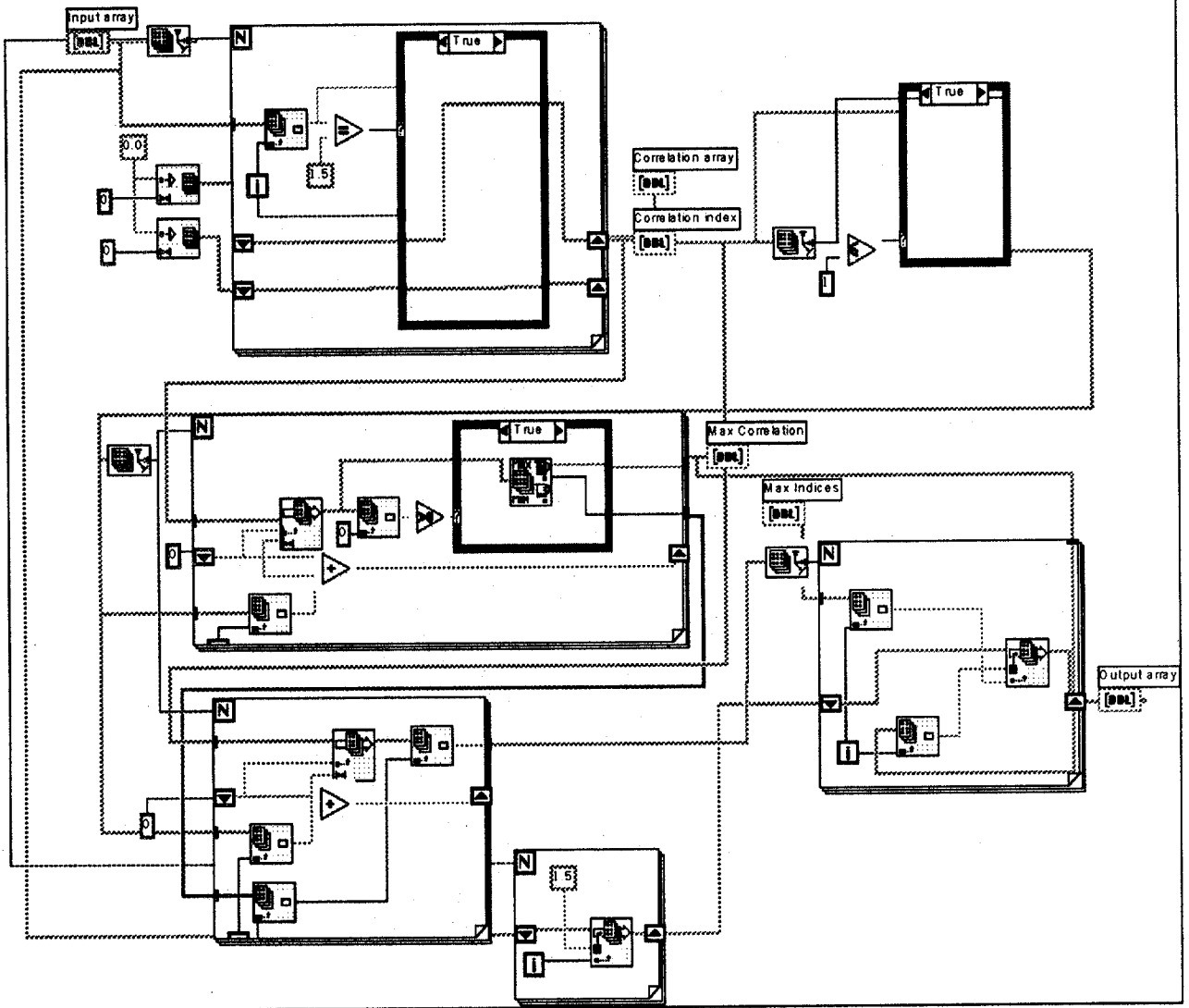
Correlation Model Subroutine:

The function of this subroutine is to define the mathematical model that is used in the correlation analysis.



Correlation Graph Peak Identification Subroutine:

The function of this subroutine is to identify and label peaks in the correlation graph that are higher than a pre-specified threshold.



REFERENCES

1. Kusenberger, F.N., and Barton, J.R., *Detection of Flaws in Reinforcing Steel in Prestressed Concrete Bridge Members*. Final Report, Report No. FHWA/RD-81/087, Federal Highway Administration, 1981.
2. Kusenberger, F.N., and Birkelbach, R.S., *Detection of Flaws in Reinforcing Steel in Concrete Bridge Members*. Final Report, Report No. FHWA/RD-83/081, Federal Highway Administration, 1983.
3. Beissner, R.E., and Barton, J.R., *Laboratory Test of Magnetic Field Disturbance (MFD) System for Detection of Flaws in Reinforcing Steel in Prestressed Concrete Bridge Members*. Draft Final Report, Contract No. DTFH61-83-C-00090, Federal Highway Administration, 1984.
4. Ghorbanpoor, A., Steber, G.R., and Shew, T.E., *Evaluation of Steel in Concrete Bridges: The Magnetic Field Disturbance (MFD) System*. Final Report, Report No. FHWA-SA-91-026, Federal Highway Administration, 1991.





HRDI-09/4-00(700)E
